Abstract

Title of Dissertation: Magnetic Fields Around Black Holes

David A. G. Garofalo, Doctor of Philosophy, 2008

Dissertation directed by: Professor Christopher Stephen Reynolds
Department of Astronomy

Active Galactic Nuclei are the most powerful long-lived objects in the universe. They are thought to harbor supermassive black holes that range from 1 million solar masses to 1000 times that value and possibly greater. Theory and observation are converging on a model for these objects that involves the conversion of gravitational potential energy of accreting gas to radiation as well as Poynting flux produced by the interaction of the rotating spacetime and the electromagnetic fields originating in the ionized accretion flow. The presence of black holes in astrophysics is taking center stage, with the output from AGN in various forms such as winds and jets influencing the formation and evolution of the host galaxy. This dissertation addresses some of the basic unanswered questions that plague our current understanding of how rotating black holes interact with their surrounding magnetized accretion disks to produce the enormous observed energy. Two magnetic configurations are examined. The first involves magnetic fields connecting the black hole with the inner accretion disk and the other involves large scale magnetic fields threading the disk and the hole. We study the effects of the former type by establishing the consequences that magnetic torques between the black hole and the inner accretion disk have on the energy dissipation profile. We attempt a plausible explanation to the observed "Deep Minimum" state in the Seyfert galaxy MCG-6-30-15. For the latter type of magnetic geometry, we study the effects of the strength of the magnetic field threading the black hole within the context of the cherished Blandford & Znajek mechanism for black

hole spin energy extraction. We begin by addressing the problem in the non-relativistic regime where we find that the black hole-threading magnetic field is stronger for greater disk thickness, larger magnetic Prandtl number, and for a larger accretion disk. We then study the problem in full relativity where we show that our Newtonian results are excellent approximations for slowly spinning black holes. We proceed to address the issue of the spin dependence of the Blandford & Znajek power. The result we choose to highlight is our finding that given the validity of our assumption for the dynamical behavior of the so-called plunge region in black hole accretors, rotating black holes produce maximum Poynting flux via the Blandford & Znajek process for a black hole spin parameter of about $a \approx 0.8$. This is contrary to the conventional claim that the maximum electromagnetic flux is achieved for highest black hole spin.

Magnetic Fields Around Black Holes

by

David A. G. Garofalo

Dissertation submitted to the Faculty of the Graduate School of the
University of Maryland at College Park in partial fulfillment
of the requirements for the degree of
Doctor of Philosophy
2008

Advisory Committee:

       Professor Christopher Stephen Reynolds, chair
       Professor Kevork Abazajian
       Professor Paulo Bedaque
       Professor M. Coleman Miller
       Professor Peter Shawhan

Preface

Chapter 2 has been published in essentially this form in the Astrophysical Journal (Garofalo & Reynolds, 2005, ApJ, vol. 624, pp.94). Chapter 3 is based on material published in the Astrophysical Journal (Reynolds, Garofalo & Begelman, 2006, ApJ, vol. 651, pp. 1023). The material presented in Chapter 4 is currently being prepared for submission to the Astrophysical Journal. An early version of the results of Chapter 2 were presented as a poster paper (Garofalo & Reynolds) at the "Constellation-X Science Workshop" in New York in May 2003. The results of Chapter 3 were presented as an oral presentation (Garofalo, Reynolds & Begelman) at the "Supermassive Black Holes" conference in Santa Fe, New Mexico, July 2006.

To Luca

Contents

List of Tables

List of Figures

Figure 1: An accretion disk and a magnetic field around a black hole. An artist view taken from the Hubble Space Telescope website.

Chapter 1

Introduction

Observations reveal the presence of small regions of space appearing point-like to all current observatories from which enormous quantities of energy are emitted. The most energetic of these objects reside at the center of galaxies and sometimes outshine the rest of the galaxy by up to three orders of magnitude. These astronomical powerhouses are called active galactic nuclei (AGN). Theory and observations have converged on a paradigm for such objects whose primary components are rotating supermassive black holes that accrete matter via a surrounding accretion disk.

Much of the observed electromagnetic radiation is thought to be energized, ultimately, by conversion of the gravitational potential of the accreting matter into radiation. However, it has been suspected for some time that the rotational energy of the black hole itself may be an astrophysically important source of energy, especially for the relativistic jets of plasma that are often seen emanating from black hole systems. Through the seminal work of Blandford & Znajek (1977), it is thought that the most plausible way that Nature can tap the rotational energy of a black hole is via large scale magnetic fields that are generated by currents in the accretion disk and thread the event horizon of the black hole.

The importance of black holes to astrophysics is difficult to exaggerate. On the one hand, detailed studies of processes close to black holes (including the extraction of black

hole spin energy via large scale magnetic fields) allow us to test predictions of the General Theory of Relativity (GR) in its strong-field regime. X-ray observatories are already making the first steps in this direction. Currently, there is evidence for the frame-dragging effects of black hole spin from, for example, X-ray spectroscopic analyses of the iron emission line from several supermassive black hole accretion disks (Brenneman & Reynolds, 2006). The ultimate development of these observational techniques using future X-ray observatories (such as NASA's proposed Constellation-X Observatory) will allow us to essentially map out the spacetime around these isolated supermassive black holes, and compare the result to the expected Kerr metric.

On the other hand, the enormous output of energy from an accreting supermassive black hole can heat the interstellar medium on the scale of the galaxy, influencing the rate of star formation and thus of the evolution of the host galaxy. Observations during the last decade have revealed a tight connection between the mass of the supermassive black hole that lies at the center of a galaxy and the stellar velocity dispersions of stars in the galaxy's bulge. More precisely, it is found that

$$M \approx 1 \times 10^8 \left(\frac{\sigma}{200\,\mathrm{km\,s^{-1}}} \right)^4 M_\odot, \tag{1.1}$$

where M is the mass of the central supermassive black hole and σ is the velocity dispersion of the galaxy's bulge measured at the half-light radius (Gebhardt et al. 2000; Ferrarese & Merritt 2000). This result, the so-called $M - \sigma$ relation, indicates a previously unrecognized connection between the central supermassive black hole and the properties of the galaxy on spatial scales orders of magnitude larger than the black hole's actual gravitational sphere of influence. Although the details have yet to be fully understood, the favored scenario for explaining this relation is one in which the accretion of gas onto the central supermassive black hole accompanies periods of star formation (since both processes rely on the supply of large amounts of gas). Both electromagnetic radiation and jets from the accreting supermassive black hole can heat the interstellar medium and act

to suppress star formation. Numerical simulations suggest that this "AGN feedback" can readily reproduce the $M - \sigma$ relationship (see Di Matteo, Springel & Hernquist 2005).

This thesis attempts to shed light on some of the mechanisms behind the large output of energy from these tiny regions of space. In particular, we focus on the interaction between the black hole spacetime and the large scale magnetic field that may be key to jet formation. But before delving into these ideas, we wish to give the reader a sense of why black holes, accretion disks, and magnetic fields, form the paradigm for the objects of our study.

1.1 The black hole paradigm for AGN

1.1.1 Basic Considerations

Consider one of these high energy systems producing $10^{47}\,\mathrm{erg\,s}^{-1}$ from a region of space that light-crossing time arguments constrain to no larger than the Solar System. The light-crossing time argument goes as follows. The observed emissions from many AGN are characterized by significant time variability, with typical timescales of hours or less. Now, any disturbance in the system will propagate at a finite speed less than the speed of light. This means that it takes a time δt for the observed emissions to change by a significant amount, restricting the physical extent of the region producing that emission to be no larger than $l = c\delta t$. This allows us to use time-variability of AGN emissions to determine a maximum physical extent to the energy producing region in the AGN and, as mentioned above, it is not uncommon to find Solar System scale extents as a result. We note that this argument must be modified in systems where the emission originates from material moving at relativistic velocities towards us (e.g. Blazars and Gamma-Ray Bursts).

The enormous sustained luminosities have implications for the mass of the AGN.

If the radiation pressure exceeds the gravitational force, accreting material gets blown out and the AGN would quickly turn off. The balance between gravitational force and radiation pressure gives a limiting value to the sustained luminosity that a mass M can produce. This limiting luminosity is called the Eddington luminosity. For a pure hydrogen plasma, the balance between gravity and radiation pressure is expressed as

$$\frac{GMm_p}{r^2} = \frac{L\sigma_T}{4\pi cr^2}, \tag{1.2}$$

where we have considered a region far from the black hole where the gravity is Newtonian and have assumed that the luminosity is emitted isotropically. This expression follows from the fact that the inertia of the plasma is dominated by the protons whereas the radiation interacts primarily with the electrons with Thomson cross-section σ_T.

The Eddington luminosity is therefore

$$L_{Edd} = \frac{4\pi GMm_p c}{\sigma_T} \approx 1.3 \times 10^{38} \frac{M}{M_\odot} \, erg \, s^{-1}, \tag{1.3}$$

where $M_\odot$ is one solar mass. Thus, AGN with luminosity of $10^{47} \, erg \, s^{-1}$ require a mass of $10^9 M_\odot$.

Such enormous powers prompts us to consider highly efficient mechanisms of energy production. The efficiency is characterized by the fraction of accreted rest mass that is radiated, i.e. $L = \eta \dot{M} c^2$, where $\dot{M}$ is the mass accretion rate onto the black hole. The most efficient mechanism known is matter-antimatter annihilation but it is not believed that large quantities of anti-matter are present in the universe. The next most efficient mechanism is accretion onto relativistic objects such as neutron stars and black holes. Neutron stars have a maximum mass of $\sim 2M_\odot$, so accretion onto neutron stars cannot be the central power source in AGN. We are thus led to consider massive black holes.

1.1.2 Accretion Disks

The earliest models for accretion onto a central object were spherically symmetric (Bondi, 1952). It was quickly realized, however, that any realistic accretion flow will have sufficient angular momentum about the black hole to form a rotationally supported disk. This lead to the development of the standard non-relativistic accretion disk model of Shakura & Sunyaev (1973) and its relativistic generalization of Novikov & Thorne (1974). The efficiency of a standard relativistic disk is set by the binding energy at the radius of marginal stability, inside of which the matter is assumed to plunge into the black hole in an approximate ballistic manner (i.e. conserving energy and angular momentum). Around a non-rotating black hole the efficiency is 6% while the efficiency for a maximally spinning black hole with a prograde disk is 42%.

The dynamics of an accretion disk are almost entirely determined by the transport of angular momentum in the flow. Assuming Newtonian gravity for illustrative purposes and a radiatively-efficient geometrically thin disk with small radial pressure gradients so that gas flows on Keplerian orbits, the specific angular momentum of a parcel about a black hole of mass M is $l = \sqrt{GMr}$. Thus, for such an element of gas to accrete, it must lose angular momentum. Until the early 1990's, the principal uncertainty in disk models was the mechanism by which matter lost its angular momentum. The resolution of this problem brings us to the magnetohydrodynamic (MHD) paradigm for accretion flows.

1.1.3 The MHD paradigm

Balbus & Hawley (1991) showed that a powerful MHD instability (previously found by independently by Vavilov and Chandrasekhar between 1959 and 1961 but not adopted to solve the disk angular momentum transfer problem) will affect any magnetized ionized accretion flow. They showed that the instability leads to turbulent fluid motion charac-
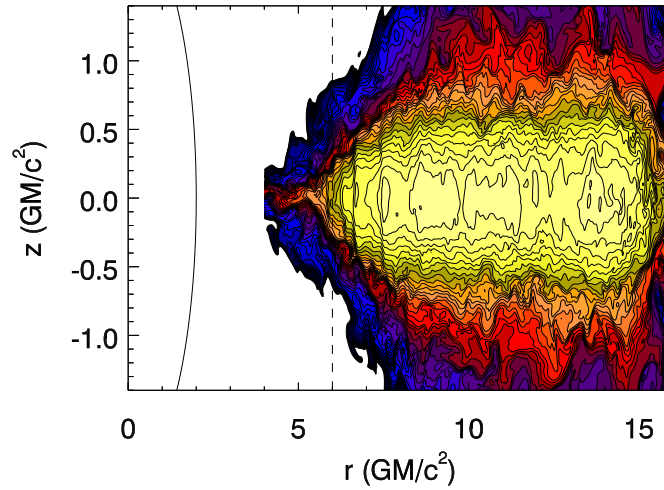
Figure 1.1: Magnetorotational instability producing turbulence leading to accretion. Azimuthal cross section of the density in logarithmic scale. Black hole event horizon is on the left (solid black line). From Reynolds & Fabian (2008).

terized by magnetic field correlations that transport angular momentum outward. To understand the basic operation of this instability, consider two nearby gas parcels at slightly different radii, connected via a magnetic field line that for illustrative purposes can be treated as an elastic band. The gas parcel at smaller radius from the compact object is orbiting faster than the gas parcel at larger radius. Therefore, there will be a torque produced by the inner gas parcel on the outer one, giving angular momentum to the latter. Because the inner gas parcel has lost angular momentum, it spirals further toward smaller radius and speeds up in its orbital velocity. The outer gas parcel moves further away to larger radius to satisfy the dynamics resulting from an increase in its angular momentum. The transfer of angular momentum is thus unstable and runs away. This is exactly what was needed to solve the angular momentum problem in accretion disks. Due to the generic nature of this instability, it was widely accepted as operating in real accretion disks. Nowadays, both non-relativistic and GRMHD simulations show that the instability produces turbulence in accretion flows and that angular momentum is indeed transferred
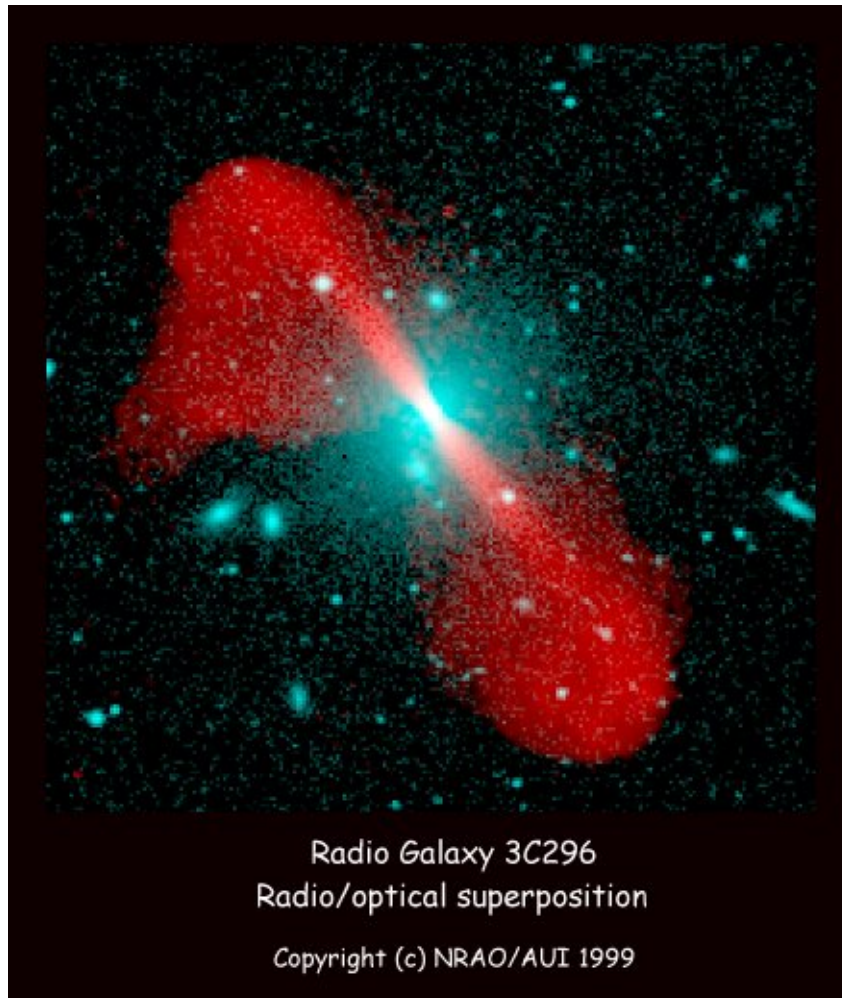
Figure 1.2: A radio/optical composite image of the radio galaxy 3C296. The optical (blue) component shows starlight from the large elliptical host galaxy. The radio emission (red) is synchrotron radiation from energetic electrons in the jets produced by the central AGN.

outward producing accretion onto a central body (Figure 1.1). This magnetorotational instability (MRI) highlights the central role that magnetic processes play in black hole accretion.

1.2   Black hole jets

In about 10 percent of AGN, the luminous central core is accompanied by oppositely directed beams of relativistic plasma called jets that are directly observed (Figures 1.2 and
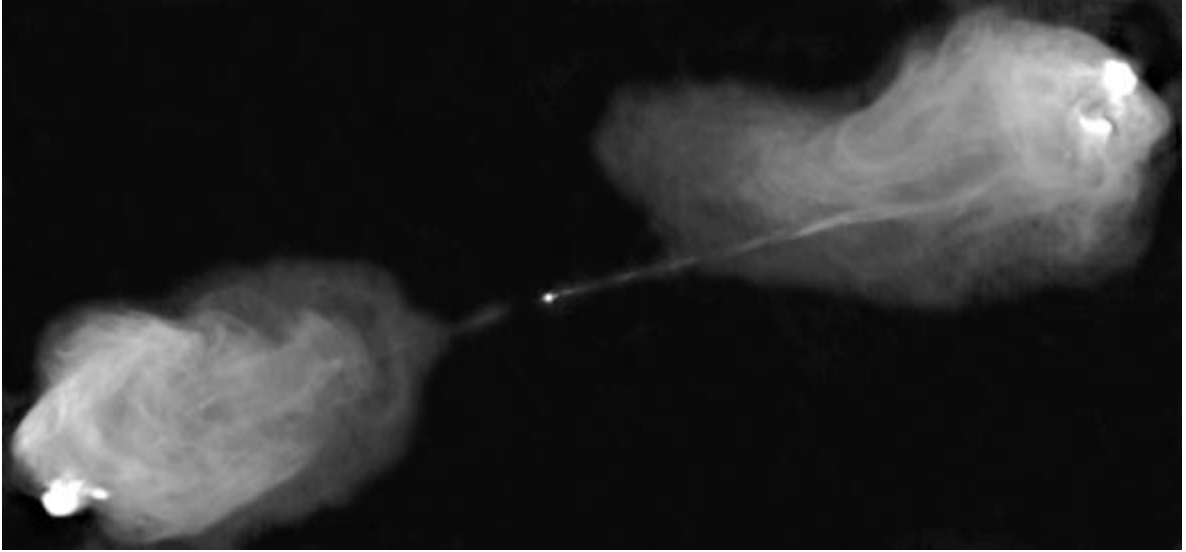
Figure 1.3: The radio galaxy Cygnus A as seen by the VLA in New Mexico showing the extended radio lobes extending in both directions over a region of about 500,000 light years.

1.3). The most prominent radiation from the jets is synchrotron radiation in the radio band, the signature of relativistic plasma flow through magnetic fields. These jets are seen to propagate over large distances, in some cases out to Mega-parsec scales. Two facts suggest that the matter flow in some of these jets is highly relativistic, with bulk Lorentz factors of up to $\Gamma \sim 10$ or more. Firstly, the jets in many AGN are observed to be one sided (e.g. M87 in Fig. 1.4 and 1.5). It is hard to envisage any process which would produce intrinsically one-sided jets from a black hole system, thus these observations are interpreted in terms of special relativistic boosting of the intensity of the approaching jet, and de-boosting of the intensity of the receding jet. Secondly, high-resolution observations (e.g. with VLB interferometry in the radio band) reveal features within the central regions of these jets that appear to move on the plane of the sky at superluminal velocities. This phenomenon was actually predicted by Rees (1966) on account of observations of radio-loud AGN and is indicative of relativistic motion along a direction close to our line of sight.

Many aspects of the acceleration and collimation of these jets remain mysterious.
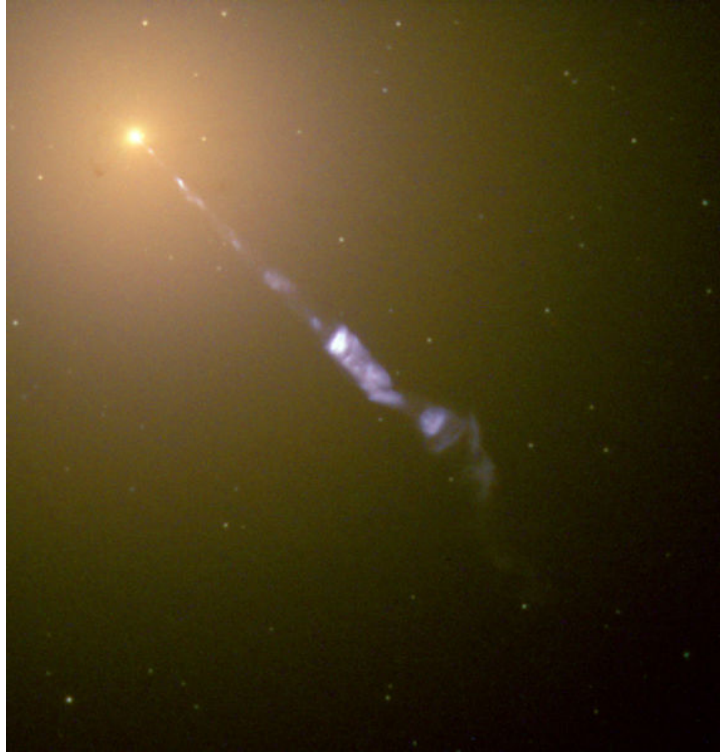
Figure 1.4: The radio galaxy M87 showing the one-sided jet, as seen by the Wide Field Planetary Camera 2 on the Hubble Space Telescope.
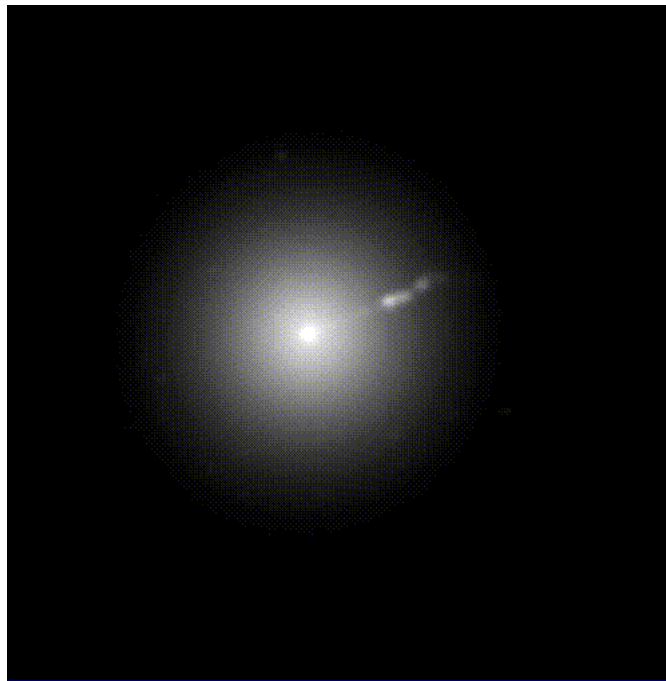
Figure 1.5: The M87 jet and host galaxy. Image taken at the Kitt Peak 2.1 meter telescope. M87 is 50 million light-years from Earth.

However, all successful models for jet formation employ a large scale magnetic field anchored in the accretion disk and, possibly, the rotating black hole (the hole anchored field is not, however, intrinsic to the black hole). The rotation of the disk and black hole can take an initially poloidal field and produce a magnetic "coil". In generic terms, it is postulated that the unwinding of the coil acts to gradually accelerate the jet matter to high velocities, and the magnetic tension forces within the magnetic coil act to collimate the jet flow.

1.2.1 From stellar mass to supermassive black holes

The black hole accretion disk picture applies on a range of scales starting from stellar mass systems, such as Cygnus X-1, to the supermassive black hole systems described above. AGN with powerful jets are referred to as radio-loud because of the prodigious amounts of radio emission from the jets. Stellar mass accreting black holes are thought to display the same physics as their larger AGN counterparts, albeit with shorter characteristic timescales and lower powers. In these stellar mass systems, the accreting matter originates from a companion star (Fig.1.6).

Stellar mass black holes are seen to undergo transitions between well defined states (characterized, principally, by their X-ray spectrum) that are believed to be driven by changes in the rate at which matter is accreted. During the so-called low/hard state, these systems display radio-emitting jets that appear to be scaled down versions of jets from radio-loud AGN (Fender & Belloni 2004). During this state, the X-ray spectrum suggests that the accretion disk is a geometrically-thick, optically-thin advection dominated accretion flow (ADAF), a mode of accretion that is only possible when the accretion rate is much smaller than that needed to produce the Eddington luminosity. However, once the stellar-mass black hole systems make the transition to the so-called high/soft state, which is believed to correspond to a more rapidly accreting geometrically-thin disk, jet activity
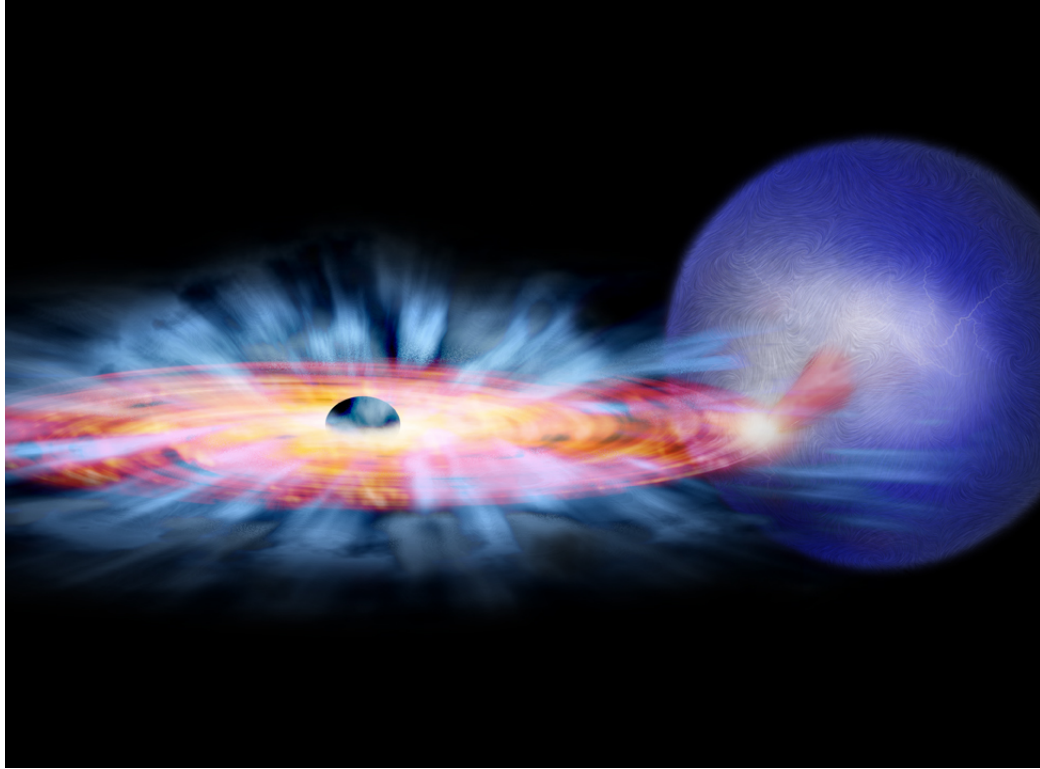
Figure 1.6: Artist sketch of a companion donor star providing material for the accretion disk of a stellar-mass black hole

appears to cease. During the actual transition itself, very powerful relativistic ejections are sometimes seen (Fender & Belloni 2004). Once the accretion rate declines again, the system makes a transition back to the low/hard state and the jet activity resumes. These transitions must be providing important clues about the physics underlying jet formation, and can be observed in stellar-mass black holes on timescales of days to weeks. Since all characteristic timescales scale linearly with black hole mass, the same processes in AGN will take millions of years and thus cannot be observed on a human timescale.

1.2.2   Theoretical issues

Although the magnetic acceleration and collimation model is becoming increasingly favored, it is mostly as a result of the exclusion of other possible mechanisms. It has been shown that both thermal and radiative acceleration models are self-limiting and thus fail to produce the relativistic outflows observed (Phinney, 1982). The basic uncertainty in magnetic jet models arises from the fact that there are currently major holes in our understanding of how energy is transferred from the magnetic field to plasma, a topic vigorously pursued in current plasma physics research. Despite these holes in our knowledge, two magnetic jet models have taken center stage. The first involves large scale field threading the accretion disk with a field geometry favoring loading of field by disk plasma (Blandford & Payne, 1982). The rotation of the disk leads to a centrifugally driven outflow of mass resulting from plasma on field lines experiencing greater centrifugal force than inward gravitational attraction. However, it is unclear whether a Blandford-Payne disk wind can produce the highly relativistic jets observed. In contrast to this kinetic outflow mechanism, another magnetically based method for black hole systems involves direct production of Poynting flux (Blandford & Znajek, 1977). This mechanism extracts the rotational energy of the black hole via field lines threading the event horizon connected to distant regions. The field structure connecting the horizon with distant regions gets twisted as a consequence of the hole's rotation, producing torsional Alfven waves propagating outward in an attempt to establish rotational equilibrium. Plasma close to the horizon (within the ergosphere) is placed onto negative energy orbits allowing the production of Poynting flux carrying the rotational energy of the hole to infinity. It is unclear precisely how and when the Poynting flux jet is transformed into a matter-dominated jet. The greatest uncertainties associated with the application of the Blandford-Znajek (hereafter BZ) mechanism to real systems are the spin rates of supermassive black holes in

radio-loud AGN, and the strength/geometry of the magnetic field threading the black hole event horizon.

1.2.3 Outline of thesis

In Chapter 2 we begin the exploration of the interaction between black holes and magnetic fields by considering magnetic coupling between the black hole itself (or plasma near the horizon), with the inner edge of a radiatively efficient accretion disk. This coupling has the effect of adding energy and angular momentum to the inner accretion disk; the source of this energy and angular momentum is either the accretion flow within the radius of marginal stability, or the black hole rotation itself. In order to appreciate the context of our treatment of this coupling, one needs some sense of how viscosity transports angular momentum outward in accretion disks, allowing the plasma to flow inward. As we discussed previously, it is now recognized that the presence of magnetic fields in accretion disks is vital to the accretion process. Plasma closer to the central accreting object can transfer its angular momentum to plasma further out due to correlations in the MHD turbulence. However, studies have indicated that an effective kinematic viscosity of the kind characterizing the Shakura & Sunyaev (1973) disk model can capture essential properties of the more realistic MHD turbulence based angular momentum transport mechanism. Within the context of these viscous disk models, the magnetic coupling between the black hole or plasma near the hole with the inner disk is first tackled in the Newtonian regime where the disk structure equations are appropriately modified to take the coupling into account. We then generalize to the relativistic regime where the effect of the coupling is studied in Schwarzschild spacetime as well as in the $a = 0.998$ limit of the Kerr metric. We characterize the behavior of a disk (and the radial dependence of the dissipation within the disk) that is subjected to a time-variable magnetic coupling. We then show that the so-called "Deep Minimum" state observed in the Seyfert galaxy MCG-

6-15-30 can be plausibly explained as the result of a time variable inner edge coupling between the rotating black hole and the accretion disk.

In Chapter 3 we continue the exploration of the interaction between black holes and magnetic fields by addressing the issue of how a large scale poloidal magnetic field is dragged to the black hole by the accretion flow. In order for the BZ process to explain the powerful jets observed, the black hole-threading field must be large. As we will explain in greater detail in Chapter 3, MHD studies of accretion disks throughout the 1990's have uncovered a characteristic difficulty in these systems that appears to limit their ability to bring strong fields toward the black hole. Basically, turbulent MHD accretion disks appear to be strongly diffusive to large scale poloidal fields. Thus, it has been argued that field-line diffusion acts to make the horizon-threading magnetic field approximately equal in strength to the large-scale magnetic field of the accretion disk. Since magnetic pressure in the disk must be an order of magnitude less than the total (gas+radiation+magnetic) pressure in order for the MRI (and hence MHD turbulence) not to be quenched (Balbus & Hawley 1991), it has been argued that the horizon-threading magnetic field is too weak to produce the observed powerful jets (Ghosh & Abrahmowicz 1997). What such studies have neglected, though, is the dynamical role of the plunging region of black hole accretion disks within the radius of marginal stability, which we claim to be fundamental in its ability to drag strong magnetic fields to the black hole. We show that the plunging region can enhance the black hole-threading field by one or more orders of magnitude compared to the studies that ignored it. In the process, we also uncover a strong dependence of the hole-threading field magnitude on the disk thickness and effective magnetic Prandtl number of the turbulent disk flow.

In Chapter 4 we extend the Newtonian treatment of Chapter 3 to the relativistic regime in Kerr metric. The main goal is to study the spin dependence of the strength of the horizon-threading magnetic field. We find that the horizon threading magnetic field is

15

stronger for lower spin systems and that the BZ mechanism produces maximum power for intermediate values of spin, in opposition to conventional wisdom which has it that strong jet systems have the highest black hole spin. We also confirm that the Newtonian treatment of Chapter 3 is a valid approximation in the low spin limit. Finally we show that our model explains some curious aspects of the recently observed correlation between accretion rate and jet power in a sample of nearby radio-loud AGN in elliptical galaxies (Allen et al. 2006)

Chapter 2

Torqued Accretion Disks Around Black Holes

Even before the observational evidence for black hole accretion disks became compelling, the basic theory of such disks had been extensively developed. Building upon the non-relativistic theory of Shakura & Sunyaev (1973), Novikov & Thorne (1974) and Page & Thorne (1974) developed the "standard" model of a geometrically-thin, radiatively-efficient, steady-state, viscous accretion disk around an isolated Kerr black hole. In addition to the assumptions already listed, it is typically assumed that the viscous torque operating within the disk becomes zero at the radius of marginal stability, $r = r_{\mathrm{ms}}$. Physically, this was justified by assuming that the accretion flow would pass through a sonic point close to $r = r_{\mathrm{ms}}$ and hence fall ballistically (i.e., "plunge") into the black hole.

Even while setting up this boundary condition, Page & Thorne (1974) noted that magnetic fields may allow this zero-torque boundary condition (ZTBC) to be violated. Given the modern viewpoint of accretion disks, that the very "viscosity" driving accretion is due to magnetohydrodynamic (MHD) turbulence, the idea that the ZTBC can be violated has been revived by recent theoretical work, starting with Gammie (1999) and Krolik

17

(1999a). In independent treatments, these authors show that significant energy and angular momentum can be extracted from matter within the radius of marginal stability via magnetic connections with the main body of the accretion disk. Agol & Krolik (2000) have performed the formal extension of the standard stationary Novikov & Thorne accretion disk model to include a torque at $r = r_{\mathrm{ms}}$ and show that the extra dissipation associated with this torque produces a very centrally concentrated dissipation profile. As shown by Gammie (1999), Agol & Krolik (2000), and Li (2002), this process can lead to an extraction (and subsequent dissipation) of spin energy and angular momentum from the rotating black hole by the accretion disk. In these cases, the magnetic forces might be capable of placing the innermost part of the flow on negative energy orbits, allowing a Penrose process to be realized. A second mechanism by which the central accretion disk can be torqued is via a direct magnetic connection between the inner accretion disk and the (rotating) event horizon of the black hole. In this case, as long as the angular velocity of the event horizon exceeds that of the inner disk, energy and angular momentum of the spinning black hole can be extracted via the Blandford-Znajek mechanism (Blandford & Znajek 1977). We note that field lines that directly connect the rotating event horizon with the body of the accretion disk (Figure 2.1) through the plunging region *are* seen in recent General Relativistic MHD simulations of black hole accretion (e.g., Hirose et al. 2004).

Interest in these torqued relativistic disks has received a boost from recent X-ray observations. The X-ray spectra of many AGN (and, indeed, Galactic Black Hole Candidates) reveal the signatures of "X-ray reflection" from optically-thick matter. In some cases, examination of these features allows us to detect strong Doppler and gravitational shifts indicative of circular motion close to a black hole (Fabian et al. 1989; Tanaka et al. 1995; Fabian et al. 2000; Reynolds & Nowak 2003). In these cases, the observed range of Doppler and gravitational shifts can be used to map the X-ray emission/irradiation across the surface of the accretion disk. The *XMM-Newton* satellite is particularly well suited to
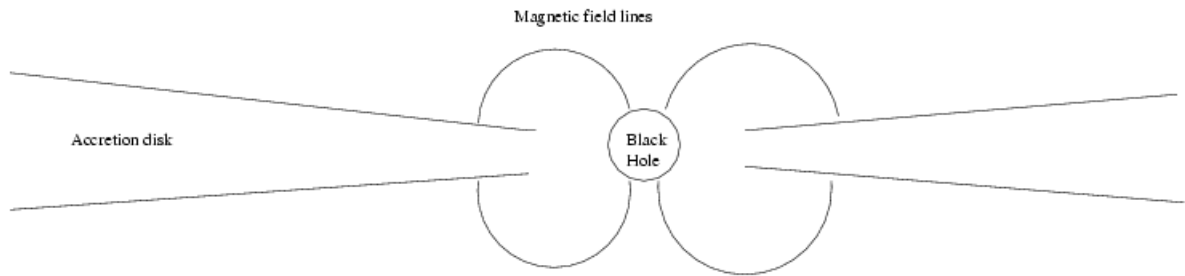
Figure 2.1: Torqued accretion disk caused by magnetic field lines connecting the black hole event horizon with the accretion disk. The system that we study in this chapter involves either field lines connecting the disk with the black hole as shown above, or field lines connecting plasma near the black hole with the disk.

the study of these features due to its combination of good spectral resolution and large collecting area. Using *XMM-Newton*, Wilms et al.(2001) and Reynolds et al.(2004) studied the Seyfert-1 galaxy MCG–6-30-15 in its peculiar "Deep Minimum State" first discovered by ASCA (Iwasawa et al. 1996). Confirming the principal result of Iwasawa et al. (1996), the X-ray reflection features were found to be extremely broad (Fig. 2.2). The degree of gravitational redshifting required the majority of the X-ray emission to emerge within a radius of $r \sim 2GM/c^2$ from a near-extremal Kerr black hole (i.e., a black hole with a spin parameter of $a = 0.998$). As explicitly shown in Reynolds et al. (2004), it is very problematic to explain these data within the framework of the standard accretion disk model. Fabian & Vaughan (2003) and Miniutti & Fabian (2004) suggest that gravitational focusing of the primary continuum X-rays might produce such a centrally-concentrated emissivity profile. Alternatively, Reynolds et al. (2004) have shown that a torqued disk can readily explain the Deep Minimum spectrum provided the source is assumed to be in a torque-dominated state whereby the power associated with the innermost torque is
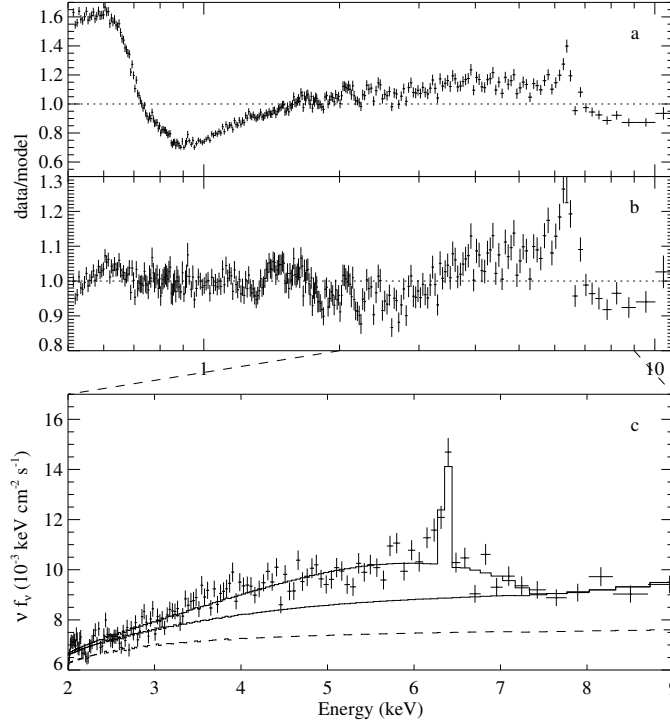
Figure 2.2: XMM-Newton data for the "Deep Minimum State" of the AGN MCG-6-30-15. (a) Ratio between data and model from fitting a power law to the 0.5-11 keV data. (b) Ratio from fitting a power law and the empirical warm absorber model; remaining residues are interpreted as an extremely broadened iron emission line from the central accretion disk. (c) Deconvoluted spectrum of the Fe Kα band, showing the accretion disk model and the continuum with and without (dashed) the reflection component for a model with reflection from an ionized disk. From Wilms et al. (2001).

instantaneously dominating the accretion power (Fig. 2.3). In other words, the X-ray data suggest that during this Deep Minimum state of MCG–6-30-15 the power derived from the black hole spin greatly exceeds that derived from accretion.

Of course, this state of affairs cannot last forever or else the central black hole in MCG–6-30-15 would spin down to a point where it could no longer provide this power. At some point in its history, the system must be in an accretion-dominated phase in which the black hole is spun up. However, even in its spin-dominated state, the spin-down timescale of the central black hole is of the order of 100 million years or more. Thus we could envisage a situation in which the system shines via a quasi-steady-state, spin-dominated accretion disk.
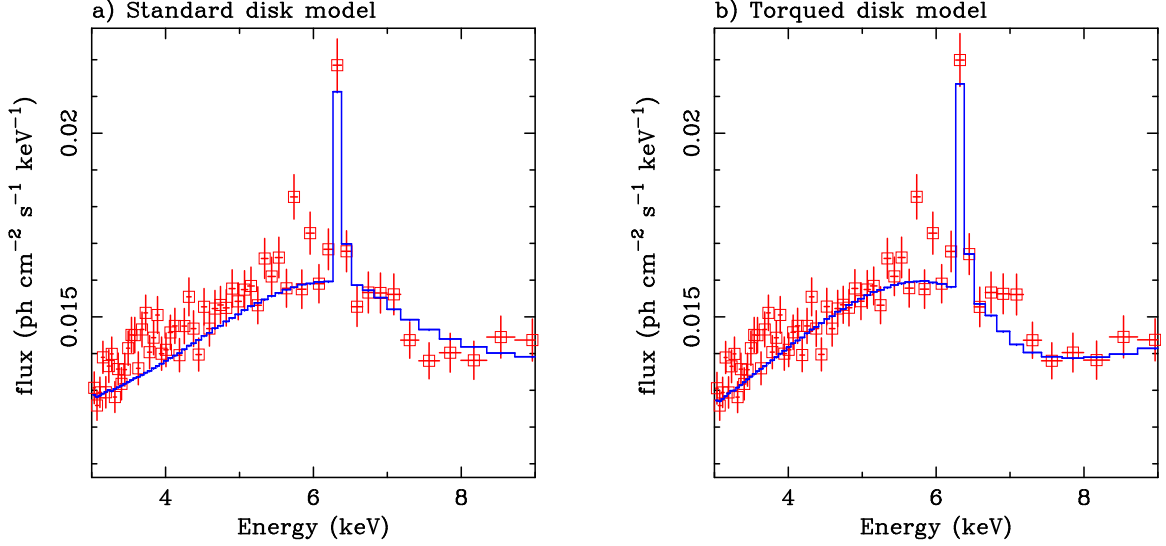
Figure 2.3: Broad iron line fit assuming that the line emission tracks the underlying disk dissipation of (a) a standard (Novikov & Thorne model) accretion disk and (b) a stationary torqued disk model (Agol & Krolik, 2000). From Reynolds, Brenneman & Garofalo (2005).

There are hints, though, that accretion disks may switch between spin-dominated and accretion-dominated on much shorter timescales. In its normal spectral state, the X-ray reflection features in MCG–6-30-15 are much less centrally concentrated than in the Deep Minimum State, suggesting that the normal state might be accretion-dominated. It is also important to note that this system can switch between its normal state and the Deep Minimum State in as little as 5–10 ksec (Iwasawa et al. 1996), which corresponds to only a few dynamical timescales of the inner accretion disk. On the theoretical side, rapid (dynamical timescale) changes in these inner disk torques were noted in the MHD simulations of Reynolds & Armitage (2001). Thus, it is of interest to consider the physics of an accretion disk that undergoes a rapid torquing event. That is the prime motivation for this Chapter.

In Section 2.1 we will begin our study of sporadically torqued accretion disks by investigating an analytic solution for a torqued Newtonian disk. In Section 2.2, we generalize to the fully relativistic equations and obtain numerical solutions. In Section 2.3, we relate

our results with the observed properties of the "Deep Minimum State" of MCG–6-30-15, and consequently discuss the effect that a torquing event may have on the physics of the X-ray emitting disk corona. In particular, we suggest that the enhanced Returning Radiation associated with a torquing event might suppress the 0.5–10 keV coronal emission in all but the inner portion of the disk. Section 4.4 summarizes our main conclusions.

2.1 An analytic "toy" model of a time-dependent non-relativistic torqued disk

We begin our investigation of sporadically torqued disks via the study of a simple case that lends itself to a straightforward analytic solution. We shall construct a non-relativistic model of a radiatively-efficient accretion disk following the usual approach of Pringle (1981). We shall assume that the accretion disk is axisymmetric, geometrically-thin and in Keplerian motion about a point-mass M. Using a cylindrical polar coordinate system (r, ϕ, z) with the axis passing through the central mass normal to the disk plane, we shall denote the surface density of the disk by $\Sigma(r,t)$, the angular velocity of the disk about M as $\Omega(r)$ and the radial velocity of the disk material as $v_r(r,t)$. The equations that determine the structure of the thin disk assuming radiative efficiency are mass and angular momentum conservation,

$$r \frac{\partial \Sigma}{\partial t} + \frac{\partial (r v_r \Sigma)}{\partial r} = 0, \tag{2.1}$$

$$r \frac{\partial (\Sigma r^2 \Omega)}{\partial t} + \frac{\partial (r \Sigma v_r r^2 \Omega)}{\partial r} = \frac{1}{2\pi} \frac{\partial G}{\partial r}, \tag{2.2}$$

respectively, where $G(r,t)$ is the torque exerted by the disk *outside* of radius r on the disk *inside* of that radius.

In standard disk models, the torque G is the integrated value of the only stress tensor component ($S_{r\phi}$) that survives the condition of axisymmetry and geometric-thinness.

From Krolik (1999b) we have,

$$G = \int r S_{r\phi} \, dz \int r \, d\phi = 2\pi r^3 \nu \Sigma \frac{\partial \Omega}{\partial r},$$

(2.3)

where we have introduced an "effective kinematic viscosity", ν. To generalize these models to the case of an externally imposed torque, we set

$$G = 2\pi r^3 \nu \Sigma \frac{\partial \Omega}{\partial r} + G_T$$

(2.4)

where G_T is the externally imposed torque (due to the magnetic couple to the black hole or plunging region) that is in general a function of radius and time. Combining eqns. 2.1, 2.2 and 2.4, and specializing to a Keplerian rotation curve,

$$\Omega = \left(\frac{GM}{r^3} \right)^{1/2},$$

(2.5)

we get the usual diffusion equation for surface density modified for the effects of the external torque,

$$\frac{\partial \Sigma}{\partial t} = \frac{3}{r} \frac{\partial}{\partial r} \left[r^{1/2} \frac{\partial (\nu \Sigma r^{1/2})}{\partial r} \right] - \frac{1}{r\pi (GM)^{1/2}} \frac{\partial}{\partial r} \left(r^{1/2} \frac{\partial G_T}{\partial r} \right).$$

(2.6)

For the rest of this chapter, we shall work in units where $GM = 1$. Changing variables to $x = r^{1/2}$ and $\psi = \nu \Sigma x$ and assuming that ν has no explicit time dependence, we get

$$\frac{\partial \psi}{\partial t} = \frac{3\nu}{4x^2} \frac{\partial^2}{\partial x^2} \left(\psi - \frac{G_T}{3\pi} \right).$$

(2.7)

We now consider a particular torquing event. Suppose that the disk suffers no external torques for the period $t < 0$. Then, at $t = 0$, we engage an external torque (possibly resulting from a newly formed magnetic connection to the plunging region or spinning event horizon) that deposits angular momentum into a narrow annulus at $r = r_0$. If the rate at which angular momentum is being deposited is β, we have

$$\frac{\partial G_T}{\partial r} = \beta \delta(r - r_0) \Theta(t),$$

(2.8)

23

giving

$$G_T(r,t) = \beta \Theta(r - r_0)\Theta(t), \tag{2.9}$$

where Θ is the Heaviside step function. At this point, we specialize to a particular viscosity law. While we lose generality, this will enable us to construct a readily soluble system that can be used to study the general qualitative behavior of torqued disks. We set $\nu = kr$ for mathematical convenience. We can now rewrite eqn. 2.7 as

$$\frac{\partial \xi}{\partial t} = \frac{3k}{4}\left[\frac{\partial^2 \xi}{\partial x^2}\right] - \frac{\beta}{3\pi}\Theta(x - x_0)\delta(t), \tag{2.10}$$

where

$$\xi = \psi - \frac{\beta}{3\pi}\Theta(x - x_0)\Theta(t), \tag{2.11}$$

and the delta-function in time results from the time-derivative of the $\Theta(t)$ term.

Suppose that the disk is in the untorqued steady state at $t < 0$. From eqn. 2.10, one can easily see that such a steady state is given by,

$$\xi_{ss} = \psi = A(x - x_i) \qquad (t < 0), \tag{2.12}$$

where A is a normalization constant and $r_i \equiv x_i^2$ is the inner edge of the untorqued disk defined as the location where the "viscous" torques vanish. Examination of eqn. 2.10 shows that the time-dependent behavior of the torqued disk at times $t > 0$ is given by the simple diffusion equation,

$$\frac{\partial \xi}{\partial t} = \frac{3k}{4}\frac{\partial^2 \xi}{\partial x^2}, \tag{2.13}$$

with an initial condition set by integrating through the delta-function in time, $\xi(x, t = 0) = \xi_{ss} - \beta\Theta(x - x_0)/3\pi$. The appropriate boundary condition is $\xi \to \xi_{ss}$ as $t \to \infty$. Standard methods (i.e., separation of variables) give the following solution:

$$\xi(x,t) = \xi_{ss}(x) + \frac{\beta}{3\pi^2}\int_0^\infty \frac{1}{\lambda}[\sin\lambda x_0 \cos\lambda x - (\cos\lambda x_0 + 1)\sin\lambda x]\exp\left[-3k\lambda^2 t/4\right]\,d\lambda. \tag{2.14}$$

24

With this solution, we can compute the surface density of the disk at any given radius and time. Armed with the surface density, we can then compute all other quantities of interest including the viscous dissipation rate per unit surface area of the disk:

$$D(r) = \frac{\nu \Sigma r^2}{2} \Omega'^2, \tag{2.15}$$

where $\Omega' = d\Omega/dr$. Plots of the radial dependence of $\Sigma(r)$ and $D(r)$ for various times are shown in Figures 2.4-2.8 and 2.10-2.14. Also shown in Figure 2.9 and Figure 2.15 is the time dependence of the total viscous dissipation obtained by integrating $D(r)$ across the whole disk (i.e. luminosity). We can see that the response of the disk to the onset of an external torque can be separated into two phases. In the first phase, the accretion flow is "dammed" at $r = r_0$ due to the inability of the accretion flow to transport the angular momentum deposited by the external torque. This leads to a build-up of mass (i.e., an increase in the surface density) in the region $r > r_0$. Concurrently, matter in the region $r < r_0$ continues to accrete thereby partially draining away the surface density. The inevitable result is a growing discontinuity in the surface density at $r = r_0$. The angular momentum transport associated with this discontinuity grows until mass can, once again, flow inwards across this radius. One then enters the second phase of evolution, whereby the surface density in the region $r < r_0$ is replenished back to its original level while the surface density discontinuity is maintained at approximately a constant level. Eventually, one achieves the torqued steady-state solution (e.g., Agol & Krolik 2000). The two sets of figures (2.4-2.9 and 2.10-2.15) are for an external torque at $r = 4$ and one closer to the inner edge at $r = 2$, respectively. Note how, for a given injection rate of angular momentum, the effect on the disk structure is much more dramatic for smaller radius.

Since our disks are assumed to be radiatively-efficient, the instantaneous total luminosity of the accretion disk can be formally decomposed into two components, one due to the decrease in gravitational potential energy of the accreting gas, and a second due to
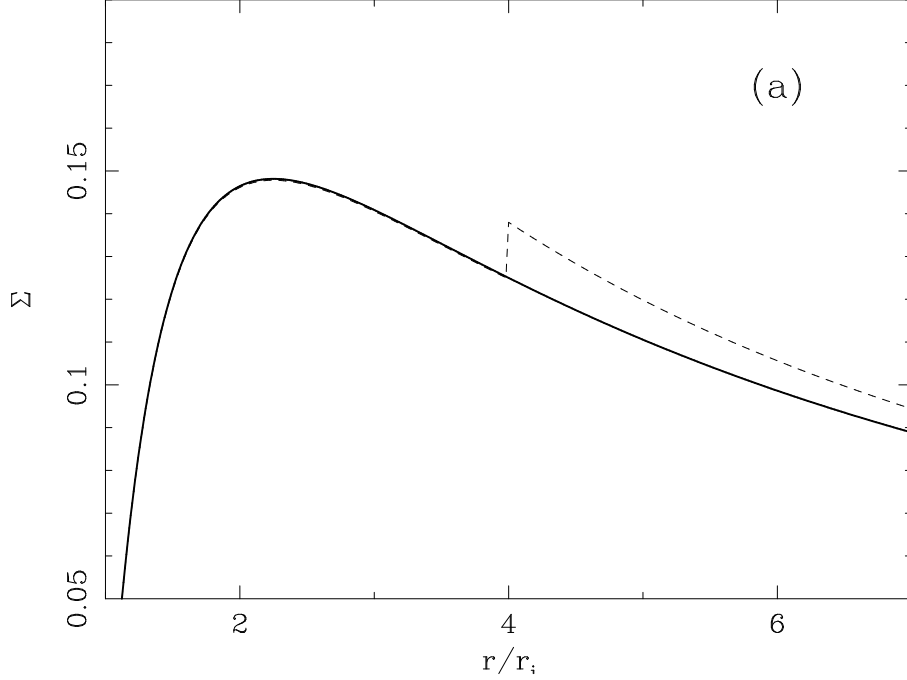
Figure 2.4: Evolution of our "toy" model disk with a torque acting at $r = 4$. Figure shows the initial state of the surface density profile for the non torqued disk (solid line) and the resulting final torqued steady-state (dashed line).

the work done by the external torque, i.e.,

$$L = 2 \int 2\pi r D(r) dr = \frac{1}{2} \int \frac{GM\dot{M}}{r^2} dr + \int \Omega \frac{\partial G_T}{\partial r} dr. \qquad (2.16)$$

As can be seen from Fig. 2.9 and Fig. 2.15, the luminosity dips before climbing up to a new elevated level that includes the work done by the external torque as well as the accretion energy. The temporary dip in luminosity is due to the damming of the accretion flow in the early evolution of the torquing event.

Now that we have explored a torquing event via the analytical solution of an extremely simplified accretion disk model, we move on to somewhat more realistic models. In the next section, we present a semi-analytic analysis of a geometrically-thin general relativistic accretion disk.

26
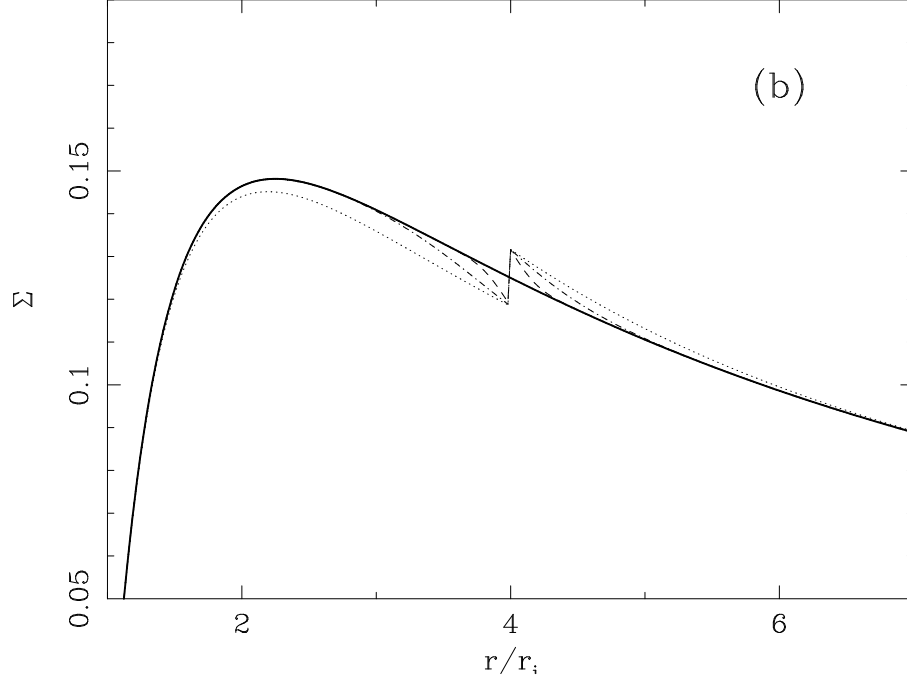
Figure 2.5: Early evolution of our "toy" non-relativistic model disk with a torque acting at $r = 4$. Shown are four times in the early evolution of the surface density profile (solid-line:$t = 0$ the untorqued steady-state, dashed-line:$t = 10^{-3}$, dot-dashed-line:$t = 10^{-2}$, dotted-line:$t = 10^{-1}$; we use units such that $k = 1$ which corresponds to scaling with respect to the viscous timescale of the inner disk). Notice how the initial evolution is such that density drops inward of the torque location and increases outward of it due to the "damming" of the accretion flow.

2.2   Relativistic torqued accretion disks

Relativity produces two complications to the analysis. Firstly, the equations governing the structure of the accretion disk are rather more complex and drive us to use numerical rather than analytic techniques. Secondly, the relationship between the emitted and observed fluxes becomes non-trivial, with gravitational light bending, relativistic aberration/beaming, and Doppler/gravitational redshifting all becoming important. We shall deal with these issues in turn.

The time-dependent equations describing the structure of a geometrically-thin accretion disk in the $\theta = \pi/2$ plane of a Kerr spacetime are given in Boyer-Lindquist coor-
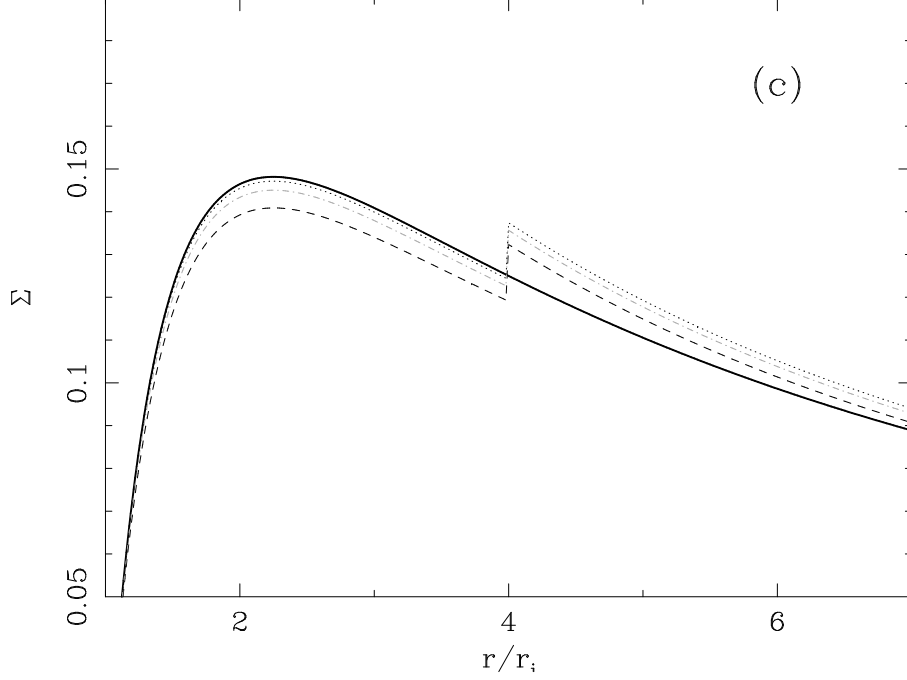
Figure 2.6: Late evolution of our "toy" non-relativistic model disk with a torque acting at $r = 4$. The subsequent late evolution towards the torqued steady-state (solid-line:$t = 0$, or untorqued steady-state, dashed-line:$t = 1$, dot-dashed-line:$t = 10$, dotted-line:$t = 100$).

dinates (t, R, θ, ϕ) by Eardley & Lightman (1974). Taking $\Sigma(R)$ to be the proper surface density of the disk (i.e., the surface density measured by a local observer moving with the fluid), the disk evolution is described by

$$\frac{\partial \Sigma}{\partial t} = \frac{C^{1/2}}{\mathcal{B}R} \frac{\partial}{\partial R} \left[\frac{\Gamma}{\frac{\partial L^{\dagger}}{\partial R}} \frac{\partial}{\partial R} (\mathcal{W}R^2 \mathcal{D}) \right], \tag{2.17}$$

where,

$$\mathcal{B} = \left(1 + \frac{aM^{1/2}}{R^{3/2}} \right), \tag{2.18}$$

$$\mathcal{C} = \left(1 - \frac{3M}{R} + \frac{2aM^{1/2}}{R^{3/2}} \right), \tag{2.19}$$

$$\mathcal{D} = \left(1 - \frac{2M}{R} + \frac{a^2}{R^2} \right), \tag{2.20}$$

$$\Gamma = \frac{\mathcal{B}}{C^{1/2}}, \tag{2.21}$$

$$L^{\dagger} = M^{1/2}R^{1/2} \left(1 - \frac{2aM^{3/2}}{R^{3/2}} + \frac{a^2M^2}{R^2} \right). \tag{2.22}$$

28
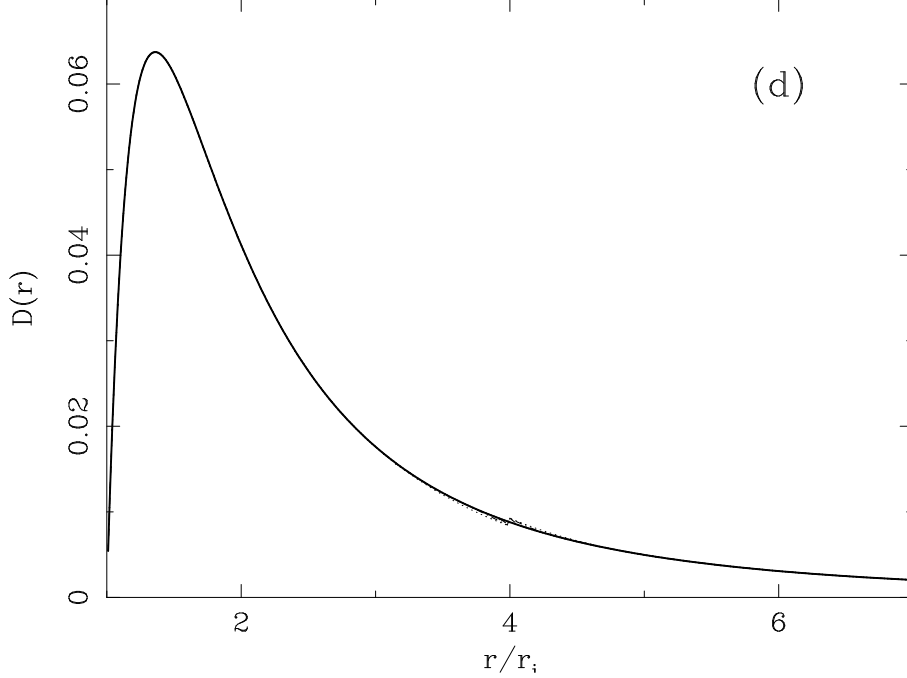
Figure 2.7: Early evolution of our "toy" model disk with a torque acting at $r = 4$. The dissipation profiles $D(r)$ in the early stages of the evolution with the type of line and time corresponding to those of figure (b).

Here, a is the dimensionless spin parameter of the black hole (denoted as a_* by Eardley & Lightman 1975) and $L^\dagger$ is the specific angular momentum of the fluid for prograde orbits. The local $r\phi$ shear in this flow is $\sigma = -3\Omega\mathcal{C}^{-1}\mathcal{D}$, where the angular velocity in the comoving frame is $\Omega = (M/r^3)^{1/2}$. Thus, guided by the non-relativistic prescription, we set the vertically-integrated $r\phi$ component of the stress tensor in the absence of an external torque to be

$$W = -\nu\sigma\Sigma = \frac{3}{2}\nu\Sigma\frac{M^{1/2}}{R^{3/2}}\frac{\mathcal{D}}{\mathcal{C}}, \tag{2.23}$$

where ν is the same effective viscosity that appeared in the non-relativistic expressions. Noting that the total *torque* is given by $G = 2\pi W R^2 \mathcal{D}$, we see that the appropriate relativistic diffusion equation describing a sporadically torqued disk (i.e., the counterpart to eqn. 2.6) is

$$\frac{\partial\Sigma}{\partial t} = \frac{\mathcal{C}^{1/2}}{2\pi\mathcal{B}R}\frac{\partial}{\partial R}\left[\frac{\Gamma}{\frac{\partial L^\dagger}{\partial R}}\frac{\partial}{\partial R}\left(\frac{3\mathcal{D}^2}{2\mathcal{C}}\nu\Sigma M^{1/2}R^{1/2} - \frac{G_T}{2\pi}\right)\right]. \tag{2.24}$$

It is straightforward to verify that eqn. 2.24 reduces to eqn. 2.6 in the non-relativistic

29

Figure 2.8: Late evolution of our "toy" model disk with a torque acting at $r = 4$. The dissipation profiles $D(r)$ in the late stages of the evolution toward steady-state with the type of line and time corresponding to those of figure (c).

limit (i.e., $\mathcal{B}, \mathcal{C}, \mathcal{D} \to 1; L^{\dagger} \to (MR)^{1/2}$). The complications introduced by the relativistic factors render this equation intractable to elementary analytic solution methods. Thus, we use a simple explicit scheme to numerically solve this diffusion equation following the treatment of Press et al. (1992), using a finite difference scheme to evaluate first and second spatial derivatives. Figures 2.16-2.21 and 2.22-2.27 show the temporal behavior of an accretion disk around Schwarzschild ($a = 0$) and near maximal Kerr ($a = 0.998$) black holes respectively. To facilitate comparison with the non-relativistic case, we have chosen the same viscosity law, $\nu = kR$ (i.e. ν scales with the radial Boyer-Lindquist coordinate and not the proper distance). As in the Newtonian case, this prescription does not change the results qualitatively. Note that the behavior is similar to that found in the non-relativistic model. The two phases of evolution, the damming phase and the replenishing phase, are reproduced.

The differences are mostly due to the fact that in the relativistic regime there are
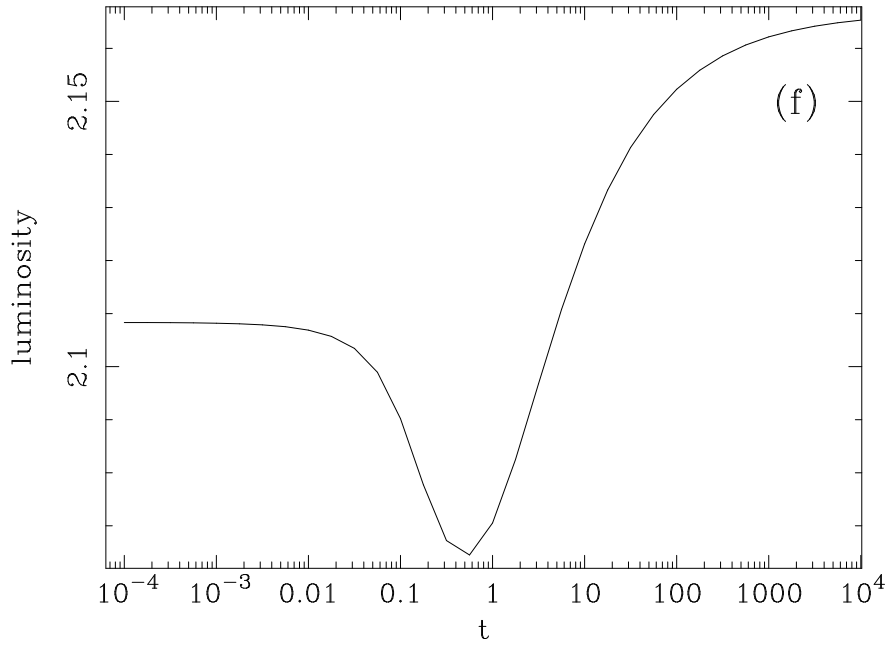
Figure 2.9: Evolution of our "toy" model disk with a torque acting at $r = 4$. The luminosity profile obtained by integrating the dissipation profile over the disk surface. The final steady-state torqued luminosity profile is enhanced with respect to the non-torqued steady-state profile due to work done by the torque.
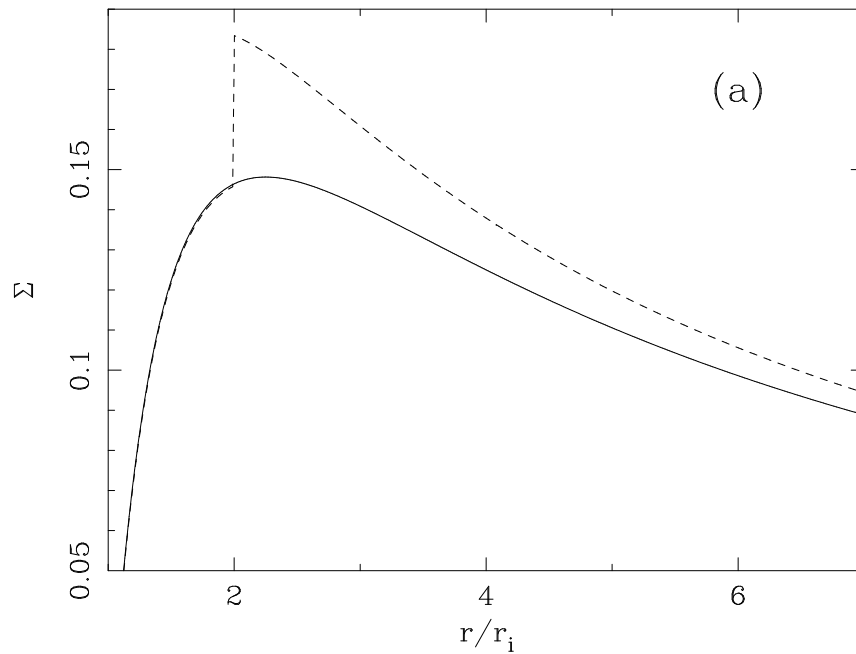
Figure 2.10: Early evolution of our "toy" model disk with a torque acting at $r = 2$. The initial state of the surface density profile for the non torqued disk (solid line) and the resulting torqued steady-state (dashed line).
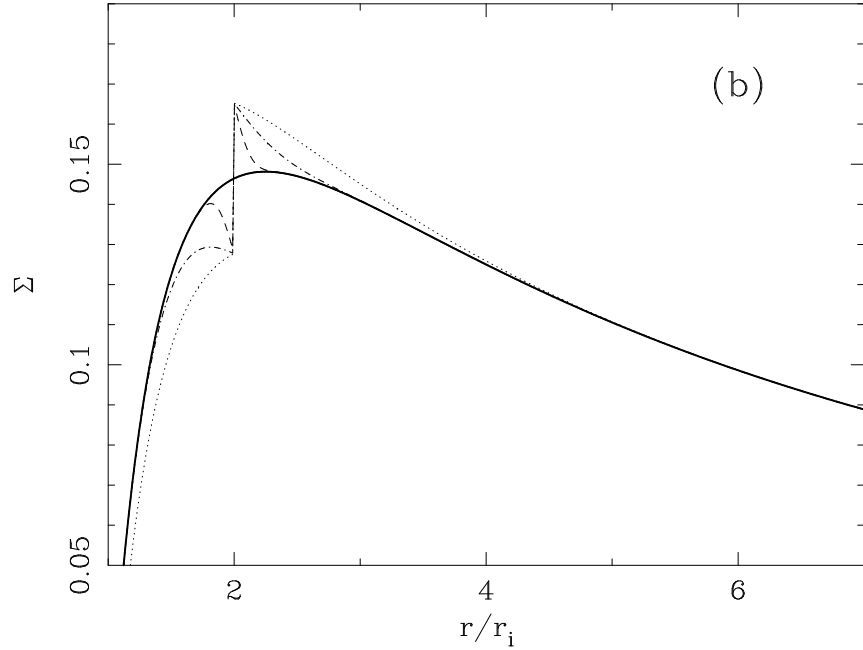
Figure 2.11: Evolution of our "toy" model disk with a torque acting at $r = 2$. Four times in the early evolution of the surface density profile (solid-line:$t = 0$, dashed-line:$t = 10^{-3}$, dot-dashed-line:$t = 10^{-2}$, dotted-line:$t = 10^{-1}$).
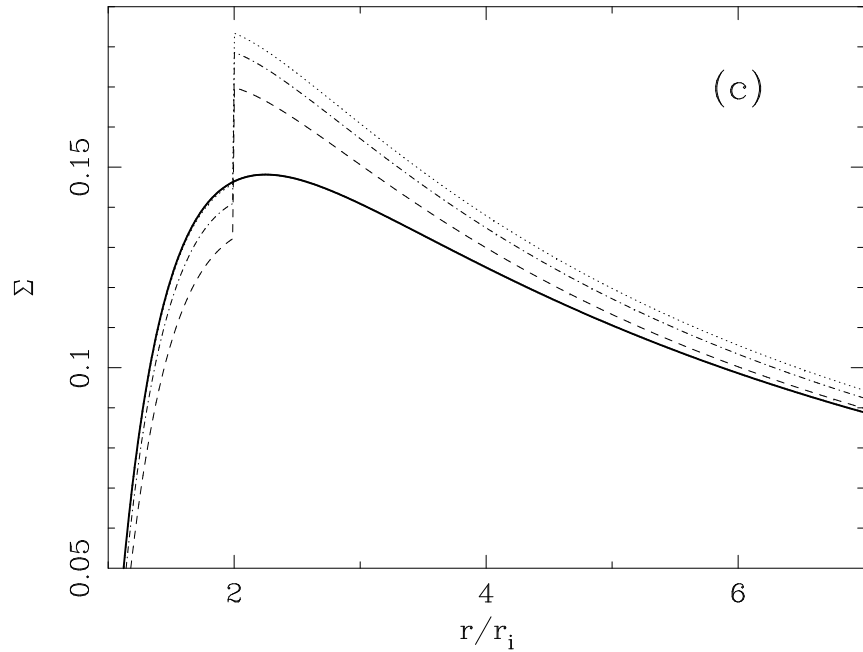
Figure 2.12: Late evolution of our "toy" model disk with a torque acting at $r = 2$ (dashed-line:$t = 1$, dot-dashed-line:$t = 10$, dotted-line:$t = 100$). For reference, the lower solid-line shows the untorqued steady-state disk.

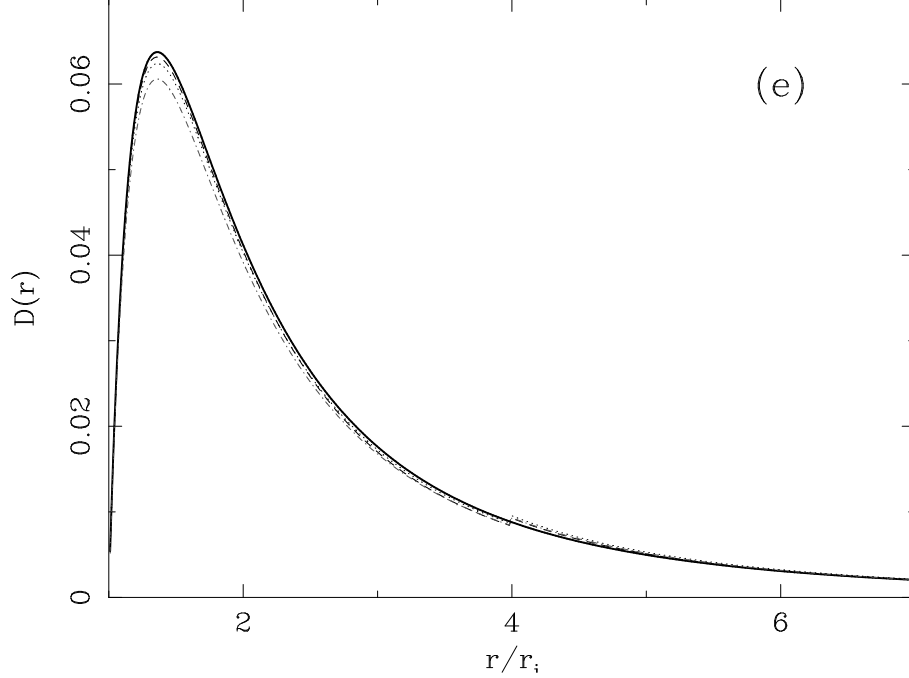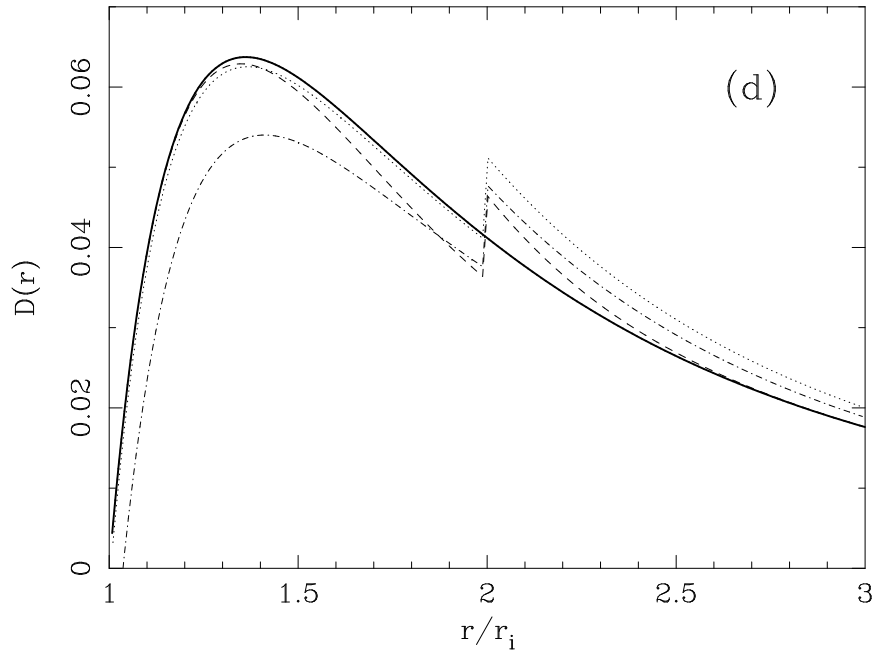Figure 2.13: Evolution of our "toy" model disk with a torque acting at $r = 2$. The dissipation profiles $D(r)$ in the early evolution (with line types and times corresponding to those of Fig. 2.11.
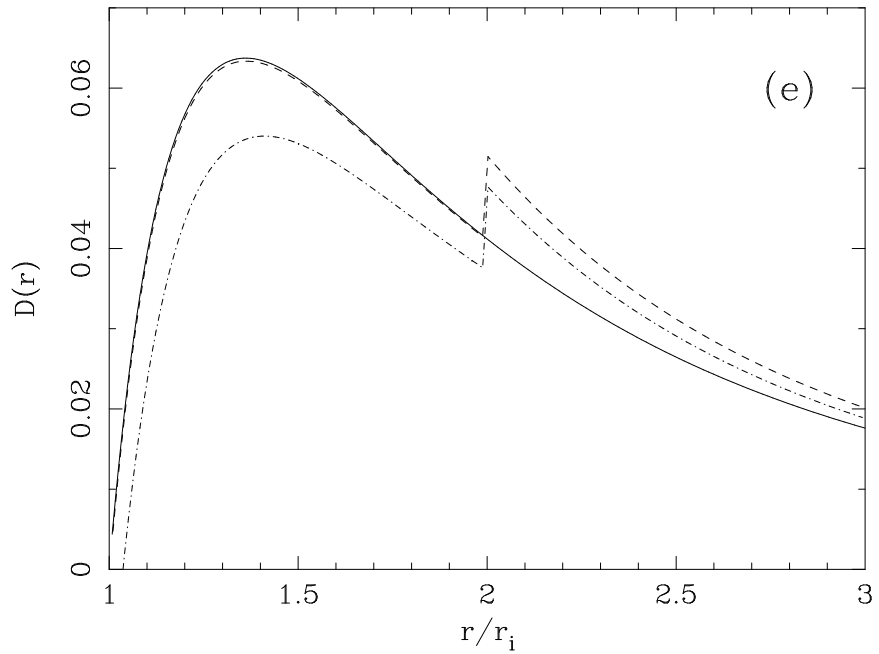
Figure 2.14: Evolution of our "toy" model disk with a torque acting at $r = 2$. Figure shows the dissipation profiles $D(r)$ in the late evolution with times and line-style equal to those of Fig. 2.12.
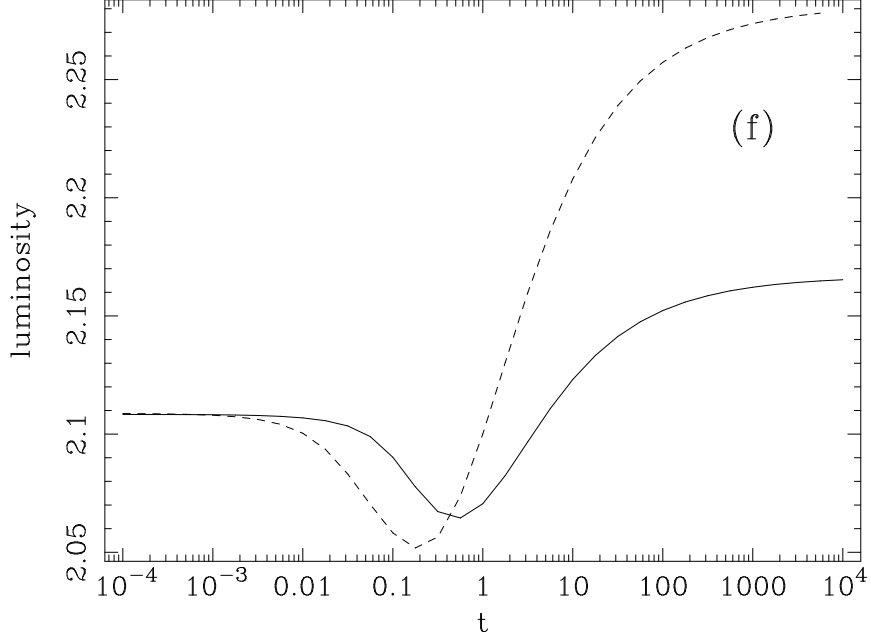
Figure 2.15: Evolution of our "toy" model disk with a torque acting at $r = 2$. The luminosity profile obtained by integrating the dissipation profile over the disk surface for both torques at r=2 (dashed line) and r=4 (solid line).

two natural inner boundaries for the disk at the location of the marginally stable circular orbits. $R = 6M$ for Schwarszchild spacetime and $R = 1.23M$ for the near-maximal Kerr spacetime.

Relating the observed radiative flux to the fundamental disk structure is substantially more complex in the relativistic case due to the complexities of general relativistic photon propagation. For a given value of the stress W, energy conservation gives that the total radiative flux from one side of the disk, measured in the locally orbiting frame, is (Novikov & Thorne 1974),

$$F(R) = \frac{3\mathcal{D}}{4\mathcal{C}}\Omega W. \tag{2.25}$$

Suppose that the corresponding energy-integrated (but angle-dependent) intensity is $I_e(R, \theta)$, where θ is measured from the normal to the disk plane (in the locally orbiting frame of reference). Following Cunningham (1975), an observer at infinity will see an integrated

34

luminosity,

$$L_0 = \int \int 2\pi I_e \Upsilon g^3 (g^* - g^{*2})^{-1/2} dg^* d(\pi R^2) \qquad (2.26)$$

where we have followed the notation of Cunningham (1975) with the exception of Υ; here Υ is the relativistic transfer function that encodes the effect of light bending and results from ray-tracing null-geodesics through the Kerr metric from the disk to the observer. The quantity g is the ratio of observed energy to emitted energy, and g^* is the "relative redshift" defined by,

$$g^* = (g - g_{min})/(g_{max} - g_{min}), \qquad (2.27)$$

where g_{max} and g_{min} are the extremal values of g over the family of geodesics from a given emission radius and a given viewing inclination of the disk. We have used the code of R. Speith (Speith, Riffert & Ruder 1995) to compute Υ and hence perform this integral in order to examine how the observed luminosity changes through the torquing event.

These calculations uncover a fundamental difference between the Newtonian and relativistic cases. In the relativistic case, the observed changes in luminosity are a function of the inclination angle of the observer due to the effects of light bending and relativistic beaming of the disk emission. Figures 2.21 and 2.27 show the temporal behaviour of the observed flux (normalized to the flux for the untorqued disk) for various observing angles for our Schwarzschild and near-extremal Kerr cases, respectively. The final fractional increase in observed flux depends on the beaming pattern of the torque-energized region of the disk compared with that of the untorqued disk. For our Schwarzschild case (Fig. 2.21), one can see that the final fractional increase in observed luminosity depends very weakly on the observing angle, implying that the untorqued disk and the torque-energerized region of the torqued disk have very similar beaming patterns. There is, however, a much more pronounced temporary decrease in observed flux at higher inclinations due to the temporary dimming of the (more highly beamed) inner regions of the disk. For our near-extremal Kerr case, the final fractional increase in observed luminosity

35
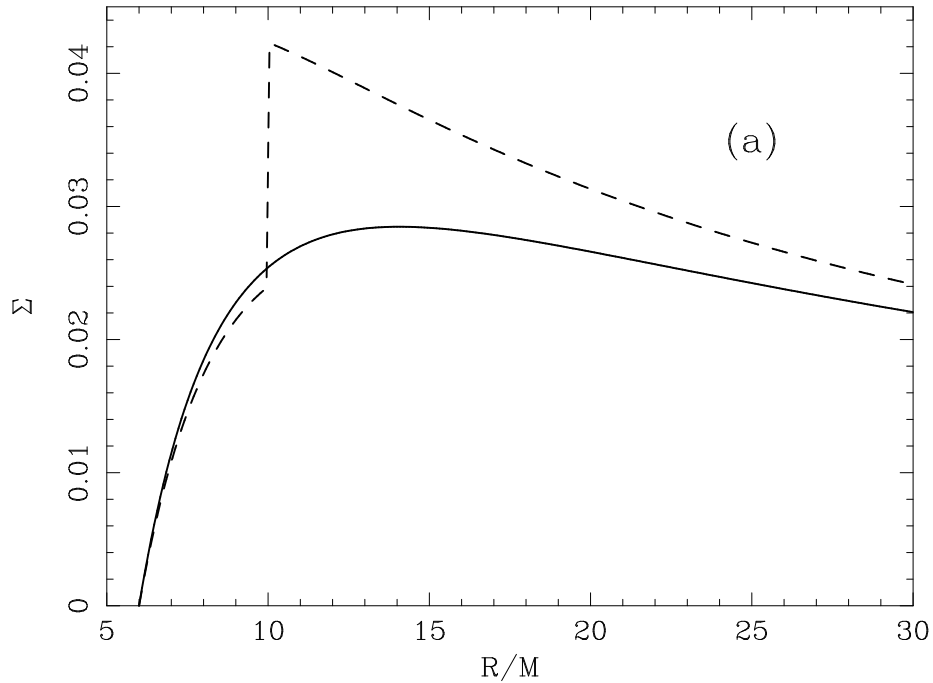
Figure 2.16: Evolution of disk in Schwarzschild spacetime for torque at R/M=10. Figure shows the surface density profile just after the torquing event begins as well as when the steady-state torqued profile is approached (dashed-line:$t = 10000$).

increases by almost a factor of two as one moves from almost face-on to almost edge-on disks, implying that the torque-energized disk is significantly more beamed than the un-torqued disk. A temporary decrease is only observed for the most edge-on cases, again due to a temporary dimming of the inner most regions of the disk.

These features are all symptomatic of the fact that the black hole torques the accretion disk and deposits energy and angular momentum in the disk. This extra source of energy that is dumped into the disk and that tends to affect the disk outward of the external torque location constitutes the starting point for the analysis of Section 2.3 where we attempt to explain the "deep minimum state" of the Seyfert galaxy MCG-6-30-15 as the result of just such a sporadic torquing event.
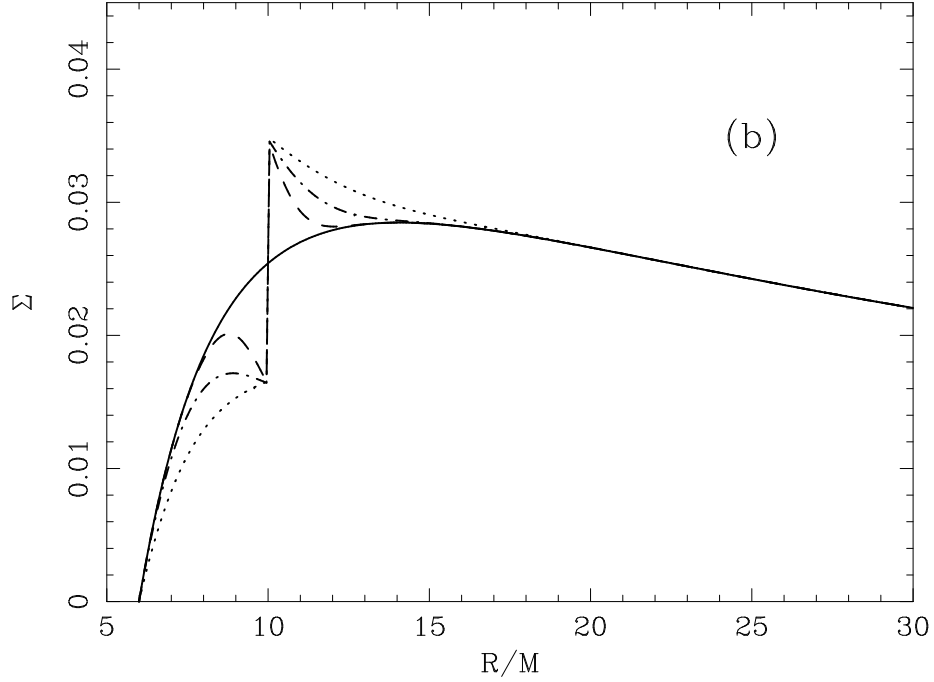
Figure 2.17: Evolution of disk in Schwarzschild spacetime for torque at R/M=10. Figure shows the early stages in the evolution of the surface density profile with the solid line being the untorqued steady-state profile (dashed-line:$t = 0.8$, dot-dashed-line:$t = 2.53$, dotted-line:$t = 8.0$).
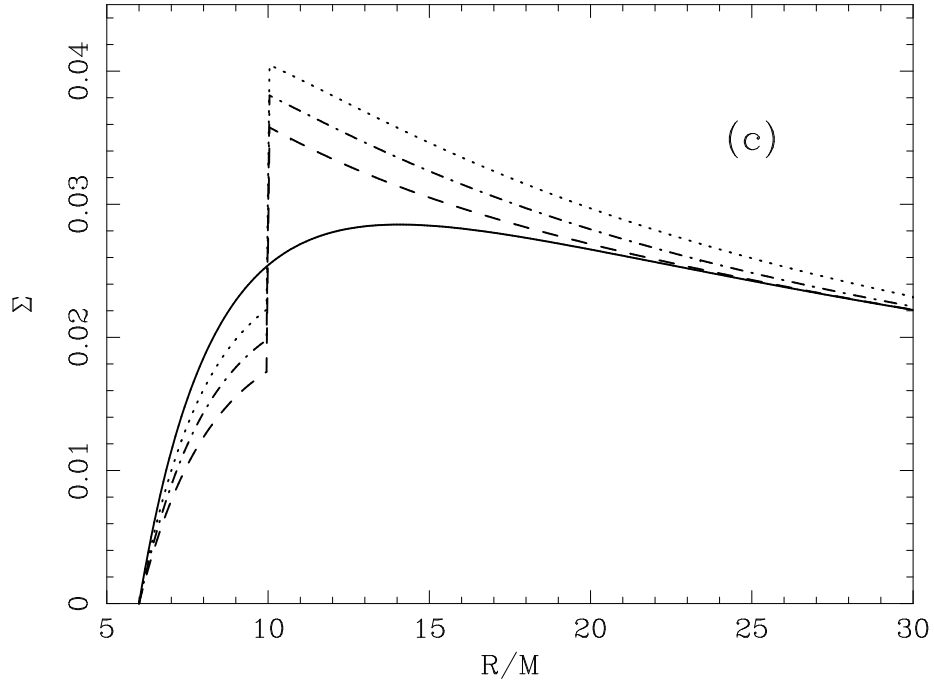
Figure 2.18: Evolution of disk in Schwarzschild spacetime for torque at R/M=10. Figure shows the untorqued steady-state profile (solid-line) as well as the late-time evolution of the torqued profile (dashed-line:$t = 25$, dot-dashed-line:$t = 80$, dotted-line:$t = 253$).
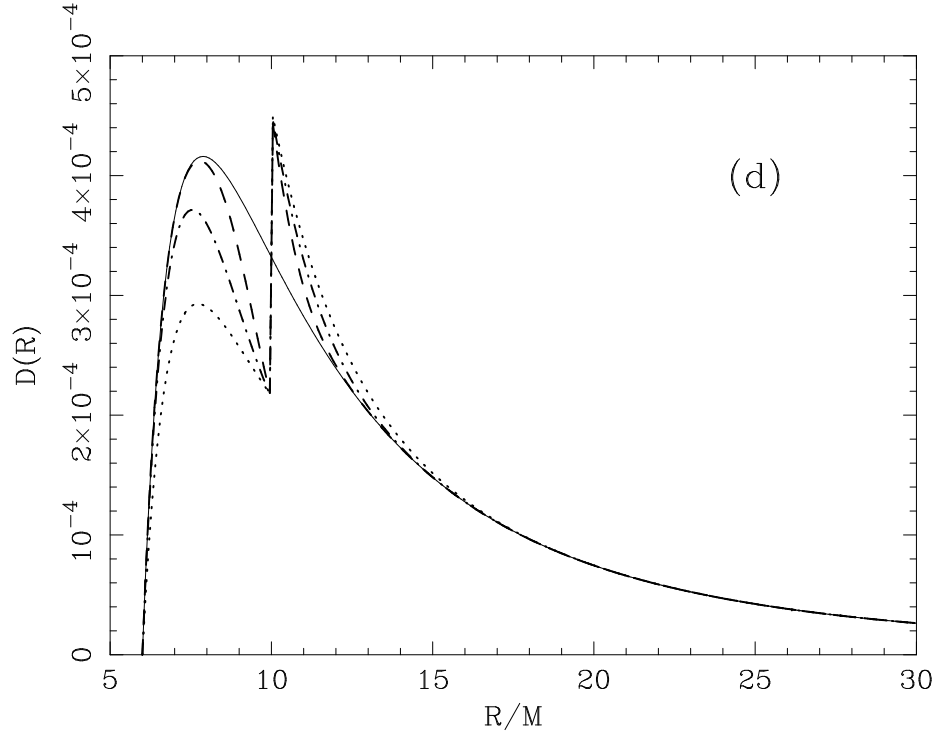
Figure 2.19: Evolution of disk in Schwarzschild spacetime for torque at R/M=10. Figure shows the early evolution of the dissipation function with lines and times corresponding to those of figure 2.18. The qualitative feature is again a drop inward of the torque location and an increase outward.

2.3 Can we interpret the "Deep Minimum State" of MCG–6-30-15 as a sporadic torquing event?

In addition to exploring the general characteristics of sporadically-torqued disks, a central motivation for this study are the *XMM-Newton* observations of the Seyfert galaxy MCG–6-30-15. In particular, we would like to explore whether the enigmatic "Deep Minimum State" of this AGN could correspond to a sporadic torquing event, possibly induced by the formation of a temporary magnetic connection between the inner accretion disk and either the plunging region of the disk or the rotating event horizon. There are two defining characteristics of the Deep Minimum State that must be reproduced by any successful model, the extremely broadened X-ray reflection features (implying a very centrally concentrated
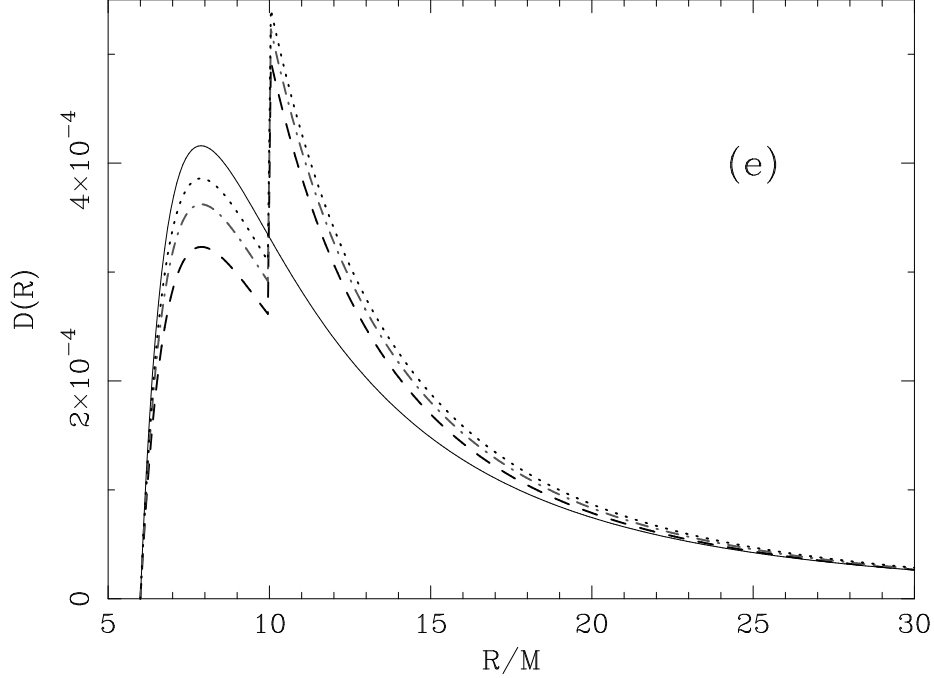
Figure 2.20: Evolution of disk in Schwarzschild spacetime for torque at R/M=10. Figure shows the late-time evolution of dissipation function with lines and times analogous to those of figure 2.18.

X-ray irradiation pattern) and the factor 2–3 drop in the observed X-ray continuum flux.

A major uncertainty when relating disk models to X-ray observations is always the relation between the dissipation within the disk (predicted by the models) and the emission of the observed X-rays. If we suppose that a local disk-corona radiates a fixed fraction of the underlying dissipation into the X-ray band, the results of this Chapter quickly lead to a contradiction between the sporadically-torqued disk model and the observations. While the model does predict a temporary dip in observed luminosity for some observer inclinations (that one might be tempted to identify with the continuum drop in the Deep Minimum), this dip is due to a dimming of the innermost regions of the accretion flow as a result of the damming of the mass flux. This is precisely the part of the flow that we wish to be enhanced in order to explain the simultaneous broadening of the X-ray reflection features.

Within the (standard) accretion disk corona framework, the relation between the dis-
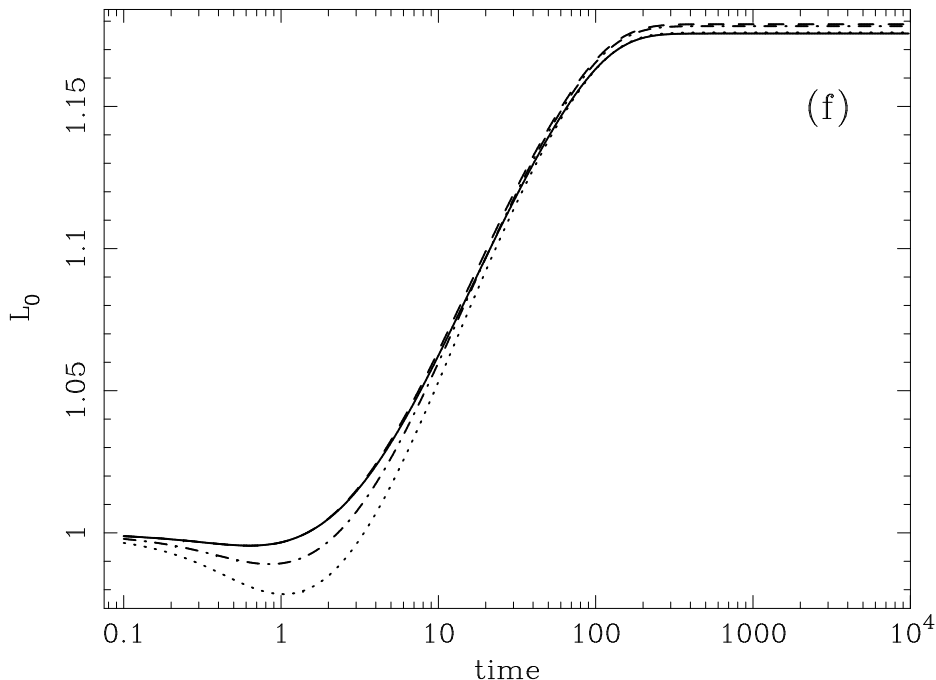
Figure 2.21: Evolution of disk in Schwarzschild spacetime for torque at R/M=10. Figure shows the observed luminosity starting at untorqued steady-state with t=0. The observed luminosity is determined for angles of 10 (solid-line), 30 (dashed-line), 60 (dot-dashed line) degrees, and 80 degrees (dotted line). Although the magnitude of the observed luminosity is not the same in the untorqued steady-state for all angles, we have normalized them in order to see the change with respect to the untorqued state. Note the presence of a drop in the luminosity as the angle of inclination decreases.

sipation within the disk and the emission of the observed X-rays depends on the reprocessing of disk photons by the corona. We suggest this relation changes when the system departs from steady-state as the sporadic torque engages and will use this, in the next section, to discuss a scenario for the Deep Minimum spectrum.

2.3.1 Quenching the X-ray corona with returning radiation

The assumption that the X-ray emission from the disk corona locally tracks the dissipation in the underlying accretion disk is clearly an oversimplication. For example, Krolik & Hawley (2001) have used high-resolution pseudo-Newtonian simulations to show that there is a rather extended transition (occurring near but slightly outside of the radius of

Figure 2.22: Evolution of disk in Kerr spacetime for torque at R/M=2 and spin parameter $a = 0.998$. Figure shows the surface density profile in untorqued steady-state (solid-line) as well as the approach to steady-state torqued profile (dashed-line:$t = 10000$).

marginal stability) from the pure MHD turbulent region characterizing the bulk of the disk to the more laminar flow present in the plunging region. Since the heating of the corona is almost certainly due to reconnection and MHD wave heating from the underlying disk, the fraction of the dissipated energy transported to the corona will certainly change within this transition region, leading to a violation of the simple assumption employed in our toy models. A time-variable magnetic torque of the kind we envision in this paper might alter the MHD and thermodynamic properties of the gas and such a scenario might not be compatible with the one we describe in the thin-disk approximation. In other words, we can imagine that the external torque changes both the radiative efficiency of the gas as well as local MHD properties thereby invalidating the treatment of the magnetorotational instability as a local kinematic viscosity. Global disk simulations focusing on the formation and properties of the corona are required to address this issue and, hence, are beyond
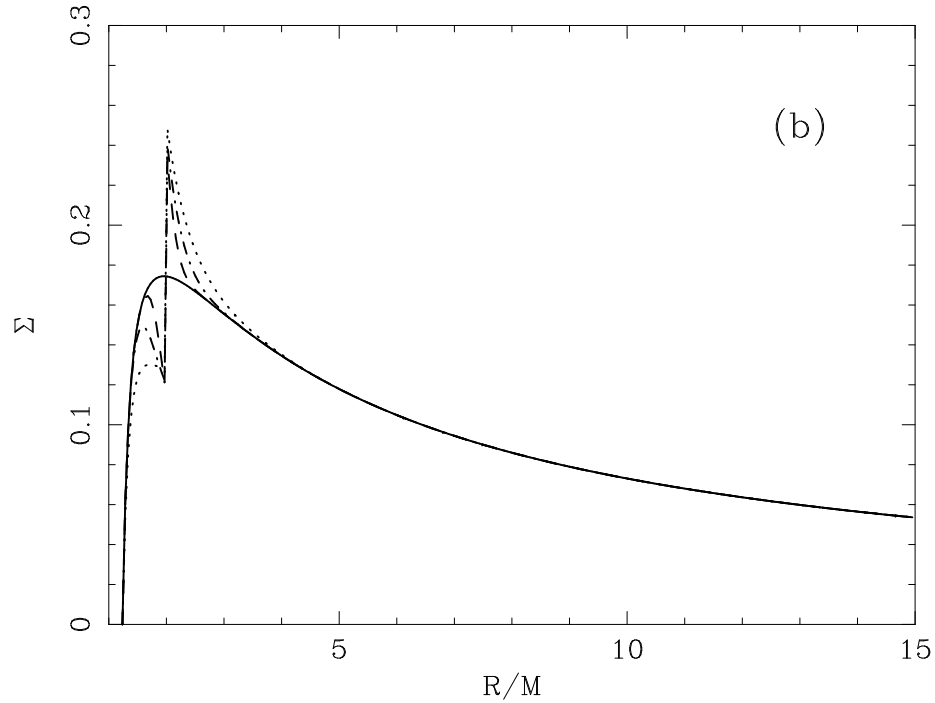
Figure 2.23: Early evolution of disk in Kerr spacetime for torque at R/M=2 and spin parameter $a = 0.998$. Figure shows the density profile with the solid line being the un-torqued steady-state profile (solid-line:$t = 0$) and the other profiles matching the times and line styles for figure 2.17 of the Schwarzschild figure.

the scope of this Chapter.

We do, however, note an important and previously neglected physical effect that could substantially change the structure of a disk corona in a strongly torqued disk — Compton cooling by flux emitted elsewhere in the accretion disk and, in particular, by "Returning Radiation". Consider a geometrically-thin accretion disk around a near-extremal Kerr black hole, and suppose that it possesses a disk-hugging X-ray corona energized from the underlying disk. Now suppose that the central regions of the disk are subjected to a significant torquing event. As shown above, the work done by the torque is rapidly radiated from the accretion disk in a very centrally concentrated manner. The torque-induced emission will be a combination of both thermal optical/UV radiation and hard X-ray emission produced by the corona associated with the torque-energized regions of the disk. Now, some fraction of the torque-induced emission will strike the disk at larger
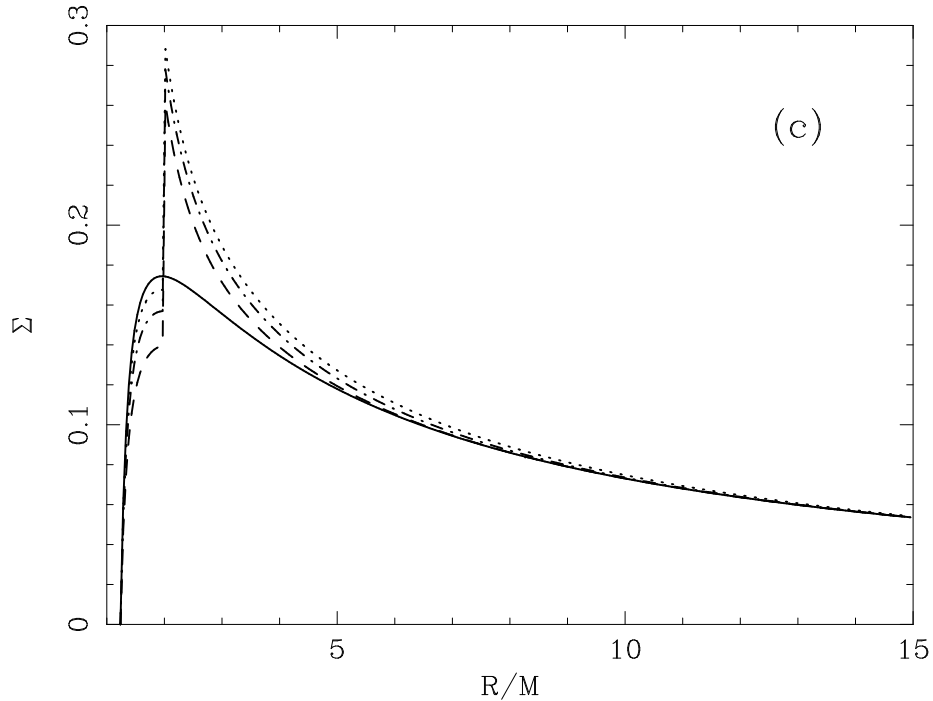
Figure 2.24: Late evolution of disk in Kerr spacetime for torque at R/M=2 and spin parameter $a = 0.998$. Figure shows the untorqued steady-state profile (solid-line) as well as the late-time evolution of the torqued profile (dashed-line:$t = 25$, dot-dashed-line:$t = 80$, dotted-line:$t = 253$).

radii — this will be particularly prevalent if the disk is flared or warped, but will occur even in flat disks due to strong relativistic light bending effects (i.e., Returning Radiation; Cunningham 1973). This extra irradiation will enhance the Compton cooling of the corona at these larger radii. At the very least, the additional cooling will lead to a decrease in the Compton amplification factor of the corona and a spectral steepening of the coronal emission. One could envisage a situation, however, in which the Compton cooling becomes so extreme that the corona completely collapses and local EUV/X-ray emission ceases.

Some essential aspects of this scenario can be captured in a simple model based on energy conservation, following Haardt & Maraschi (1991, 1993). Consider the X-ray emitting corona above a unit-area patch of the disk at a radius r. If a fraction f of the

43
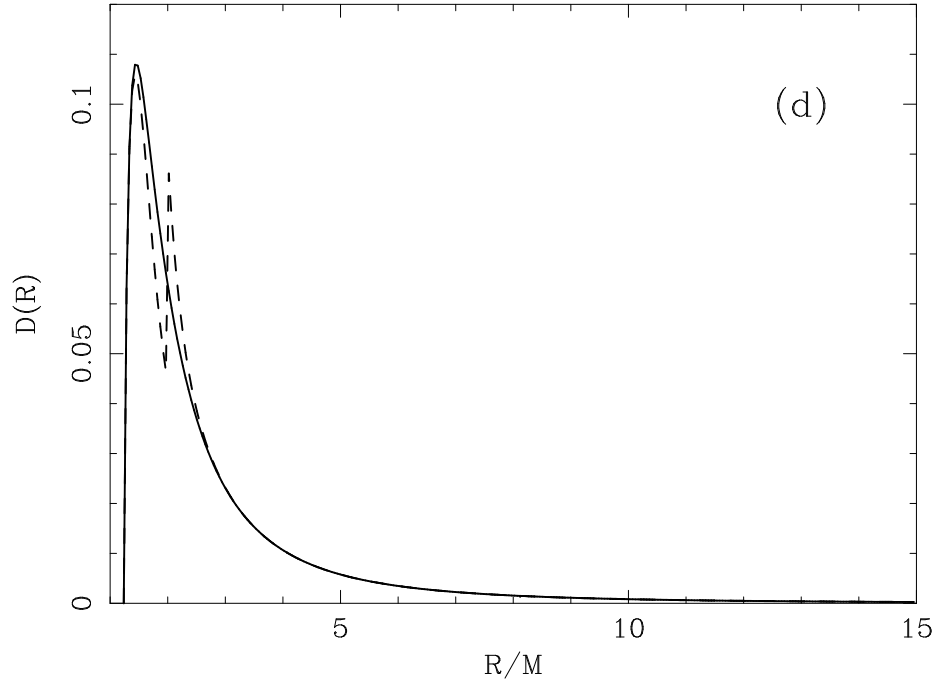
Figure 2.25: Late evolution of disk in Kerr spacetime for torque at R/M=2 and spin parameter $a = 0.998$. Figure shows the early evolution of the dissipation profile in addition to the untorqued steady-state (solid-line) for the same times and line styles of the Schwarzschild Fig. 2.17.
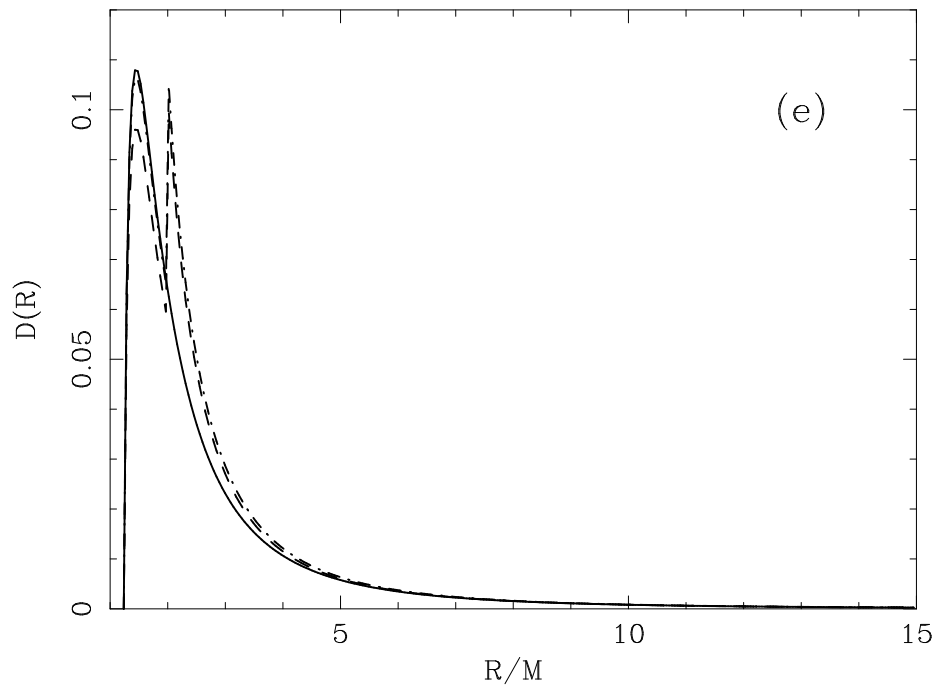
Figure 2.26: Evolution of disk in Kerr spacetime for torque at R/M=2 and spin parameter $a = 0.998$. Figure shows the late stage evolution of the dissipation function with times and line-styles compatible with those of Fig. 2.18.
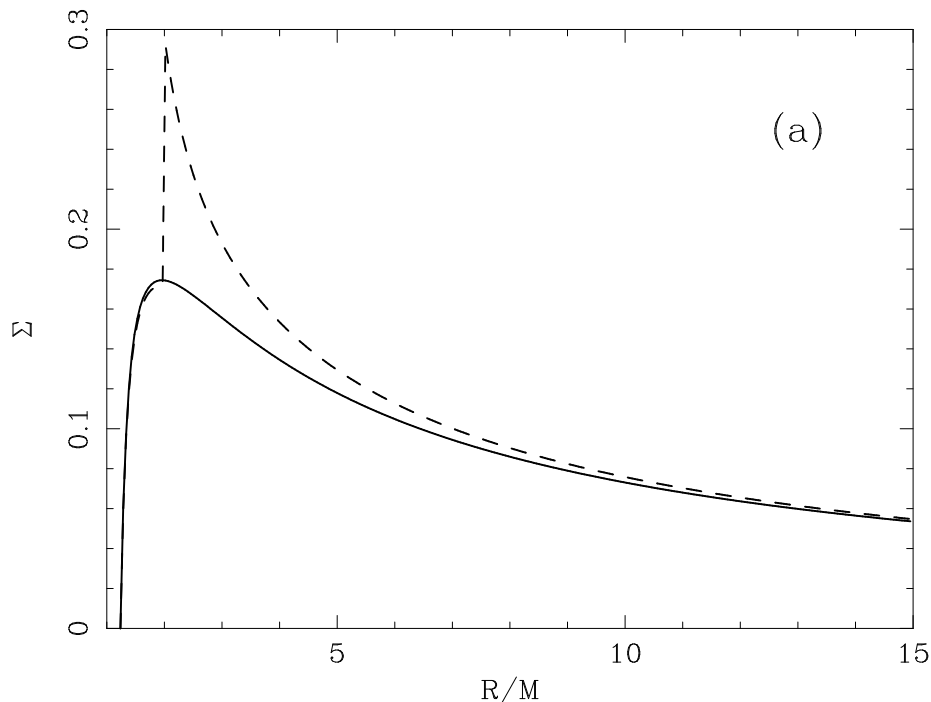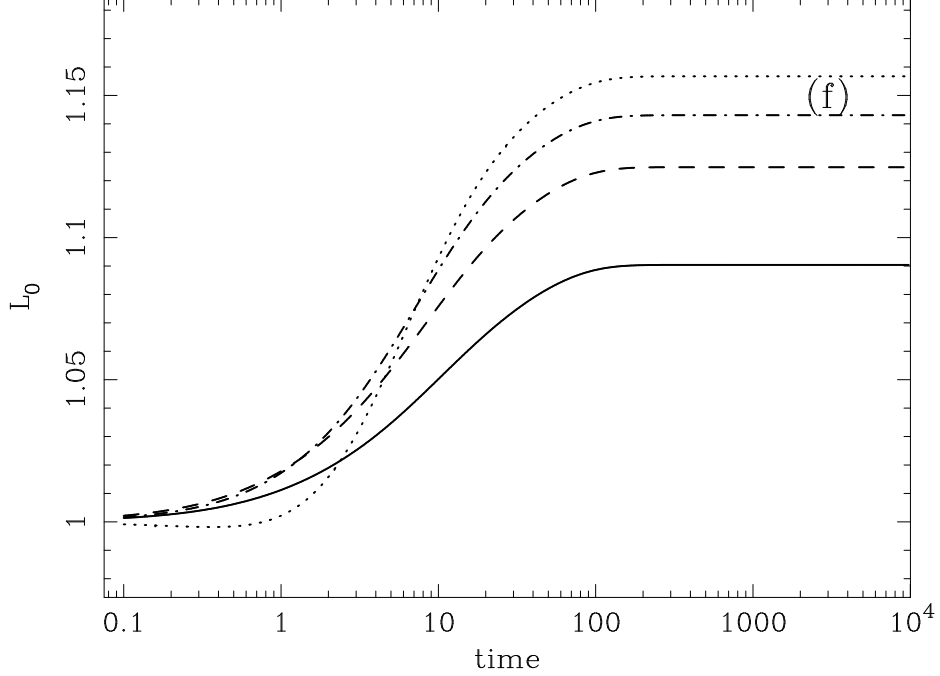
Figure 2.27: Evolution of disk in Kerr spacetime for torque at R/M=2 and spin parameter $a = 0.998$. Figure shows the luminosity observed at the same angles as in the Schwarzschild case (10 degrees, solid-line; 30 degrees, dashed-line; 60 degrees, dotted-dashed-line; 80 degrees, dotted line). Note how the smallest torqued steady-state rise occurs for the intermediate angle of 55 degrees. The lack of a drop in the observed luminosity comes from the presence of the external torque nearer to the inner boundary in the radial coordinate than in the Schwarzschild case.

energy dissipated in the underlying disk goes into heating the corona, the heating rate is

$$\mathcal{H}(r) = fD(r). \tag{2.28}$$

By definition, the (Compton) cooling rate of the corona is $(A-1)F_\mathrm{s}$, where A is the Compton amplification factor and F_s is the soft photon flux passing through the corona which will act as seed photons for the inverse Compton scattering process that generates the X-rays. Because the thermal timescale of the corona is very short, it is appropriate to assume an instantaneous balance between heating and cooling. Equating heating and cooling gives,

$$fD(r) = (A-1)F_\mathrm{s}. \tag{2.29}$$

We now determine F_s by examining energy conservation of the colder disk underlying

45

the corona. There are three contributions to that we must consider. Firstly, the portion of the internal dissipation within the disk that does *not* get transported into the disk will become thermalized in the cold disk and contribute an amount $(1-f)D(r)$ to the disk heating. Secondly, some fraction of the locally generated coronal flux $\xi_1 f D(r)$ will impinge on the disk and be reprocessed into soft flux. The parameter ξ_1 encapsulates possible anisotropies in the coronal flux and the albedo of the disk, but will typically be of the order of $\xi_1 \sim 0.2 - 0.5$. Finally, as noted above, irradiation of our coronal patch from other radii in the disk will contribute to the soft flux and hence the Compton cooling. This will cool the corona due to both the direct action of the irradiating soft flux, and the reprocessing/thermalization of the soft and hard irradiating flux. Suppose that the non-local irradiating flux is $\mathcal{R}(r)$ times the locally produced flux. The corresponding soft flux contributing to the Compton cooling will be $\xi_2 \mathcal{R} D(r)$, where $\xi_2 \leq \sim 1$ parameterizes the fraction of this non-local emission that ends up as soft flux. Hence, the total soft flux at a particular location in the disk will be

$$F_s = \xi_1 f D(r) + \xi_2 \mathcal{R}(r) D(r) + (1-f)D(r). \tag{2.30}$$

Solving for A from equation 2.29, we get

$$A = 1 + \frac{f}{\xi_2 \mathcal{R}(r) + 1 - f(1 - \xi_1)}. \tag{2.31}$$

Of course, within this simple model the total energy dissipated within the corona is a fixed fraction of the underlying dissipation irrespective of the (cooling) soft flux. However, the amplification factor is significantly reduced by Returning Radiation if

$$R(r) > \xi_2^{-1}[1 - f(1 - \xi_1)] \tag{2.32}$$

which, for canonical values of $f = 1$ and $\xi_1 = \xi_2 = 0.5$, corresponds to $\mathcal{R}(r) > 1$. The resulting coronal spectrum from the affected regions of the disk would be expected to steepen significantly, possibly placing a large fraction of the emission into the unobservable EUV band.

For a flat disk at large radii subjected to returning radiation, we have $\mathcal{R}(r) = R_0(a) + \Delta\eta R_\infty(a)$, where $\Delta\eta$ is the enhancement in the efficiency of the disk due to the inner torque and $R_\infty(a)$ and $R_0(a)$ are dimensionless functions of the black hole spin parameter given by the fitting formulae of Agol & Krolik (2000). For a near-extremal Kerr black hole ($a = 0.998$), we have $R_0 \approx 0.2$ and $R_\infty \approx 1$. Thus, we can see that even in the absence of disk flaring or warping, returning radiation alone could significantly depress coronal X-ray activity at large radii if

$$\Delta\eta > \frac{1 - f[1 - \xi_1]}{\xi_2} - 0.2. \tag{2.33}$$

Thus, although there is some dependence on the properties (e.g., isotropy and patchiness) of the corona and the ability of the disk to reprocess and thermalize any incoming flux, the corona will be depressed if the disk is in a "spin-dominated" state ($\Delta\eta \approx 1$ or greater), i.e., a state in which the disk is shining via the release of black hole spin energy rather than gravitational potential energy.

2.3.2   A proposed scenario for the MCG-6-30-15 Deep Minimum State

Let us now return to MCG–6-30-15 and the sporadic external torque model for its Deep Minimum State. We suppose that the normal state of this system is that of a standard untorqued accretion disk that might well be described by the standard accretion models of Novikov & Thorne (1974) and Page & Thorne (1974). We then suppose that some shift in magnetic configuration caused the accretion disk to become magnetically torqued by either the plunging region or the rotating black hole itself. We hypothesize that this event signals the onset of a Deep Minimum State.

On timescales shorter than the viscous timescale of the inner disk ($t_{\mathrm{visc}} \sim 1\,\mathrm{hour}$), we expect this torquing event to lead to a damming of the accretion flow and a true dimming of the disk interior to the location where the connection has occurred. Current instru-

ments are not able to define the broad iron line profile on a 1 hour timescale and, hence, the predicted temporary narrowing of the broad iron line would not have yet been observed. However, on longer timescales, the disk will tend to the new torqued steady-state (provided the torque is sufficiently long-lived).

If the magnetic torquing occurs in the very centralmost regions of the disk (which is likely in all of the scenarios that we are envisaging), the torqued steady-state will possess a much more centrally concentrated dissipation pattern. As described above, some fraction of this central flux will strike the disk further out (the Returning Radiation phenomenon) and possibly lead to a Compton suppression of the X-ray emitting corona there. Only the central portions of the X-ray emitting corona which are being vigorously energized will contribute significantly to the observed X-ray flux.

It is simple to see that the *overall X-ray luminosity* escaping the system is unlikely to drop, and will probably rise, within this scenario — the non-local cooling is only important for $\Delta\eta > 1$, in which case the part of the disk directly energized by the torque will produce coronal luminosity in excess of $f\dot{M}c^2$. Even accounting for the fact that half of this may strike the disk and be reprocessed into soft flux, the *overall* X-ray luminosity of the torqued disk will inevitably exceed that of the untorqued disk ($0.3f\dot{M}c^2$). However, the highly centrally concentrated nature of the torqued emission coupled with the suppression of the X-ray emission at larger radii means that this X-ray luminosity is highly beamed into the plane of the disk, and the *observed X-ray flux* for an observer with an inclination of $30°$ can readily drop (Fig. 2.28). In other words, the observed coronal activity is suppressed by cooling from a powerful photon source that goes largely unobserved due to beaming effects.
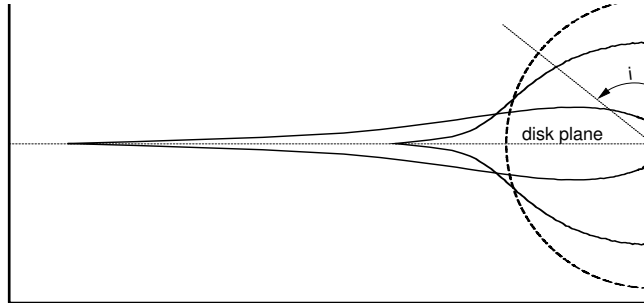
Figure 2.28: Polar diagram showing observed intensity as a function of viewing angle for the case of a near-maximal Kerr black hole ($a = 0.998$) and (from left to right) a ring source at $r = 2r_g$ and $r = 8r_g$. The circular curve is for isotropic emission. From Dabrowski et al. (1997).

2.4   Conclusions

Both non-relativistic and fully-relativistic MHD simulations of black hole accretion suggest the ubiquity of weak torques across the radius of marginal stability (Hawley & Krolik 2000, 2001; De Villers, Hawley & Krolik 2003; Gammie, Shapiro & McKinney 2004). However, it is still far from clear whether these torques can ever achieve the strength required to allow a decline of the overall mass-energy of the black hole, due to spin-down of the hole, a requirement for the kind of spin-dominated accretion disks that we have been discussing within the context of MCG–6-30-15. Significantly more simulation work is needed to address this question.

If one makes the assumption that such strongly torqued disks are possible, they provide a plausible and theoretically-attractive explanation for the extremely broadened X-ray reflection features seen in the Deep Minimum State of MCG–6-30-15 (Wilms et al. 2001; Reynolds et al. 2004) as well as the Galactic Black Hole Binary XTEJ1650–500 (Miller et al. 2002). Given this hypothesis, we can ask whether the onset of the Deep Minimum State corresponds to the occurrence of a strong torquing event.

We address this question through analytic and semi-analytic time-dependent toy models of torqued accretion disks. Using these models, we have shown that the simple model of a sporadically-torqued disk *fails* to explain the phenomenology of the Deep Minimum State transition. However, it would be premature to dismiss torqued-disk models on the basis of this failure. In particular, the real culprit may be the assumption that the local X-ray emission is a fixed fraction of the dissipation in the underlying disk. We discuss a particular scenario in which all but the innermost X-ray emitting corona is quenched by returning radiation when the torque is engaged. Other possibilities include changes in the structure of the MHD turbulence as a result of the strong torquing event that, in turn, could readily change the fraction of the dissipated energy that is transported into the corona.

An alternative paradigm is the gravitational light-bending model of Fabian & Vaughan (2003) and Miniutti & Fabian (2004). Here, the primary X-ray source is located on the black hole spin axis. A transition into the Deep Minimum State corresponds to a migration of the X-ray source down to 2–$3\,GM/c^2$, with the light bending producing both an enhancement in the central illumination of the accretion disk and a dimming of the observed X-ray continuum flux. While the physical nature of the axial X-ray source remains unclear, it is an appealing aspect of this model that it reproduces the long-term temporal behavior of the iron line strength (Miniutti & Fabian 2004).

It is uncertainty in the geometry of the primary X-ray source that prevents us from distinguishing between the torqued-disk and light-bending models. The most promising observational approach is to search for a reverberation delay between short timescale flickering in the X-ray continuum and the corresponding response in the X-ray reflection signatures. If measurements of this time-delay demonstrate that the X-ray source in the Deep Minimum is indeed 2–$3\,GM/c^2$ [corresponding to $10-15\,(M/10^6 M_\odot)$ light seconds] above the central disk plane, strong light-bending must occur and the need for a

torqued disk is removed. Measurements of this time-delay will constrain the X-ray source geometry and allow the degeneracy between these two models to be resolved but require future high-throughput observations. Also, future high throughput missions may be able to look for the short-lived damming phase via a temporary narrowing of the broad iron line.

Chapter 3

Magnetic Flux-Trapping Around Black Holes

Despite years of observational and theoretical work, we are at present still uncertain of the basic mechanism behind jets. Whatever this mechanism is, it must tap into one or both of two available energy sources. The first is the gravitational potential energy of matter in the accretion disk, and the second is the rotational energy of the black hole. The most probable way that an accretion disk can drive a wind is by field lines threading the disk with geometry that favors loading of field lines by disk plasma (Blandford & Payne 1982). Unfortunately, this method seems to fail to produce the highly collimated, highly relativistic jets (essentially due to the mildly relativistic velocities that characterize disk rotation). The alternative involves spin-energy extraction of the black hole itself via the BZ mechanism (Blandford & Znajek 1977). The power extracted from a Kerr black hole with dimensionless spin parameter a_* threaded by a magnetic field of strength B_H (in the membrane paradigm sense; see Thorne, Price & Macdonald 1986) is

$$L_{BZ} \approx \frac{1}{32}\omega_F^2 B_H^2 r_H^2 a_*^2 c \qquad (3.1)$$

where r_H is the radius of the event horizon and $\omega_F^2 = \Omega_F(\Omega_H - \Omega_F)/\Omega_H^2$, with Ω_H and Ω_F being the angular velocities of the black hole and magnetic field lines, respectively. It is often argued (e.g., see BZ) that the magnetic field structure adjusts itself such that $\Omega_F = \Omega_H/2$ (Phinney 1983), hence maximizing ω_F^2 to a value of 1/4. Although the original formula of Blandford & Znajek was derived via perturbation theory and hence is strictly valid only for low values of spin, numerical simulations have shown that equation 3.1 is valid at least up to a spin of $a_* = 0.9$ (Komissarov, 2001).

While the initial work of BZ was based on force-free black hole magnetospheres, the basic mechanism is seen to operate in the recent generation of fully relativistic MHD accretion disk simulations (e.g., see Koide et al. 2000; Komissarov 2004, De Villiers et al. 2004, McKinney & Gammie 2004, McKinney 2005a,b,c). Furthermore, these simulations do indeed support the hypothesis that the field structure adjusts so as to give $\Omega_F = \Omega_H/2$ for those field lines that thread the horizon.

A major uncertainty in the study of the BZ mechanism, however, is the strength of the black hole-threading magnetic field, B_H. Until the early 1990's, the maximum strength of the hole-threading magnetic field was determined by considering the strength of the disk-threading field. If the horizon-threading field exceeded the disk field strength, the argument went, the former would push its way off the hole via magnetic pressure and back into the disk until the hole-threading field strength was no larger than the disk field strength. Two major untested assumptions go into this scenario. The first is that the hole-threading field is confined via Maxwell pressure by the disk-threading field, while the second is that the disk-threading field grows to a large enough value to confine a sufficiently intense black hole-threading field to explain the most powerful jets. In 1991, Balbus & Hawley rekindled interest in an MHD instability (the MRI) uncovered by Chandrasakhar in 1961, showing how it formed the foundation for angular momentum transport in accretion disks. This revelation came at a price, in the sense that it operates only if the disk magnetic field

is characteristically weak, or more precisely, when magnetic pressure in the disk is at least an order of magnitude less than the gas pressure in the disk. These realizations form the basis for the arguments starting with Lubow, Papaloizou & Pringle (1994), through Ghosh & Abramowicz (1997), and ending with Livio et al (1999), pointing to basic constraints on the strength of the hole-threading field. The picture that emerged was bleak for the BZ mechanism. The indication was that the disk field must be smaller than believed possible before the 1991 conclusions. To compound the problem, turbulent accretion was found to be sufficiently diffusive (Lubow, Papaloizou & Pringle, 1994), making the already weaker than hoped disk-threading field difficult to drag toward the black hole. Under these circumstances, Livio et al. (1999) showed that the accretion energy always exceeds black hole spin energy. The upshot of these conclusions would be that hole-threading fields must be weak, to the extent that the BZ power would be insufficient to explain the highly relativistic jets.

We challenge the argument that Maxwell pressure from the large-scale magnetic field threading the disk solely determines the field on the hole on the basis that such a conclusion ignores the dynamics of the so-called plunge region. We argue that the plunge region is effective in trapping a strong black hole-threading field despite weak disk-threading fields. In contrast to Ghosh & Abramowicz (1997), we claim that the plunge region plane cannot be force-free.

In more detail, the goal of this Chapter is to construct a non-relativistic model of accretion around a black hole to illustrate the strength of the black hole threading magnetic field that results from the assumption of an inertially dominated accretion flow in the plunge region. We consider the dragging of a poloidal magnetic field through a diffusive accretion disk toward a black hole, for different values of the effective magnetic Prandtl number of the disk and varying disk thickness. We show that the strength of the hole-threading magnetic field can be substantially larger than the field in the disk and that the
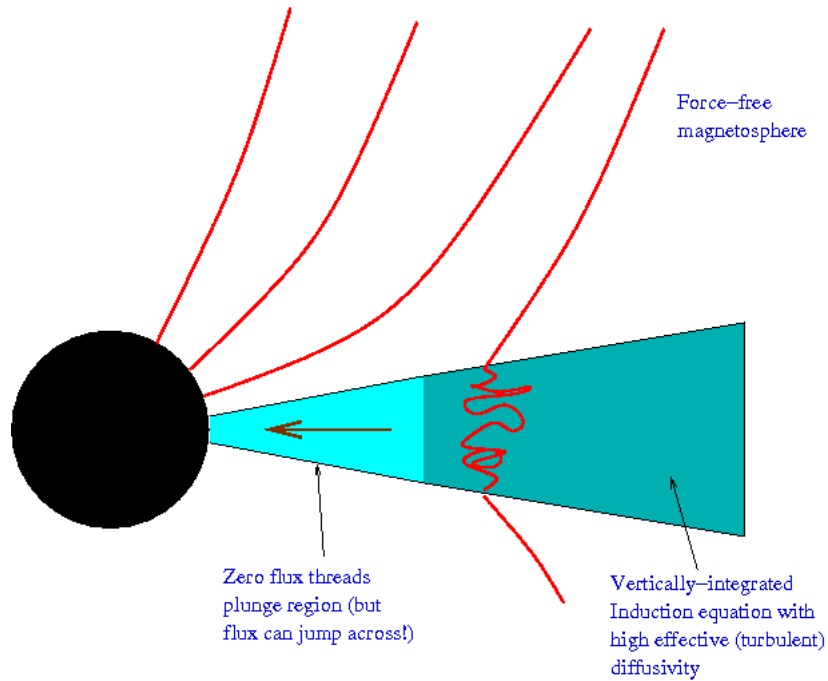
Figure 3.1: Toy model setup for a diffusive accretion disk surrounding a black hole. Courtesy of C. Reynolds.

increase in the field strength on the horizon increases with larger Prandtl number and disk thickness. The relativistic generalization of this model will be presented in the next chapter.

3.1   The toy model

Here we construct a simple model to study the dragging of an external magnetic field by an MHD turbulent black hole accretion disk. While the magnetic field will be (essentially) perfectly frozen into the accreting plasma on small scales, we follow Lubow et al. (1994) and Heyvaerts, Priest & Bardou (1996) in assuming that reconnection within the MHD turbulence allows a large scale magnetic field to diffuse through the turbulent plasma with an *effective* magnetic diffusivity η. The question we want to address is the nature of the balance between inward dragging of the magnetic field by the accretion flow and the outward diffusion of the magnetic field. This competition determines the strength of the

magnetic field threading the black hole. Figure 3.1 shows a cartoon of our toy model.

Our accretion disk is a standard geometrically thin Shakura-Sunyaev (1973) disk. We describe angular momentum transport in the disk using the usual α-prescription, and assume that the velocity field within the disk is not affected by the large scale magnetic field (i.e., we do not allow the large scale field to act back and affect the dynamics of the accretion disk). Within the body of the accretion disk, the large scale electromagnetic field of interest is taken to satisfy Maxwell's equations,

$$\vec{\nabla} \times \vec{E} = -\frac{\partial \vec{B}}{\partial t} \tag{3.2}$$

$$\vec{\nabla} \times \vec{B} = \mu \vec{J} \tag{3.3}$$

and a simple Ohm's law of the form

$$\vec{J} = \frac{1}{\mu \eta}(\vec{E} + \vec{v} \times \vec{B}) \tag{3.4}$$

where $\vec{v}$ is the flow velocity of the plasma, and we are assuming that the field will vary slowly thereby allowing us to neglect the displacement current in equation 3.3. We now derive the equation that governs the structure of the magnetic field in the accretion disk. By writing the current in terms of $\vec{B}$ from equation (3.3) and the electric field in terms of $\vec{B}$ from equation (3.4), we can rewrite the induction equation (eq. 3.2) in terms of $\vec{B}$,

$$\vec{\nabla} \times \left(\eta \vec{\nabla} \times \vec{B} \right) - \vec{\nabla} \times \left(\vec{v} \times \vec{B} \right) = -\frac{\partial \vec{B}}{\partial t}. \tag{3.5}$$

Using the usual form of the vector potential

$$\vec{B} = \vec{\nabla} \times \vec{A} \tag{3.6}$$

and imposing the gauge condition

$$\vec{\nabla} \cdot \vec{A} = 0 \tag{3.7}$$

we have

$$\nabla \times \left[-\eta \nabla^2 \vec{A} - \vec{v} \times \left(\vec{\nabla} \times \vec{A} \right) + \frac{\partial \vec{A}}{\partial t} \right] = 0. \tag{3.8}$$

For the rest of this chapter, we shall work in a cylindrical polar coordinate system (r, ϕ, z), with the origin $r = 0$ at the center of the disk (i.e., the location of the center of the black hole), and the plane $z = 0$ coincident with the mid-plane of the accretion disk. From Stokes' Theorem, we can write the flux threading a ring described by fixed r and fixed z in terms of the ϕ component of the vector potential as,

$$\psi = \int_S \vec{B} \cdot d\vec{a} = \int_S \vec{\nabla} \times \vec{A} \cdot d\vec{a} = \int_{\partial S} \vec{A} \cdot d\vec{l} = 2\pi r A_\phi, \tag{3.9}$$

where S denotes a circular area spanned by fixed r and z and ∂S denotes its ring boundary. At this point, we assume that the large scale magnetic field is axisymmetric. A qualitative discussion of departures from this assumption will be presented in section 3.3.2. Under this assumption, the poloidal components of equation 3.8 can be integrated to give,

$$-\eta \left[\frac{\partial^2 \psi}{\partial z^2} + r \frac{\partial}{\partial r} \left(\frac{1}{r} \frac{\partial \psi}{\partial r} \right) \right] + v_r \frac{\partial \psi}{\partial r} + \frac{\partial \psi}{\partial t} = 0. \tag{3.10}$$

This equation describes the time-evolution of the magnetic flux through any given ring described by a fixed value of r and z. The first term (involving a second-derivative with respect to z) describes the diffusion of the magnetic field due to magnetic tension associated with field-line curvature, whereas the second term (involving a second derivative with respect to r) describes diffusion driven by gradients in magnetic pressure.

We wish to apply equation 3.10 in the mid-plane of our geometrically-thin accretion disk ($z = 0$) and examine the magnetic flux enclosed as a function of radius in the disk r. The vertical structure of the disk/field only enters in the first term of equation 3.10 (i.e., the magnetic tension term). Following Heyvaerts, Priest and Bardou (1996, hereafter HPB), we assume that the flux within the disk has a z-dependence given by,

$$\psi(r,z) = \psi(r,0) + \frac{z^2}{2} \psi_2 \tag{3.11}$$

where ψ_2 is the value of $\frac{\partial^2 \psi}{\partial z^2}$ at the center plane of the disk at distance r from the black hole. This amounts to assuming that the large scale field is smooth inside of the disk. By

differentiating with respect to z we have

$$\frac{\partial \psi}{\partial z} = z\psi_2, \tag{3.12}$$

so, introducing the disk thickness h, we can relate ψ_2 to the value of $\frac{\partial \psi}{\partial z}$ at the disk surface

$$\left(\frac{\partial \psi}{\partial z}\right)_+ = h\psi_2, \tag{3.13}$$

where the plus sign denotes the upper disk surface. Thus, we can write an equation for the midplane magnetic flux function for an accretion disk characterized by a radial velocity inflow as

$$-\eta\left[\frac{1}{h}\left(\frac{\partial \psi}{\partial z}\right)_+ + r\frac{\partial}{\partial r}\left(\frac{1}{r}\frac{\partial \psi}{\partial r}\right)\right] + v_r\frac{\partial \psi}{\partial r} + \frac{\partial \psi}{\partial t} = 0. \tag{3.14}$$

We must specify the form of our externally imposed magnetic field. We suppose that the original externally imposed field is uniform with strength B_0 in the vertical direction (i.e., the direction normal to the plane of the accretion disk). Therefore, the flux function can be decomposed into three components,

$$\psi(r,z;t) = \psi_{\mathrm{BH}}(r,z;t) + a(r,z;t) + \pi r^2 B_0 \tag{3.15}$$

where $\psi_{\mathrm{BH}}(r,z;t)$ is the flux function associated with "cleaned" black hole-threading field (which, we stress, is generated by currents in the disk), the final term on the RHS is just the uniform imposed flux (generated by currents far enough away to be considered outside of our system), and $a(r,z;t)$ accounts for all other (disk-threading) magnetic field structures (generated, in principle, by currents either in or out of the disk plane). The cleaned black hole-threading field refers to the configuration of the field on the horizon membrane in the sense of Thorne & MacDonald, (1986). The basic idea is that whereas the horizon proper is outside causal contact with the external plasma and cannot influence it, the region just outside the horizon can still be important. Because of the divergent gravitational redshift as the horizon is approached, observers outside will see a magnetic field that is sluggish and compactified on the horizon. Because field features at the horizon

do not affect the outside, the membrane paradigm eliminates this region by considering an effective horizon membrane just outside of the real horizon where the magnetic field is less dramatically influenced by the gravitational redshift. We assume that in the region exterior to the disk ($|z| > h$), the black hole-threading field has the form of a split monopole,

$$\psi_{\mathrm{BH}}(r,z;t) = \psi_*(t) \left(1 - \mathrm{sgn}(z) \frac{z}{(z^2 + r^2)^{1/2}} \right) \qquad (|z| > h), \qquad (3.16)$$

where $\psi_*(t)$ is the hole-threading flux. To reiterate, this hole-threading field is generated by toroidal currents flowing in the disk ($|z| < h$) and is a vacuum solution to Maxwell's equations elsewhere. While the precise structure of the cleaned black hole field is unclear, the choice of the split monopole has support from recent General Relativistic MHD simulations (e.g., see Hirose et al., 2004; Komissarov 2005).

3.1.1   The magnetosphere

The z-derivative of the flux function at the disk surface is determined by matching the magnetic flux function in the disk onto a solution for the magnetic field outside of the disk (hereafter referred to as the disk magnetosphere). We assume that the plasma density in the magnetosphere is very low, resulting in the magnetosphere adopting a force-free configuration, i.e., $(\vec{\nabla} \times \vec{B}) \times \vec{B} = 0$. In addition, we assume that the Alfvén speed in the disk magnetosphere is sufficiently high as to reduce the toroidal field to essentially zero (through the production of torsional Alfvén waves). Setting $B_\phi = 0$, the field in the disk magnetosphere becomes potential ($\vec{\nabla} \times \vec{B} = 0$) and the flux function obeys

$$\mathcal{D}\psi = 0 \qquad (3.17)$$

where $\mathcal{D}$ is the linear differential operator

$$\mathcal{D} \equiv \frac{\partial}{\partial r} \left(\frac{1}{r} \frac{\partial}{\partial r} \right) + \frac{\partial}{\partial z} \left(\frac{1}{r} \frac{\partial}{\partial z} \right). \qquad (3.18)$$

Noting that both the imposed uniform field and (exterior to the disk) the black hole-threading field $\psi_{\mathrm{BH}}(r,z;t)$ individually obey $\mathcal{D}\psi = 0$, the structure of the disk magnetosphere is determined by solving the potential problem for $a(r,z;t)$, i.e., $\mathcal{D}a = 0$.

At this point, a brief discussion of our $B_\phi = 0$ assumption (which leads to the potential field condition) is in order. The differential rotation to which the disk plasma is subjected produces toroidal fields that propagate outward into the magnetosphere as torsional Alfvén waves. In the non-relativistic treatment here, we assume that the Alfvén speed in the disk magnetosphere is large enough such that any twist in the magnetic field is removed via a torsional Alfvén wave. We also argue that this fact carries over into the relativistic regime where the inner disk rotates at speeds close to the speed of light. The reason for this is that it is the differential rotation that produces the toroidal field component and not the direct rotational speed. In fact, detailed studies of non-rotating (or slowly-rotating) black hole magnetospheres have shown that the field line rotation associated with a Keplerian accretion disk has only a small effect on the poloidal field as compared with the equivalent non-rotating configuration (MacDonald 1984; Uzdensky 2004). In this sense, Keplerian accretion disks around slowly rotating black holes are "slow rotators" (Uzdensky 2004).

3.1.2 The disk

For the rest of this chapter, we explicitly consider the behavior of the magnetic field in the upper half of the z-plane, $z > 0$ — we suppose the system to be symmetric in the $z = 0$ plane. The tension term in eqn. 3.14 can be decomposed into

$$\left(\frac{\partial \psi}{\partial z}\right)_+ = \left(\frac{\partial \psi_{\mathrm{BH}}}{\partial z}\right)_+ + \left(\frac{\partial a}{\partial z}\right)_+. \tag{3.19}$$

The contribution from the hole-threading flux can be evaluated directly from eqn. 3.16,

$$\left(\frac{\partial \psi_{\mathrm{BH}}}{\partial z}\right)_+ \approx -\frac{\psi_*}{r}, \tag{3.20}$$

where we have neglected a term which is smaller by a factor of $(h/r)^2$. The remaining contribution to eqn. 3.19 follows from the solution to the potential problem $\mathcal{D}a = 0$ with boundary conditions $a(r=0,z;t) = 0$ and $a(r,z=0;t)$ specified. As shown by HPB, this gives

$$\left(\frac{\partial \psi}{\partial z}\right)_{z=h} = \mathcal{P} \int_0^\infty dx \frac{[a(x,0;t) - a(r,0;t)]}{\pi(r-x)^2} - \frac{a(r,0;t)}{\pi r} \tag{3.21}$$

where "$\mathcal{P}$" signifies the principal part of the integral. We can now write an explicit integro-differential equation for the time evolution of $a(r,0;t)$ in the diffusive part of the disk ($r > r_{\mathrm{ms}}$);

$$\frac{\partial a}{\partial t} + \frac{\partial \psi_{BH}}{\partial t} + v_r r B_0 + \left(v_r + \frac{\eta}{r}\right)\frac{\partial a}{\partial r} =$$
$$\eta \left[\frac{1}{h}\mathcal{P}\int_0^\infty dx \frac{[a(x,0;t) - a(r,0;t)]}{\pi(r-x)^2} - \frac{a(r,0;t)}{h\pi r} - \frac{\psi_{BH}(t)}{hr} + \frac{\partial^2 a}{\partial r^2}\right]. \tag{3.22}$$

As part of our model, we must specify $h(r)$, $v(r)$ and $\eta(r)$. For definiteness, we define $h(r)$ by taking the ratio h/r as a fixed parameter of our model (in principle, one could substitute a particular form for $h(r)$ resulting from a detailed disk model). To specify the radial velocity field, we follow Lubow et al. (1994) and split our disk into two zones which we dub an "active" and a "dead" zone. In the active zone ($r_{\mathrm{ms}} < r < r_{\mathrm{dead}}$), we set $v_r = -v(1/r - 1/r_{\mathrm{dead}})$ where $v = \alpha h^2 (GM/r^3)^{1/2}$, and $\eta = v/P_{\mathrm{m}}$. The magnetic Prandtl number P_{m} is a fixed and constant parameter of the active disk. Note that we have introduced the usual α of accretion disk theory (in contrast with HPB who implicitly employ $\alpha \sim 1$). In the dead zone ($r_{\mathrm{dead}} < r < r_{\mathrm{out}}$), the diffusivity is still given by $\eta = \alpha h^2 (GM/r^3)^{1/2}/P_{\mathrm{m}}$, but the velocity is set to zero. For computational necessities, we impose an outer cutoff on the system at $r = r_{\mathrm{out}}$. We assume that the disk beyond r_{out} is a perfect and static conductor. Hence the total magnetic flux threading a loop ($r = r_{\mathrm{out}}, z = 0$) is constant and has the value $\pi r_{\mathrm{out}}^2 B_0$. The inclusion of the dead-zone makes the evolution of the inner part of the system essentially independent of the position or exact nature of the $r = r_{\mathrm{out}}$ boundary. In particular, the dead zone acts as a reservoir of

magnetic flux that can feed the actively accreting part of the disk — only in the outermost parts of the active disk does the conservation of magnetic flux lead to a non-negligible magnetic pressure trying to "suck" magnetic flux out of the active disk. The physical nature of the dead zone will be discussed in Section 3.3.1.

Finally, we must specify boundary conditions on $a(r, 0; t)$. The implementation of the inner radial boundary condition must capture the fact that the plunge region is extremely effective at sweeping in poloidal magnetic field that crosses within $r = r_{\mathrm{ms}}$. Consider a poloidal magnetic field line which is dragged towards the plunge region on the viscous timescale $t_{\mathrm{visc}} \approx (r_{\mathrm{ms}}/h_{\mathrm{ms}})^2 (r_{\mathrm{ms}}^3/GM)^{1/2} \alpha^{-1}$. Once in the plunge region, the radial velocity of the disk material rapidly increases with no associated increase in the effective magnetic diffusivity (indeed, to the extent that the plunge region becomes a laminar rather than a turbulent flow, the effective magnetic diffusivity may well plummet to very small values). For the field strengths under consideration here (i.e., with an energy density much less than the kinetic energy density of the accretion flow) inward advection of the field line on a dynamical timescale $t_{\mathrm{dyn}} \approx (r_{\mathrm{ms}}^3/GM)^{1/2}$ will dominate all other processes. Since the characteristic evolution timescale of the system is $t_{\mathrm{visc}} \gg t_{\mathrm{dyn}}$, flux conservation gives that the vertical magnetic field in the $z = 0$ plane in the plunge region compared with that in the disk just outside is

$$\frac{B_z(\text{plunge})}{B_z(\text{disk})} \approx \frac{t_{\mathrm{dyn}}}{t_{\mathrm{visc}}} \approx \alpha \left(\frac{h}{r}\right)^2 \ll 1. \tag{3.23}$$

To a good approximation, we can say that the magnetic flux locally crossing the plunge region is zero. Thus, the only magnetic flux passing through a loop $(r < r_{\mathrm{ms}}, z = 0)$ is that which threads the black hole, i.e., $\psi(r \leq r_{\mathrm{ms}}, 0; t) = \psi_*(t)$. To cancel the contribution from the externally imposed uniform field in this region, we must have

$$a(r, 0; t) = -r^2 B_0/2 \qquad (r < r_{\mathrm{ms}}). \tag{3.24}$$

Thus, the appropriate inner radial boundary condition for eqn 3.22 is $a(r = r_{\mathrm{ms}}, 0; t) =$

$-r_{\mathrm{ms}}^2 B_0/2$ and we must use eqn. 3.24 in the evaluation of the integral term of eqn. 3.22. The fact that $\partial a(r_{\mathrm{ms}}, 0; t)/\partial t = 0$ allows us to use eqn. 3.22 to evaluate the rate of change of black hole-threading flux,

$$\frac{\partial \psi_{BH}}{\partial t} = \eta(r_{\mathrm{ms}}) \left[\frac{1}{h} \mathcal{P} \int_0^\infty dx \frac{[a(x,0;t) - a(r,0;t)]}{\pi(r-x)^2} - \frac{a(r,0;t)}{h\pi r} - \frac{\psi_{BH}(t)}{hr} + \frac{\partial^2 a}{\partial r^2} + B_0 \right]_{r=r_{ms}},$$
(3.25)

where we have used the continuity of $\partial a/\partial r$ across $r = r_{\mathrm{ms}}$ to combine the third and fourth terms on the left hand side of eqn. 3.22. We can justify this assumption of continuity as follows. Suppose that this derivative was *discontinuous* across $r = r_{\mathrm{ms}}$, resulting in a discontinuity in the strength of the vertical magnetic field. This would lead to a large magnetic pressure gradient and a very rapid rearrangement of material until continuity was achieved. We do note, however, that we expect a rather narrow transition zone just outside of $r = r_{\mathrm{ms}}$ where vertical magnetic field goes from zero to the value characteristic of the disk. We must spatially resolve this transition in our numerical model.

For the outer radial boundary condition, we set $a(r_{\mathrm{out}}, z = 0; t) = -\psi_*(t)$ for some $r_{\mathrm{out}} > r_{\mathrm{dead}}$. This amounts to bounding the entire system by a perfect and static conductor in the disk plane ($z = 0$) for all $r > r_{\mathrm{out}}$, as discussed above.

With these assumptions, eqns. 3.22 and 3.25 completely describe the evolution of $a(r,0;t)$ and $\psi_*(t)$ from some initial state once we fix the magnetic Prandtl number P_{m}, the disk thickness h/r, the characteristic radii of the problem (r_{ms}, r_{dead}, r_{out}), the external field strength B_0, and the viscosity parameter α. In fact α and B_0 are trivial parameters of the model, affecting only the scaling of the time coordinate and the absolute normalization of a, respectively. Furthermore, the inclusion of the dead-zone makes the evolution of the inner disk/field essentially independent of the location of the outer boundary $r = r_{\mathrm{out}}$. Hence, the non-trivial parameters describing this system are P_{m}, h/r, and r_{dead}. For our

initial condition, we take

$$a(r, z = 0, t = 0) = \begin{cases} -r^2 B_0/2 & (r < r_{\mathrm{ms}}) \\ -r_{\mathrm{ms}}^2 B_0/2 & (r \geq r_{\mathrm{ms}}) \end{cases} \tag{3.26}$$

This amounts to saying that the initial currents flowing in the disk are only those required to cancel the imposed uniform field in the plunge region.

3.2 Solution method and results

While equation 3.17 is solved via standard analytic techniques once we have a solution to equation 3.22, we solve eqn. 3.22 numerically by discretizing it on a logarithmic grid with 200 zones from $r_{\mathrm{ms}} = 6$ to $r_{\mathrm{out}} = 150$ with the dead-zone starting at $r_{\mathrm{dead}} = 100$. Here and for the rest of this chapter, radii will be given in units of gravitational radii GM/c^2.

All terms (including the principal part integral) are differenced to second-order spatial accuracy. The time evolution is achieved through a simple first-order explicit scheme. To ensure numerical stability, we set the time-step to be $dt = (1/dt_{\mathrm{ad}}^2 + 1/dt_{\mathrm{diff}}^2 + 1/dt_{\mathrm{field}}^2)^{-1/2}$, where the advective, diffusive and field time-steps are given by $dt_{\mathrm{ad}} = 0.5 \min[\Delta r/(v + \eta_*/r)]$, $dt_{\mathrm{diff}} = 0.5 \min[\Delta r^2/\eta_*]$ and $dt_{\mathrm{field}} = 0.5 \min[h\Delta r/\pi\eta_*]$.

Figure 3.2a shows the time-evolution of ψ_{BH} for the case of $P_{\mathrm{m}} = 2$ and various choices of h/r from 0.01 to 0.16. In all cases, the flux threading the black hole grows from zero and achieves some positive steady state. The final equilibrium flux threading the black hole always exceeds $\pi r_{\mathrm{ms}}^2 B_0$ (corresponding to $\frac{\psi_{BH}}{2\pi} = 18B_0$), thereby establishing the basic fact that the plunge region can aid in the accumulation of significant magnetic flux through the black hole. For thicker disks, the increased inward advection of the field (due to the increased radial inflow speed of the accreting matter) coupled with the decreased effectiveness of field diffusion leads to significant enhancements of the black hole-threading flux above this baseline value. The dependence of the equilibrium value

of ψ_* on disk thickness and magnetic Prandtl number is shown in Fig.3.2b. For small P_m, the enhancement of the hole-threading flux above the canonical value of $\frac{\psi_{BH}}{2\pi} = 18B_0$ is very small. However, for P_m of order unity or higher, there is a strong h/r-dependent enhancement.

The full magnetic field configuration at any given time can be derived by solving the potential problem for $a(r,z;t)$ adopting the Green's function approach laid out in HPB to solve equation 3.17.

In Figures 3.3-3.5, we show the initial field configuration as well as the final configuration for $h/r = 0.08$ and two choices of magnetic Prandtl number $P_m = 2$ and 20. The initial configuration deviates from a simple uniform field due to the fact that flux is excluded from the region $r < r_{ms}$ which leads to a "bowing" of the field lines away from the radius of marginal stability. This curvature is rapidly reversed as field is advected inwards, finally achieving a steady state in which the bend angle of field lines as they enter the diffusive part of the disk is approximately constant. As pointed out by Lubow et al. (1994) and discussed below, we expect this bend angle (away from the disk normal) to be $i \sim \tan^{-1}(hP_m/r)$. This is indeed seen in our equilibrium solutions.

The central quantity of interest in this work is the magnetic field threading the black hole event horizon. Recalling the definition of the flux function, it is straightforward to show that the magnetic field threading the event horizon is $B_H = \psi_{BH}/2\pi r_H^2$ where $r_H = 2r_g$ is the event horizon radius of the (slowly rotating) black hole considered in this work. From the results described above, we conclude that the equilibrium flux threading the black hole always exceeds the flux of the external uniform field through the plunge region ($\pi r_{ms}^2 B_0$ corresponding to $\frac{\psi_{BH}}{2\pi} = 18B_0$), sometimes by a large factor in the case of high effective magnetic Prandtl numbers and/or thick disks. Scaling to this fiducial flux, we have $B_H = 4.5\Upsilon B_0$, where $\Upsilon = \psi_{BH}/2\pi 18B_0$. Using a least squares fit to the results displayed in Fig.3.2, we find that a good approximation is $\Upsilon \approx 1 + 20P_m(h/r)$. Hence, we
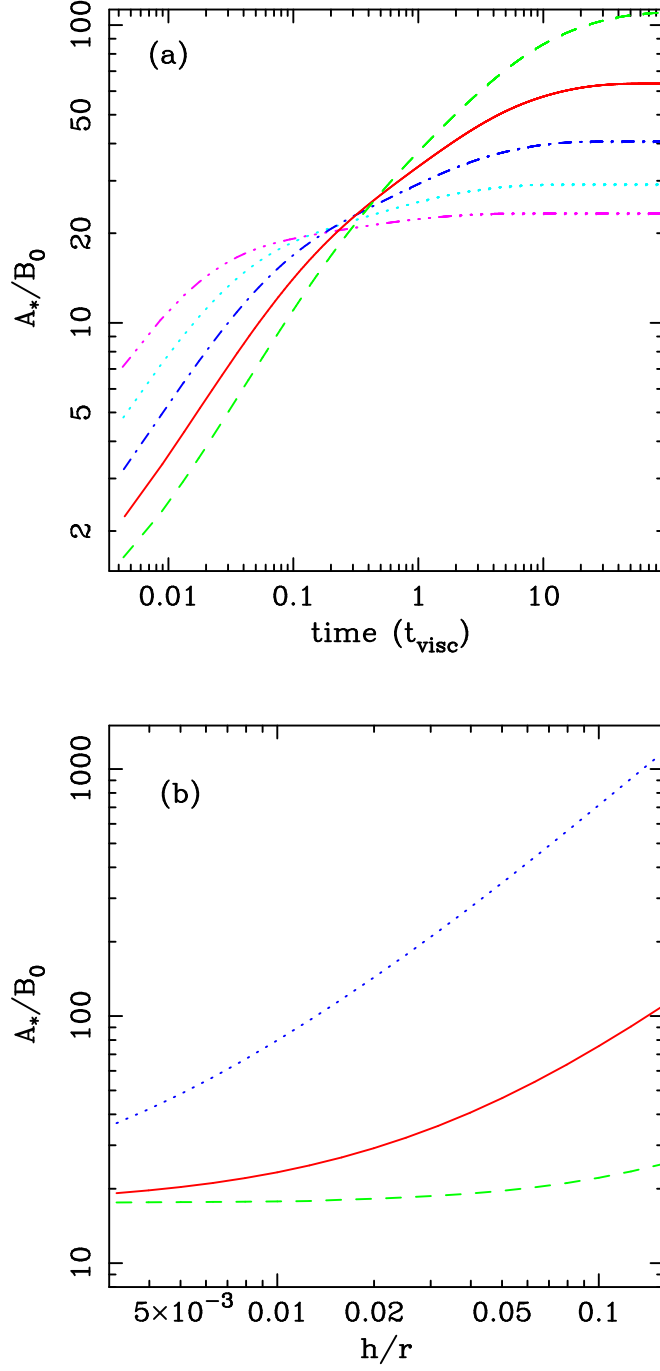
Figure 3.2: *Panel (a)* : Time dependence of the black hole-threading flux for $P_{\mathrm{m}} = 2$ and $h/r = 0.01$ (magenta dot-dot-dot-dash line), 0.02 (cyan dotted line), 0.04 (blue dot-dash line), 0.08 (red solid line), and 0.16 (green dashed line). For comparison, $A_*/B_0 = 18$ corresponds to the flux of the uniform external field threading the radius of marginal stability. Time is in units of the viscous timescale at r_{ms}, $t_{\mathrm{visc}} = r^2 (R^3/GM)/\alpha h^2$. *Panel (b)* : Equilibrium value of A_*/B_0 as a function of h/r for $P_{\mathrm{m}} = 0.2$ (green dashed line), 2.0 (red solid line) and 20.0 (blue dotted line).
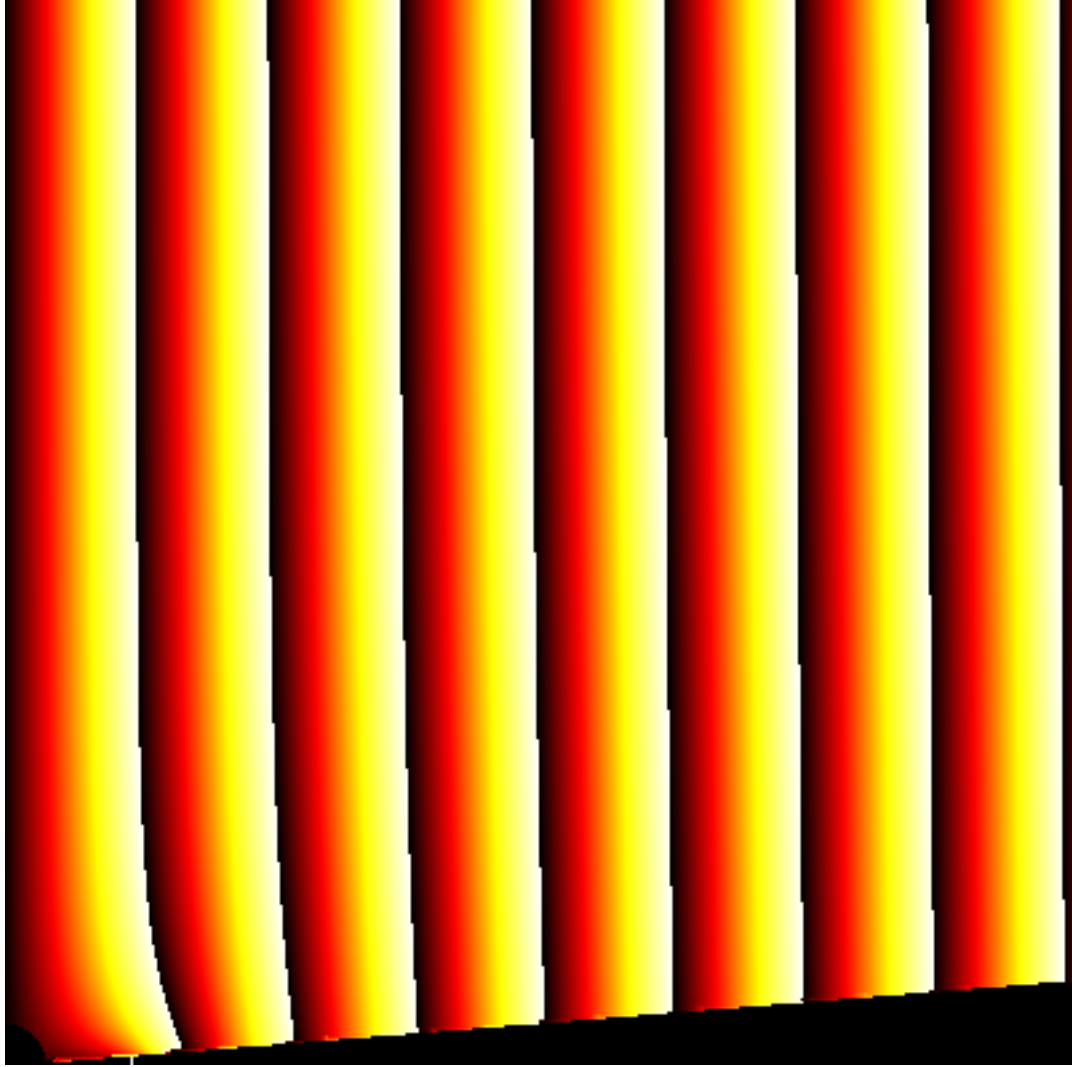
Figure 3.3: Magnetic field configuration for the initial condition of the $h/r = 0.08$ case. The white line is the location of the radius of marginal stability and the black hole is in the lower left corner. The scale is 50 gravitational radii ($\frac{50GM}{c^2}$) on a side.

have

$$B_{\mathrm{H}} \approx 4.5 \left[1 + 20 P_{\mathrm{m}} \left(\frac{h}{r}\right)\right] B_0, \tag{3.27}$$

which is accurate to the 20% level for $P_{\mathrm{m}} < 20$. As we discuss below, the factor multiplying the $P_{\mathrm{m}} h/r$ term in eqn. 3.27 has a dependence on the size of the dead zone; the precise form of eqn. 3.27 is strictly valid only for $r_{\mathrm{dead}} = 100$.
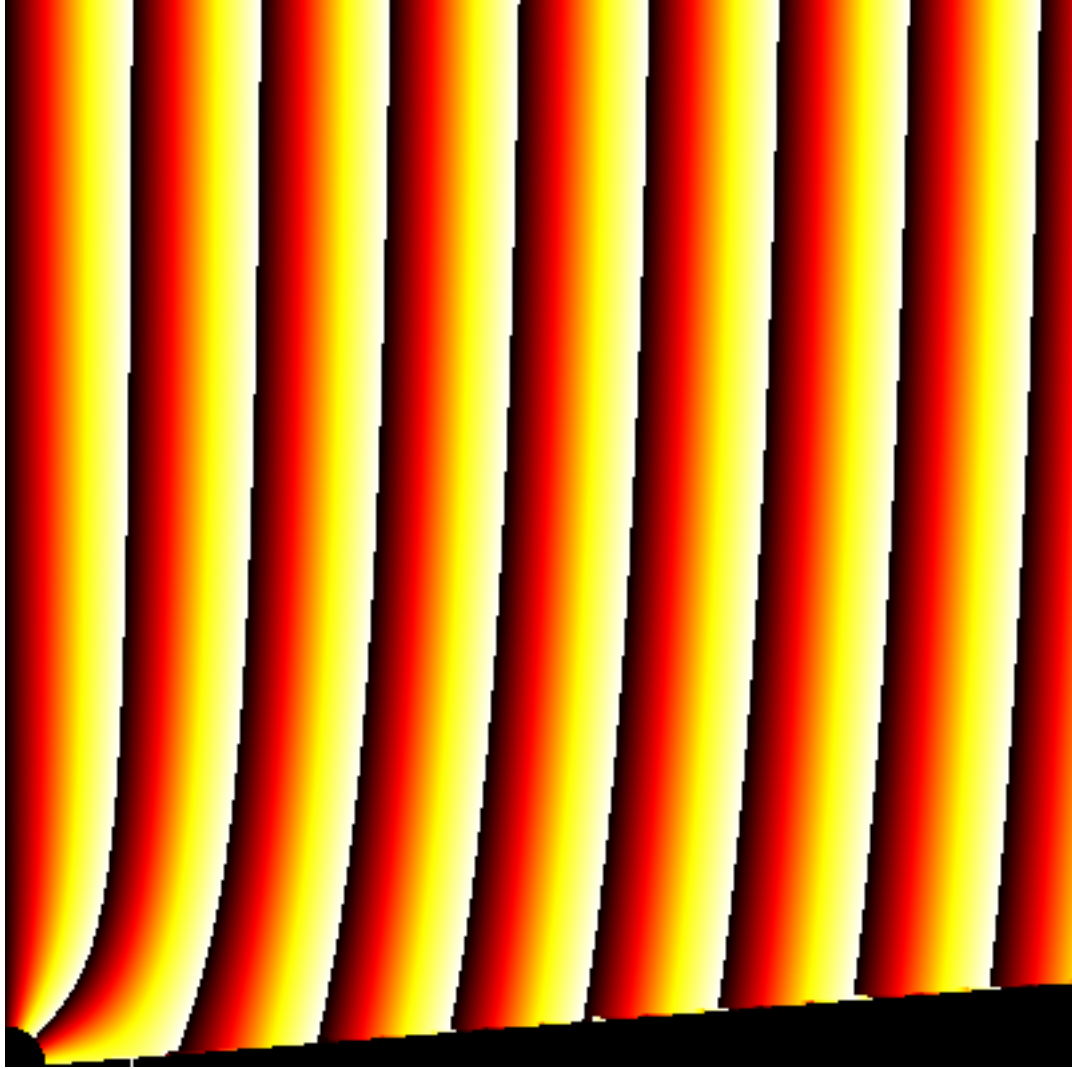
Figure 3.4: Magnetic field configuration for the final state of the $P_m = 2$, $h/r = 0.08$ case with the same dimensions as the previous figure.

3.3 Discussion

3.3.1 Dependence on the size of the dead zone

At first glance, the dragging of magnetic flux by the accretion disk leads to a surprisingly large enhancement in the black hole-threading field. However, as we will now explain, simple arguments can be put forward to support the results encapsulated in eqn. 3.27.

Firstly, we note that the existence of the dead zone is crucial for setting an overall size
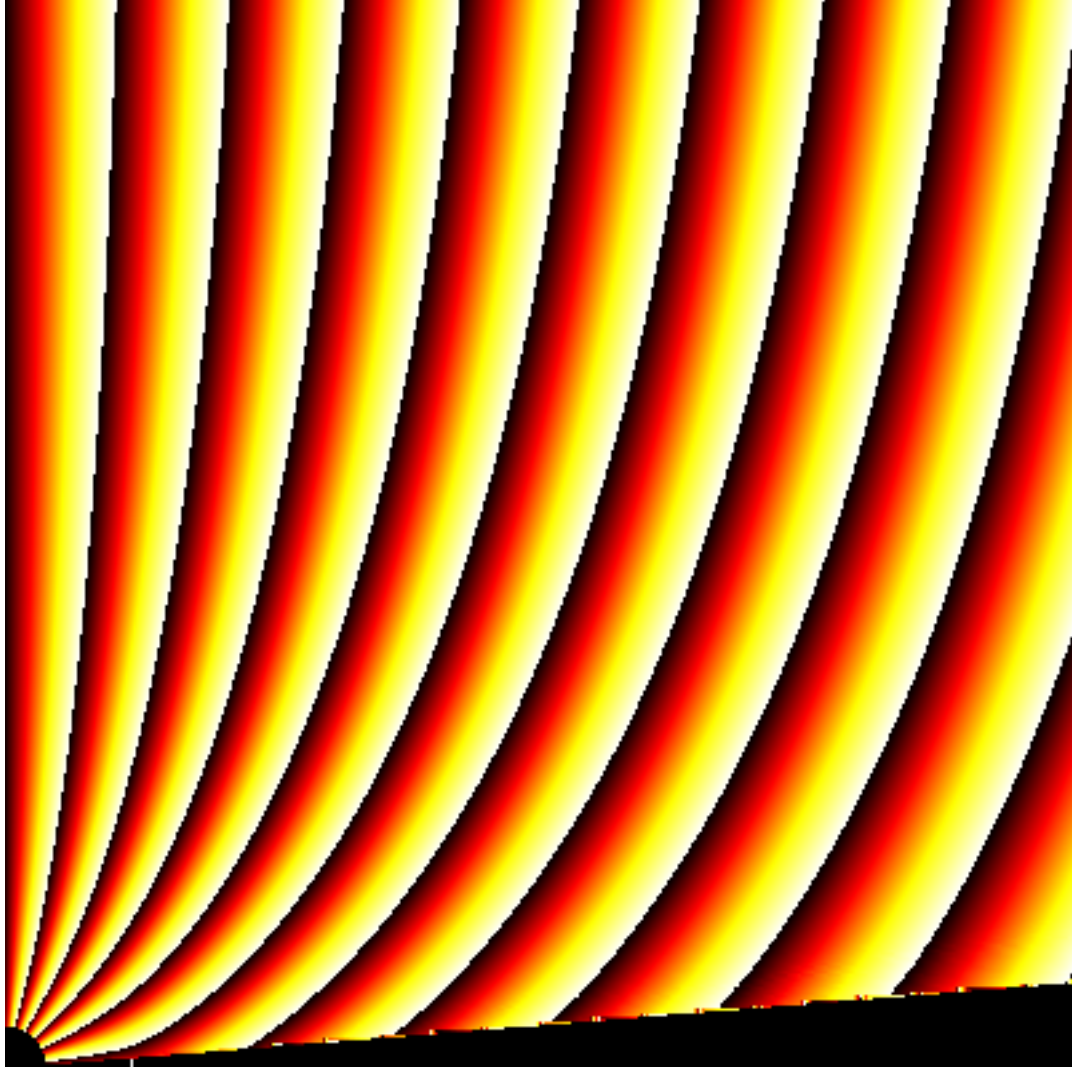
Figure 3.5: The final state of the $P_\mathrm{m} = 20$, $h/r = 0.08$ case. Note how the higher magnetic Prandtl number results in a powerful inward dragging of magnetic field and subsequent magnetization of the black hole. Each of these three figures is 50 gravitational radii ($50GM/c^2$) on a side.

scale to the magnetic disturbances introduced by the disk. To see this, consider the limit in which $r_\mathrm{dead} \to \infty$ (also requiring $r_\mathrm{out} \to \infty$, of course). In this case, the imposed uniform magnetic field is dragged inwards by the accretion flow but a balance will never be achieved between the inward advection and the magnetic tension — without an imposed spatial scale, the field curvature through the disk and hence the magnetic tension can be made arbitrarily small. A balance is possible only when one imposes an outer truncation

on the part of the disk that drags the magnetic flux. In this case, the undragged field at $r > r_{\text{dead}}$ acts as an anchor and limits the vertical extent to which the magnetic field can be appreciably distorted. Indeed, our calculations show that the magnetic field at $|z| > r_{\text{dead}}$ is essentially just the imposed uniform field.

Now, as already noted, we find that the magnetic field threads the active part of the diffusive accretion disk ($r_{\text{ms}} < r < r_{\text{dead}}$) with a bend angle (away from the disk normal) of $\tan i \equiv B_r / B_z \approx h P_{\text{m}} / r$. As shown by HPB and Lubow et al. (1994), this is a direct consequence of a balance between outward magnetic diffusion due to field-line tension and the inwards advection of magnetic field,

$$v_r \frac{\partial \psi}{\partial r} \approx \eta_* \left(\frac{\partial \psi}{\partial z} \right)_{z=h}. \tag{3.28}$$

Consider the field line that threads the inner edge of the diffusive disk at $r = r_{\text{ms}}$. This field line follows a roughly parabolic path in the magnetosphere that can be described by the flux function $\Psi = \Psi_0 (r^2 + 2\xi z) = \text{constant}$. We can determine the parameter ξ using the fact that, at the disk plane, we have $B_r / B_z \approx r / h P_{\text{m}}$,

$$\frac{B_r}{B_z} = -\frac{\partial \Psi / \partial z}{\partial \Psi / \partial r} = -\frac{\xi}{r_{\text{ms}}} \approx \left(\frac{h}{r} \right) P_{\text{m}}, \tag{3.29}$$

where we have dropped a term that is second order in (h/r). At a vertical distance of $z = r_{\text{dead}}$, this same field line has a cylindrical radius R given by

$$R^2 = r_{\text{ms}}^2 \left[1 + 2 \frac{r_{\text{dead}}}{r_{\text{ms}}} \left(\frac{h}{r} \right) P_{\text{m}} \right] \tag{3.30}$$

Using our observation above concerning the vertical extent of the field disturbances, we use the fact that the field is essentially uniform for $|z| > r_{\text{dead}}$ to read off the magnetic flux threading the plunge region and hence the black hole,

$$\Phi_{\text{H}} = \pi R^2 B_0 = \pi r_{\text{ms}}^2 B_0 \left[1 + 2 \frac{r_{\text{dead}}}{r_{\text{ms}}} \left(\frac{h}{r} \right) P_{\text{m}} \right]. \tag{3.31}$$

In terms of the field threading the hole (putting $r_{\text{ms}} = 6r_g$) we get

$$B_{\text{H}} = 4.5 \left[1 + \frac{r_{\text{dead}}}{3} \left(\frac{h}{r} \right) P_{\text{m}} \right] B_0. \tag{3.32}$$

70
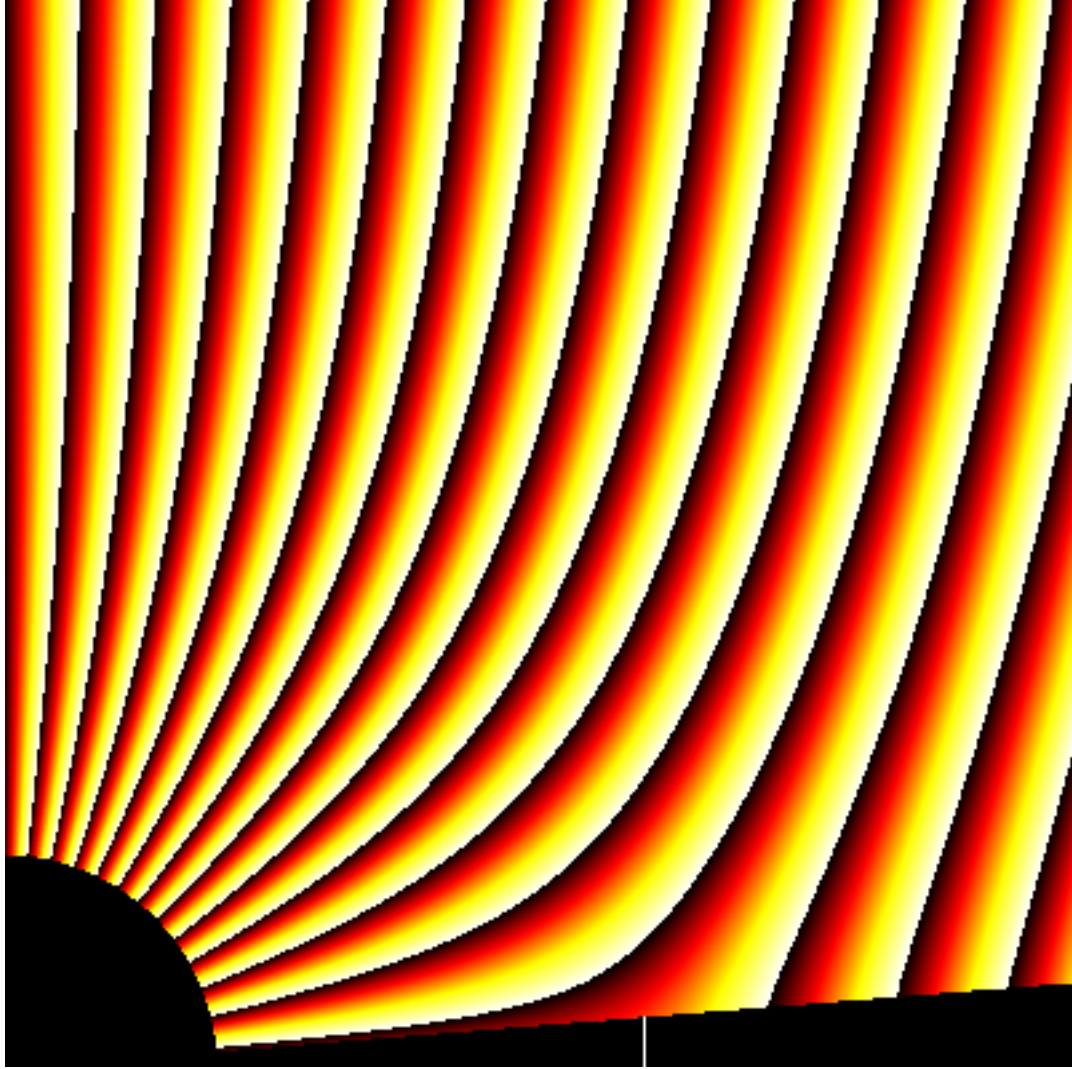
Figure 3.6: Magnetic field configuration for the plunge boundary condition. The figure shows a zoom-in ($10GM/c^2$ on a side) of the final field structure in the $P_\mathrm{m} = 2$, $h/r = 0.08$ case. A white vertical line on the accretion disk denotes the radius of marginal stability.

Thus we can see that the numerical factor multiplying the $(h/r)P_\mathrm{m}$ term in eqn. 3.27 is directly related to the value of r_dead.

The above discussion helps to elucidate the role of the plunge region in enhancing the black hole-threading flux — the plunge region "shields" the diffusive part of the disk from the large bundle of magnetic flux that threads the black hole. This bundle of flux is the ultimate repository for the magnetic flux that has been scooped up by the accretion flow. The larger the region of the disk that can drag the flux inwards, the larger is this
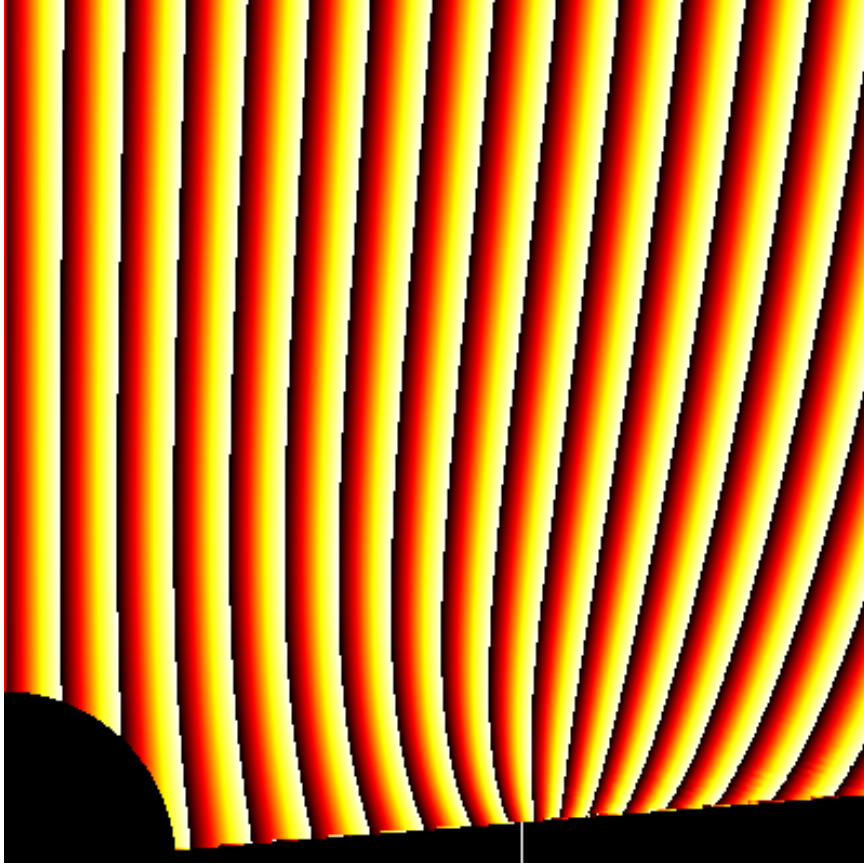
Figure 3.7: Magnetic field configuration for the uniform flux bundle boundary condition. The figure shows a zoom-in ($10GM/c^2$ on a side) of the final field structure in the $P_\mathrm{m} = 2$, $h/r = 0.08$ case. A white vertical line on the accretion disk denotes the radius of marginal stability.

repository. To illustrate this issue, we have run a modified version of our code in which the plunge region boundary condition is replaced with the assumption that the magnetic flux contained within $r = r_\mathrm{ms}$ has the form of a uniform field on the disk plane. We employ canonical values of the model parameters; $h/r = 0.08$, $P_\mathrm{m} = 2$, and $r_\mathrm{dead} = 100$. As expected, we get a weak (50%) enhancement in the flux contained within $r = r_\mathrm{ms}$, compared with over a factor of 3 for the plunge case. The magnetic field structures of the two cases are illustrated in Fig. 3.6 and 3.7.

Performing a full numerical solution to eqn. 3.22 for $r_\mathrm{dead} = 50$, $r_\mathrm{dead} = 100$ and $r_\mathrm{dead} = 200$ reveals that the enhancement of the magnetic flux increases with r_dead slightly

more slowly than the linear relationship predicted by our simple arguments in this section. Since the implementation of the dead zone is one of most artificial aspects of our toy model, we will not explore this dependence in any more detail here. In real systems, the dead zone might be identified with the outer edge of the MHD turbulence dominated accretion disk, e.g., the self-gravity region in an AGN disk or the tidal truncation radius for the disk in a Galactic Black Hole Binary (GBHB). Both of these radii are likely to be at significantly larger radius than $r_{\text{dead}} = 100$ used here. Alternatively, if the magnetosphere is treated using a full MHD wind model, the crucial length-scale which determines the magnetic field enhancement is likely be the vertical height of the Alfvénic surface. In addition, the radius of the dead zone could also represent the transition radius in an Advection Dominated Accretion Flow (ADAF) outwards of which the extreme thinness of the disk results in negligible inflow velocity. It is beyond the scope of this chapter to address such models. However, our approach allows us to illustrate an essential point; that the inward dragging of magnetic field over some region of the inner disk coupled with the existence of the plunge region allows a significant enhancement in the strength of the magnetic field threading the black hole.

3.3.2   Limitations of our approach

Before discussing the astrophysical implications of our result, we must address the three major limitations of our approach. First, we have made no attempt to include relativistic effects (beyond our simple treatment of the radius of marginal stability) on the dynamics or electrodynamics of the disk/field system. Our model is an adequate representation for slowly spinning black holes (where the radius of marginal stability is rather large and in a comparatively low-gravity region of spacetime), but we acknowledge that a full relativistic electrodynamic treatment is required to robustly treat the case of rapidly rotating black holes. While the same basic phenomenon of magnetic flux trapping by the plunge region

73

is at work around rapidly rotating black holes, the geometry of the system (i.e., the fact that the radius of marginal stability is much closer to the event horizon) is unfavorable for producing dramatic enhancements in the black hole-threading magnetic field. We show this in the next chapter when we extend this model to the relativistic regime.

Second, we assume the existence of a pre-existing large scale magnetic field. The origin of such a field depends upon the system under consideration. For the accreting black hole at the heart of a Gamma-Ray Burst (GRB) collapsar, such a field may arise naturally from the collapsed stellar envelope. In the case of AGN, the field corresponds to that of the accreting interstellar medium. For GBHBs, the presence of a large scale field probably depends on the mode of accretion, with wind-accretors likely possessing a much stronger and better organized large scale field than Roche-lobe overflow accretors.

Third, we assume axisymmetric large scale fields with a disk magnetosphere consisting of force-free and purely poloidal field. As mentioned, a more physical treatment would entail matching an MHD wind solution to the disk-plane flux function. With such an approach, one could capture the inertial effects of a disk outflow on the field structure, the hoop stresses resulting from any toroidal fields present, and the angular momentum losses in the disk due to the wind. These could have competing effects on the ultimate ability of the disk to drag the field into the plunge region. The inertial effects will tend to bend the field lines outwards, increasing the field-line curvature at the disk plane and hence increasing outward diffusion of the field. The loss of disk angular momentum to the wind, on the other hand, would lead to an increase in the radial velocity of the accretion flow but no change in the magnetic diffusivity. This, in turn, increases the inwards advection of the magnetic field. Clearly, more detailed calculations of this scenario are warranted. As for the axisymmetric assumption, we note that Spruit & Uzdensky (2005) have recently examined the dragging of a large scale magnetic field by an accretion disk under the assumption that the MHD turbulence in the disk concentrates the field into small

bundles (giving rise to the accretion disk equivalent of Sun spots). Through an analysis of the dynamics of these bundles, they conclude that this is a generally favorable scenario for accumulating a large amount of magnetic flux in the central regions of the disk. Thus, in at least one specific model, an extreme deviation from axisymmetry aids in the inward dragging of magnetic flux.

We reiterate that the principal result of this chapter is that the existence of a plunge region together with magnetic field dragging in the accretion disk can significantly enhance the black hole-threading magnetic field and hence the BZ effect. Furthermore, the enhancement becomes increasingly effective for thicker disks or higher magnetic Prandtl numbers.

3.3.3 Astrophysical implications

Given the caveats discussed above, the results of this chapter have important implications for the strength of the black hole-threading field and the relevance of the BZ process. Suppose that the magnetic pressure due to the large scale field B_0 is a fraction f of the maximum pressure in the accretion disk, p_{max}, i.e., $B_0 = (8\pi f p_{\mathrm{max}})^{1/2}$. Using this together with eqn. 3.1 and eqn. 3.27 gives, $L_{\mathrm{BZ}} \approx 5\pi\omega_F^2 f p_{\mathrm{max}} \Upsilon^2 r_{\mathrm{H}}^2 a_*^2 c$. Using the expressions for p_{max} for radiation pressure-dominated (RPD) and gas pressure-dominated (GPD) disks from Moderski & Sikora (1996) and GA97, and assuming the usual BZ impedance matching criterion is obeyed, gives

$$L_{\mathrm{BZ}} \approx \begin{cases} 1.5 \times 10^{45} \alpha^{-1} f M_8 \Upsilon^2 a_*^2 & \text{RPD} \\ 9 \times 10^{43} \alpha^{-9/10} f M_8^{11/10} \dot{m}_{-4}^{4/5} \Upsilon^2 a_*^2 & \text{GPD} \end{cases} \tag{3.33}$$

where we have scaled to a black hole mass of $M = 10^8 M_8$ and $\dot{m} = 10^{-4}\dot{m}_{-4}$ is the mass accretion rate in Eddington units. This can be directly compared with the expressions for L_{BZ} in GA97 if we set $f\alpha^{-1} \approx 0.1$ (which results from their relation between α and the disk magnetic field). For $\Upsilon = 1$ (corresponding to small effective magnetic Prandtl

numbers or very thin disks), we find low BZ luminosities that agree very well with those computed by GA97. However, as we have shown, large magnetic Prandtl numbers and/or thick disks can result in large enhancements of the black hole-threading fields, approximately described by $\Upsilon \approx 1 + 2xP_{\mathrm{m}}(h/r)$, where $x \sim O(r_{\mathrm{dead}}/r_{\mathrm{ms}})$. The BZ luminosity is then enhanced by a factor of Υ^2.

It is interesting to explore astrophysical consequences of the strong h/r dependence of the equilibrium hole-threading flux ψ_*. There is mounting empirical evidence that black hole systems produce jets only when a geometrically thick accretion disk is present. The best case can be made for the GBHBs, as discussed by Fender, Belloni & Gallo (2004). In their X-ray low-hard (LH) state (a.k.a. the power-law state; McClintock & Remillard 2004) they display steady optically-thick radio cores which, in Cygnus X-1, can be spatially resolved into a jet-like structure by VLBA (Stirling et al. 2001). It is generally believed that the inner regions of the accretion flow in a LH-state GBHB system is radiatively inefficient, hot, and hence geometrically-thick ($h/r \sim 0.5$). However, the radio jet is seen to shut off once the source has made a transition to the high-soft (HS) state (or thermal state; McClintock & Remillard 2004) which is believed to correspond to an inner accretion disk which is radiatively efficient and hence significantly thinner. We postulate that the jet in the LH state is powered by the BZ effect which is enhanced by the flux trapping effect of the plunge region. Some time after a transition to a HS state, the system will possess a disk with a similar accretion rate but significantly reduced thickness. For a fixed accretion rate, the maximum pressure in a disk scales as $p_{\mathrm{max}} \propto (h/r)^{-1}$. Using our parameterization for Υ, we expect the BZ luminosity scales as $L_{\mathrm{BZ}} \propto f(h/r)$, provided $h/r \gg 1/xP_{\mathrm{m}}$. Hence, due to the inability of a thin disk to trap flux on the black hole, the BZ luminosity of the HS state will be much reduced leading to the suppression of the radio jet.

The actual LH $\rightarrow$ HS transition itself is particularly interesting. It is during this tran-

sition (when the source crosses the "jet line" on the X-ray flux/color diagram) that powerful relativistic outflows are produced which, for example, produce the superluminal radio blobs seen from microquasars. It is likely that the transition is driven by the thermal collapse of the LH-state hot disk, producing a structure that eventually evolves into the HS-state cold disk. The nature of the intermediate structure is unclear, however. It has been suggested that the thermal collapse produces a magnetically-dominated region (e.g., Meier 2005) in which MRI-driven turbulence is suppressed and accretion proceeds only through large scale magnetic torques. If the pre-collapse disk is threaded by a large scale magnetic field, this field could readily become dynamically important in the post-collapse disk (since rapid thermal collapse will proceed at constant surface density, producing a disk pressure which scales as $p_{\mathrm{max}} \propto h/r$). Subsequent magnetic braking of the disk would lead to rapid inflow, a rapid accretion of poloidal flux onto the black hole, and a rapid increase in the importance of the BZ effect. The powerful ejections seen from GB-HBs as they undergo this transition might be the result of such a scenario. The ejections would terminate once the inner disk has ceased to be magnetically dominated (due to the accretion of matter from the outer disk), hence re-establishing a turbulent state with high effective magnetic diffusivity.

3.4   Conclusions

Black hole rotation is, in principle, a more than sufficient source of energy for energizing even the most powerful relativistic jets. The viability of magnetic extraction of black hole spin energy does, however, hinge on the strength of the horizon-threading poloidal magnetic field that can be established by the accretion flow. In this chapter, we have argued that the plunge region of the black hole accretion disk has an important role to play in enhancing the horizon-threading field well above the modest levels suggested by previous

works. We support this hypothesis by constructing a toy-model (that is non-relativistic, assumes axisymmetry, and treats the fields away from the disk plane as potential) with which we can follow the dragging of an external magnetic field by the disk and its subsequent trapping by the plunge region. Our toy model suggests that the BZ effect can be enhanced above the canonical estimates of GA97 by a factor of $[1 + x P_{\mathrm{m}}(h/r)]^2$ where P_{m} is the effective magnetic Prandtl number of the disk and $x \sim O(r_{\mathrm{dead}}/r_{\mathrm{ms}})$. Even in cases where the effective magnetic diffusivity is significant due to the MHD turbulence (i.e., $P_{\mathrm{m}} \sim 1$), the BZ effect can be enhanced by one order of magnitude (or more) above the GA97 value if the disk is geometrically-thick $h/r \approx r_{\mathrm{ms}}/r_{\mathrm{dead}}$. The h/r-dependence of this effect has an appealing resonance with the empirical evidence from GBHBs which points to a close connection between the existence of powerful black hole jets and the inferred properties of the accretion disk

Chapter 4

Relativistic generalization of the flux trapping model

Our goal in this Chapter is to construct a relativistic version of the flux-trapping model described in Chapter 3. We show that the $a = 0$ limit produces flux accumulation values close to those obtained in the non-relativistic study, establishing the validity of the Chapter 3 results for slowly spinning black holes. Our central result is that the ability of the plunge region to enhance the black hole threading field decreases as the spin of the black hole increases. We find that the BZ power is not a monotonically increasing function of black hole spin and, instead, has a maximum when $a \approx 0.8$. In section 4.1.1, we describe the formalism of the relativistic extension of the flux-trapping model. We discuss the covariant nature of the magnetic flux function and the equations it satisfies. In section 4.2 we present our results and show that the hole-threading flux decreases with increase in spin. This appears to be largely a geometrical effect connected to the radial positions of the marginally stable orbit and the horizon as a function of spin. In section 4.3, we discuss the implications of our model in view of the recently discovered correlation between jet power and accretion rate found by Allen et al. (2006). Section 4.4 presents our

conclusions.

4.1   The relativistic flux-trapping model

We consider a geometrically-thin accretion disk around a Kerr black hole threaded by a large scale poloidal magnetic field. On small scales, the magnetic field lines are frozen into the highly conductive plasma of the accretion disk. However, if we coarse-grain our view to larger scales, we expect that the large scale magnetic field lines can undergo turbulent diffusion through the disk plasma. Heyvaerts et al. (1996) have shown that the effective magnetic Prandtl number (i.e., the ratio of the effective turbulent viscosity to the effective turbulent magnetic diffusivity) is order unity. Hence a field line threading the disk will be dragged inwards by accretion, but radial magnetic pressure gradients and magnetic tension (associated with field line curvature as it threads the disk) will lead to competitive field line diffusion. We expect the region above and below the disk to possess a very low plasma density, and hence for the magnetic field in this region to have a force-free configuration. As argued in Chapter 3, poloidal field lines threading through the plunge region of the accretion flow will be dragged very rapidly onto the black hole, leaving the plunge region devoid of poloidal magnetic flux.

Below we enumerate the idealizations and construction of our model system.

1. Our accretion disk is described by a Novikov & Thorne (1974) disk truncated at the marginally stable orbit, inwards of which is the plunging region. We assume that the large scale magnetic field does not perturb the structure of the turbulent accretion flow. The central object is assumed to be a standard Kerr black hole whose gravitational potential dominates the system.

2. In the magnetosphere (the region outside of the black hole and accretion disk) we assume that the plasma density is negligible and hence that the magnetic field is

force free. In addition to this, we also impose the constraint that the poloidal mag-

netospheric currents are weak or, equivalently, that the toroidal component to the

magnetic field is negligible. Macdonald (1984) shows that spin-up of the hole has

negligible effect on the poloidal field structure which allows us to treat the magne-

tosphere in the limit of negligible currents. With these assumptions, the system is

described as a vacuum solution to Maxwell's equations (in the Kerr spacetime) in

the magnetosphere.

3. As discussed above, we assume that no poloidal magnetic flux threads the plunge

   region of the accretion disk. Any magnetic flux that is advected inwards across the

   radius of marginal stability is immediately added to the flux bundle threading the

   black hole.

4. The boundary condition on the horizon requires imposing finite electric and mag-

   netic fields as measured by freely-falling observers crossing the horizon. Znajek

   (1978) calculated the appropriate boundary condition on the horizon under this as-

   sumption for a force-free magnetosphere. This condition is imposed on the horizon

   in our model as

$$\psi = \frac{2\psi_0}{1 + \left[\sin^2\theta/(1-\cos\theta)^2\right]\exp[-2a^2\cos\theta/(r_+^2+a^2)]}, \tag{4.1}$$

   where r_+ is the radial coordinate of the horizon and ψ_0 is the magnitude of the flux

   threading the horizon which is determined by the numerical solution. In essence,

   the boundary condition imposed on the horizon amounts to fixing the a and θ de-

   pendence of the above function. Finally, the fundamental assumption of our model

   is that no magnetic flux threads the plunging region of the disk [$r_{\text{evt}} < r < r_{\text{ms}}$;

   $\theta = \pi/2 - \tan^{-1}(h/r)$].

5. Far away from the black hole and at poloidal angles above the accretion disk, we

   assume the large-scale field is uniform and impose an appropriate outer boundary

condition that captures this assumption. Therefore, the black hole magnetosphere is surrounded by a perfectly conducting sphere. Far away from the black hole but in the plane of the accretion disk we impose a "dead zone" as in Chapter 3. The only difference between this region and the active disk region is that the radial inflow velocity is set to zero. In the dead zone, therefore, magnetic field lines are not dragged toward the black hole. As pointed out in greater detail in Chapter 3, this dead zone dramatically reduces the sensitivity of the system to the treatment of the outer boundary. The physical nature of the dead zone is addressed in Chapter 3. Unlike in Chapter 3, the outer boundary condition here is fixed.
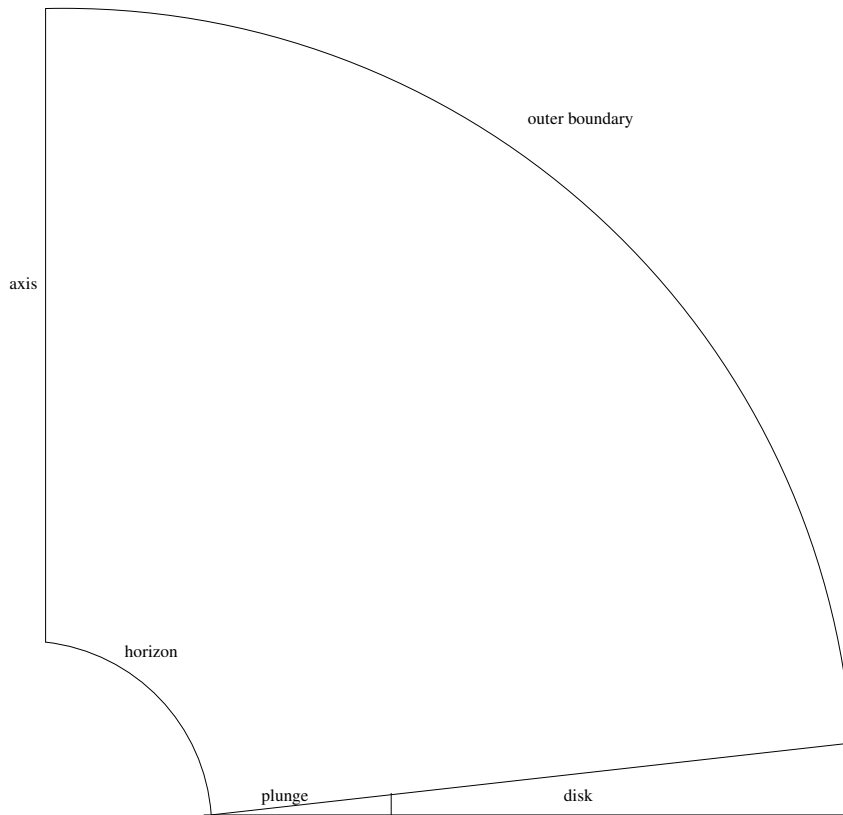

Figure 4.1: Boundaries for our axisymmetric simulations

4.1.1 Basic equations of our model

We assume that the underlying spacetime metric is the Kerr (1963) metric, i.e., that the gravitational field of the rotating black hole completely dominates over that of the accretion disk. Throughout this Chapter, we will work in Boyer-Lindquist coordinates in which the Kerr metric takes the standard form,

$$
\begin{aligned}
dS^2 &= -\left(1 - \frac{2Mr}{\rho^2}\right) dt^2 - \frac{4Mar\sin^2\theta}{\rho^2} dt\, d\phi \\
&+ \frac{\Sigma}{\rho^2}\sin^2\theta\, d\phi^2 + \frac{\rho^2}{\Delta} dr^2 + \rho^2 d\theta^2,
\end{aligned}
\tag{4.2}
$$

where

$$
\rho^2 = r^2 + a^2\cos^2\theta,
\tag{4.3}
$$

$$
\Delta = r^2 - 2Mr + a^2,
\tag{4.4}
$$

and

$$
\Sigma = (r^2 + a^2)^2 - a^2\Delta\sin^2\theta.
\tag{4.5}
$$

The basic equation describing the evolution of the (large-scale) magnetic field within the acccretion disk is obtained by following the relativistic analogue of the non-relativistic treatment of Chapter 3. One difference between our approach and that of Chapter 3 is that we only seek the stationary (time-independent) solution; this results in a significant simplification in the relativistic equations that we must deal with. As in Chapter 3, we also assume that the poloidal field structure is axisymmetric. The equation describing the field evolution within the disk is obtained by combining Maxwell's equation

$$
\nabla_b F^{ab} = \mu J^a,
\tag{4.6}
$$

with a simplified Ohm's law

$$
J^a = \sigma F^{ab} u_b - u^a J_b u^b,
\tag{4.7}
$$

where F^{ab} is the standard Faraday tensor, μ is the permeability of the plasma, J^a the 4-current, u^a the 4-velocity of the accretion disk flow, and σ is the effective conductivity of the turbulent plasma. This gives

$$\nabla_b F^{ab} = \frac{1}{\eta} F^{ab} u_b - \mu u^a u_b J^b, \tag{4.8}$$

where $\eta = 1/\mu\sigma$ is the effective magnetic diffusivity. The effective nature of these disk quantities comes from the fact that although the conductivity itself is expected to be very large in these astrophysical plasmas, they are characterized by turbulence which means that reconnection cannot be neglected. In order to capture the effect that magnetic reconnection has on the coarse-grained field geometry, one introduces a finite effective conductivity or effective diffusivity. The second term on the right-hand side of equation 4.8, which we include for completeness, is zero by the MHD assumption that proper electric charge vanishes. Therefore, the disk is governed by

$$\nabla_b F^{ab} = \frac{1}{\eta} F^{ab} u_b. \tag{4.9}$$

The equations are cast in terms of the vector potential, which is related to the Faraday tensor via

$$F_{ab} = A_{b,a} - A_{a,b}, \tag{4.10}$$

and, in particular, in terms of the component A_ϕ in the coordinate basis of the Boyer-Lindquist coordinates.

Ultimately, to examine BZ powers, we need to derive the magnetic flux threading a hoop placed at a given radius r within the accretion disk. The magnetic flux function is related to the vector potential via Stokes' Theorem applied to the Faraday tensor

$$\psi \equiv \int_S F = \int_S dA = \int_{\partial S} A = 2\pi A_\phi, \tag{4.11}$$

where S is a space-like surface with boundary ∂S consisting of a ring defined by $r =$ constant, $\theta =$ constant, and $t =$ constant. Because we work with the vector potential, A_b,

we comment briefly on the choice of gauge. Since A_b is specified up to the gradient of a scalar function Γ,

$$A_b' = A_b + \nabla_b \Gamma, \qquad (4.12)$$

the assumption of time-independence and axisymmetry gives us

$$A_t' = A_t \qquad (4.13)$$

and

$$A_\phi' = A_\phi. \qquad (4.14)$$

Thus, we need not specify the gauge uniquely beyond the statement of t and ϕ independence. Writing eqn. 4.9 in terms of the vector potential, and applying time-independence and axisymmetry, yields

$$\frac{\partial}{\partial r}\left[g^{11}\left(g^{30}\frac{\partial A_t}{\partial r} + g^{33}\frac{\partial A_\phi}{\partial r}\right)\right] + \frac{\partial}{\partial \theta}\left[g^{22}\left(g^{30}\frac{\partial A_t}{\partial \theta} + g^{33}\frac{\partial A_\phi}{\partial \theta}\right)\right] \qquad (4.15)$$

$$\frac{1}{2}\left(g^{00}\frac{\partial g_{00}}{\partial r} + 2g^{30}\frac{\partial g_{30}}{\partial r} + g^{33}\frac{\partial g_{33}}{\partial r} + g^{11}\frac{\partial g_{11}}{\partial r} + g^{22}\frac{\partial g_{22}}{\partial r}\right)g^{11}\left(g^{30}\frac{\partial A_t}{\partial r} + g^{33}\frac{\partial A_\phi}{\partial r}\right) +$$

$$\frac{1}{2}\left(g^{00}\frac{\partial g_{00}}{\partial \theta} + 2g^{30}\frac{\partial g_{30}}{\partial \theta} + g^{33}\frac{\partial g_{33}}{\partial \theta} + g^{11}\frac{\partial g_{11}}{\partial \theta} + g^{22}\frac{\partial g_{22}}{\partial \theta}\right)g^{22}\left(g^{30}\frac{\partial A_t}{\partial \theta} + g^{33}\frac{\partial A_\phi}{\partial \theta}\right)$$

$$= \frac{1}{\eta}u_r g^{11}\left(g^{30}\frac{\partial A_t}{\partial r} + g^{33}\frac{\partial A_\phi}{\partial r}\right).$$

where the $g_{\alpha\beta}$ and $g^{\alpha\beta}$ are the lower and upper metric terms in the Boyer-Lindquist coordinates, and are evaluated at the disk surface ($\theta = \pi/2 - \tan^{-1}(h/r)$ where h/r is the fractional thickness of the disk), and the numbering in the metric terms are connected to the coordinates via ($0 = t, 1 = r, 2 = \theta, 3 = \phi$). This is our final equation describing the magnetic flux threading the accretion disk.

As in the non-relativistic case (Chapter 3), we need to match the field in the disk onto the magnetospheric field in order to fully specify the solution. As described previously, our assumptions for the magnetosphere lead to the vacuum Maxwell equations

$$\nabla_b F^{ab} = 0. \qquad (4.16)$$

In the magnetosphere we also impose the ideal MHD condition

$$F^{ab}u_b = 0,$$ (4.17)

where u^b is the 4-velocity of the (tenuous) plasma in the magnetosphere and is determined by the condition that (in steady-state) field lines rigidly rotate. In terms of the vector potential, our final equation describing the vector potential in the magnetosphere is,

$$0 = \frac{\partial}{\partial r}\left[g^{11}\left(g^{30}\frac{\partial A_t}{\partial r} + g^{33}\frac{\partial A_\phi}{\partial r}\right)\right] + \frac{\partial}{\partial \theta}\left[g^{22}\left(g^{30}\frac{\partial A_t}{\partial \theta} + g^{33}\frac{\partial A_\phi}{\partial \theta}\right)\right]$$ (4.18)

$$\frac{1}{2}\left(g^{00}\frac{\partial g_{00}}{\partial r} + 2g^{30}\frac{\partial g_{30}}{\partial r} + g^{33}\frac{\partial g_{33}}{\partial r} + g^{11}\frac{\partial g_{11}}{\partial r} + g^{22}\frac{\partial g_{22}}{\partial r}\right)g^{11}\left(g^{30}\frac{\partial A_t}{\partial r} + g^{33}\frac{\partial A_\phi}{\partial r}\right) +$$

$$\frac{1}{2}\left(g^{00}\frac{\partial g_{00}}{\partial \theta} + 2g^{30}\frac{\partial g_{30}}{\partial \theta} + g^{33}\frac{\partial g_{33}}{\partial \theta} + g^{11}\frac{\partial g_{11}}{\partial \theta} + g^{22}\frac{\partial g_{22}}{\partial \theta}\right)g^{22}\left(g^{30}\frac{\partial A_t}{\partial \theta} + g^{33}\frac{\partial A_\phi}{\partial \theta}\right).$$

Our basic philosophy is to solve eqn. 4.18 for the magnetic field structure in the magnetosphere using eqn. 4.15 as a boundary condition to be applied on the disk surface. Additional boundary conditions are required. The magnetic flux is fixed to be zero on the black hole spin axis (i.e., the field is assumed to be finite on the axis). We bound the region under consideration by an outer spherical boundary at large r, and assume that the flux threading that boundary corresponds to a uniform field with strength B_0, i.e., we set $\psi = r^2\sin^2\theta B_0$. The boundary condition on the horizon is determined by the Znajek condition (Macdonald 1984) with explicit form given by equation 4.1.

4.1.2 Solution method

We adopt a relaxation method approach to solve for the time-independent magnetic flux configuration around a Kerr black hole. Through this relaxation process, we derive the steady-state solution to equation 4.18 given the boundary conditions discussed above. At the start of the numerical solution, we thread the accretion disk with uniform magnetic field everywhere which is not a steady-state solution to equation 4.15. We then jointly relax the magnetic configuration both in the magnetosphere and on the disk surface until

a solution to equations 4.18 and 4.15 is obtained. As the solution evolves, the magnetic flux at the disk inner edge changes. As previously mentioned, a consequence of our boundary condition on the plunge region is that any magnetic flux advected across the radius of marginal stability is immediately added to the flux bundle threading the black hole. As the disk supplies flux to the horizon via the plunge region, Maxwell pressure will lead to a high-latitude expansion of the hole-threading flux bundle, changing the field geometry in the magnetosphere away from the uniform initial state. As this happens, the diffusion terms in equation 4.15 increase.

Flux accumulation occurs even once the hole-threading field is significantly greater than the disk-threading field because the plunge region is shielding the disk-field from the magnetic pressure associated with the hole-threading field. However, the system does settle into steady-state when the disk-threading field is bent by the expanded black hole flux-bundle such that outward field line diffusion balances inward advection. The physics is the same as that described in Chapter 3 with the exception of relativity. The steady-state solution to equation 4.15 is the relativistic analog of the steady-state solution to equation 3.22 of Chapter 3 and the steady-state solution to equation 4.18 is the relativistic analog of equation 3.17 of Chapter 3.

In our canonical numerical solution, space is divided into a (r, θ)-grid, with 72 zones in r and 51 zones in θ. The radial coordinate runs from the horizon to an outer boundary at $r = 53$, and is spaced in a geometric progression such as to give a factor of almost 2 difference in the zone spacing at the inner and outer boundary. The θ coordinate runs from the axis ($\theta = 0$) to the disk surface, and is uniformly spaced in $\cos \theta$.

4.1.3 Newtonian vs. relativistic treatments of non-rotating black holes

It is important to examine whether the Newtonian analysis of Chapter 3 accurately describes the physics of the flux-dragging model in the slowly rotating black hole case. We choose to compare the flux-trapping that results for $a = 0$ against a Newtonian treatment, with magnetic Prandtl number fixed at $P_m = 20$ and varying disk thickness. Given our different treatment of the outer boundary condition, it would be inappropriate to compare our Schwarzschild results directly with the results of Chapter 3, however. Instead, we use our code to derive both the Schwarzschild results and the Newtonian limit ($c \rightarrow \infty$). The results are displayed in Fig. 4.2, where, to be consistent with the notation of Chapter 3, we plot the ratio $\frac{A_*}{B_0}$ where $A_* = A_\phi$. The difference between the Newtonian and relativistic cases for all disk thicknesses is a few percent. This demonstrates that the neglect of the relativistic terms for slowly rotating black holes is justified, as hypothesized in Chapter 3.

4.1.4 Resolution and convergence study

It is necessary to confirm that our results do not rely on our particular choice of numerical resolution. We chose to examine the effects of resolution on a representative model with $a = 0.4$ and $h/r = 0.1$, and $P_m = 20$, increasing in resolution from our canonical 72×51 case to 100×80. The results can be seen in Table 1, where we compare the equilibrium hole-threading flux of each case with that obtained at our canonical resolution. It can be seen that the higher resolution run agrees very well with a hole-threading flux that is only 1.5% lower despite more than doubling the number of computational cells.

It is equally important to demonstrate that our relaxation scheme achieves convergence. In Figure 4.3 we show the dependence of the hole-threading flux on the relaxation parameter t for the specific value of $a = 0.2$. It is indeed seen that the hole-threading flux
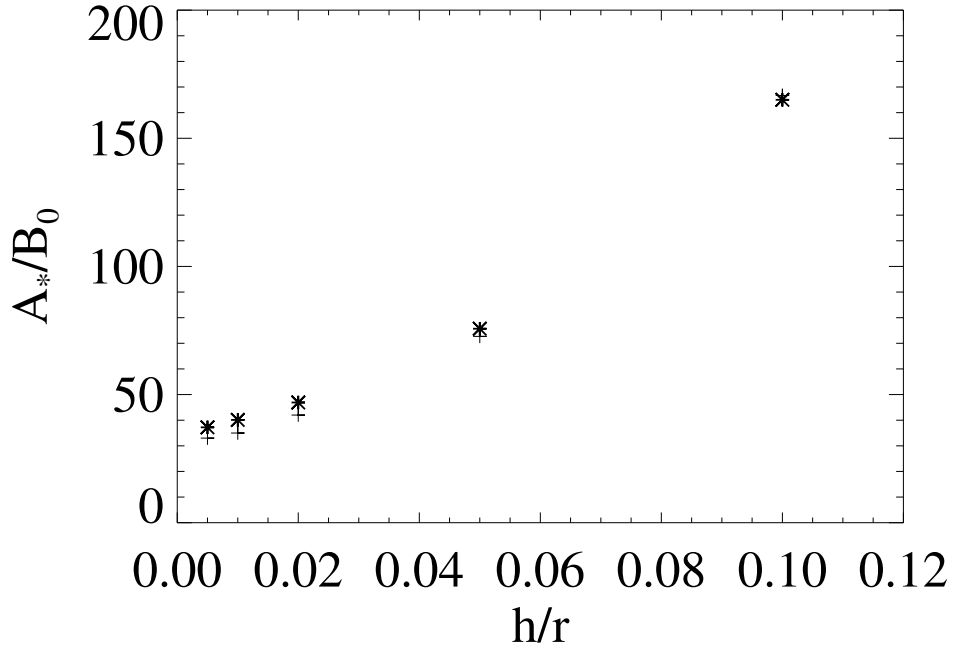
88

Figure 4.2: Equilibrium value of A_*/B_0 as a function of h/r for P_m=20.0 for Newtonian (asterisk) and Schwarzschild disk (cross). Notice how the Newtonian values are larger and by a greater amount for smaller disk thickness. As the thickness increases the difference between Newtonian and Schwarzschild decreases until for largest thickness the Schwarzschild value overtakes the Newtonian. Nevertheless, the differences are always of a few percent, establishing the fact that the Newtonian treatment is sufficiently accurate for slowly rotating black holes.

spin	r/$\theta grid$	ψ_{norm}	% difference
0.4	72 by 51	1	0
0.4	100 by 51	1.004	0.4
0.4	100 by 80	0.985	1.5

Table 4.1: Resolution study for flux obtained at $a = 0.4$.

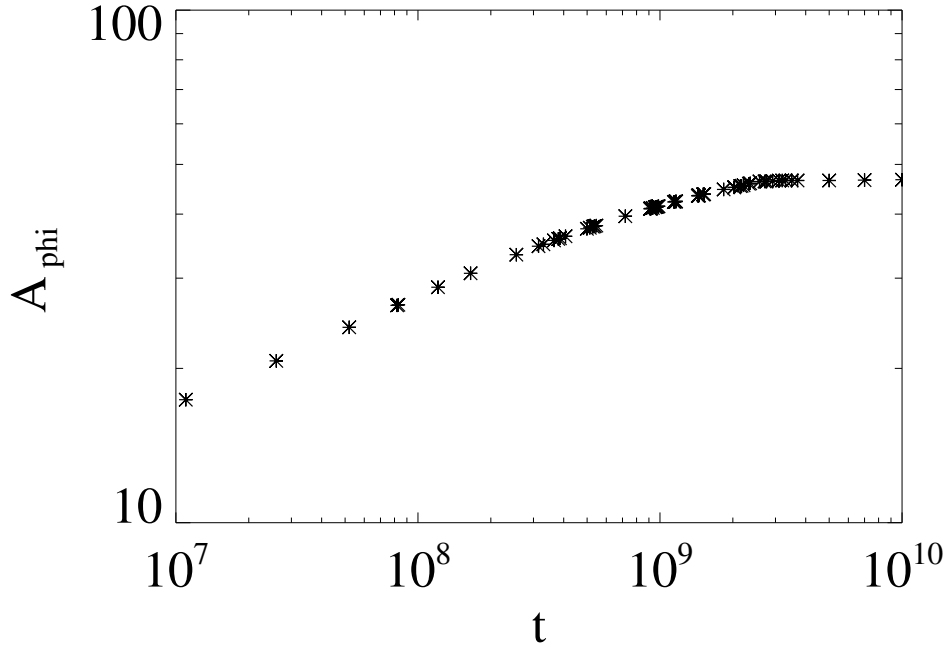appears to reach convergence. This behavior is typical for all spin runs.

Figure 4.3: Value of A_ϕ as a function of the relaxation parameter t showing the typical behavior of the runs. This one is for $a = 0.2$.

4.2 Results: spin dependence of flux trapping

We evaluate the steady-state solution to the above equations for various black hole spin values and for $P_m = 20$, a disk thickness of $h/r = 0.1$, $r_{dead} = 40$ and $r_{out} = 53$. We find that the flux accumulated on the black hole horizon decreases as the spin increases (Figure 4.4). The reason behind the decrease in flux with increase in spin appears to have a straightforward geometrical interpretation. As the spin of the hole increases, the accretion disks' inner edge (at the radius of marginal stability) gets closer to the horizon in both coordinate and proper distance. This results in a decrease of the ratio of the area within the plunge region to the area of the event horizon. Thus, as one considers more rapidly rotating black holes, the geometry becomes progressively less favorable to shielding the turbulent accretion disk from the hole-threading flux bundle. We show the
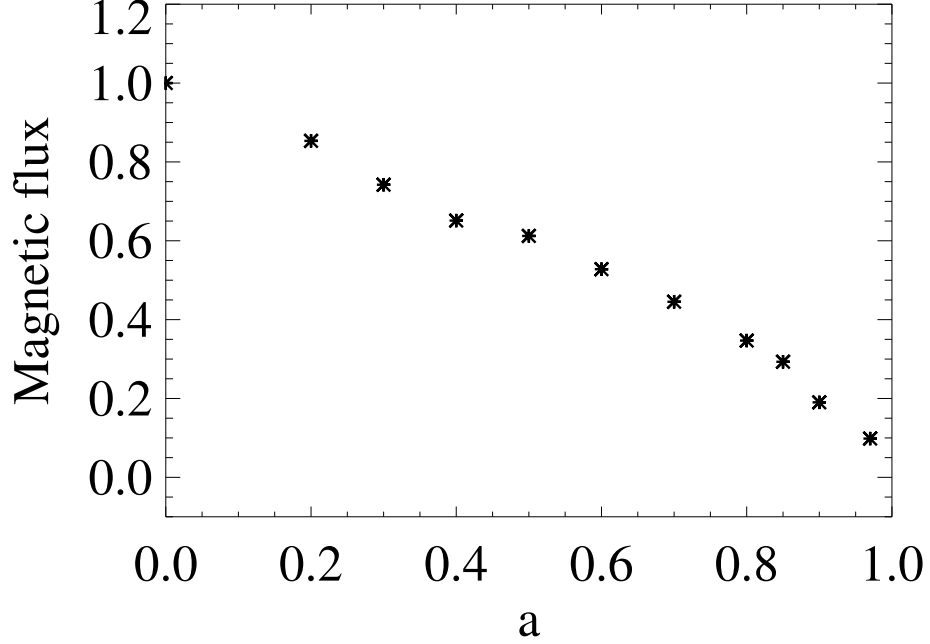
Figure 4.4: Magnetic flux threading the horizon normalized to the flux in the spin-zero case, vs. black hole spin illustrating the basic result that flux-trapping is less effective as the spin increases.

magnetic field geometry for $a = 0.85$ in Fig. 4.5.

As mentioned above, the behavior of the radius of marginal stability for rapidly spinning black holes results in ineffective shielding of the hole-threading flux bundle from the turbulent (diffusive) portion of the accretion disk. In short, flux-trapping breaks down for largest spin.

We now consider the BZ power that results from the trapped magnetic flux and its dependence on black hole spin. We start by evaluating the horizon-threading magnetic field as measured by zero-angular-momentum observers (ZAMO) from the flux values we obtain,

$$B_H = \sqrt{g_{11}} B^r \tag{4.19}$$
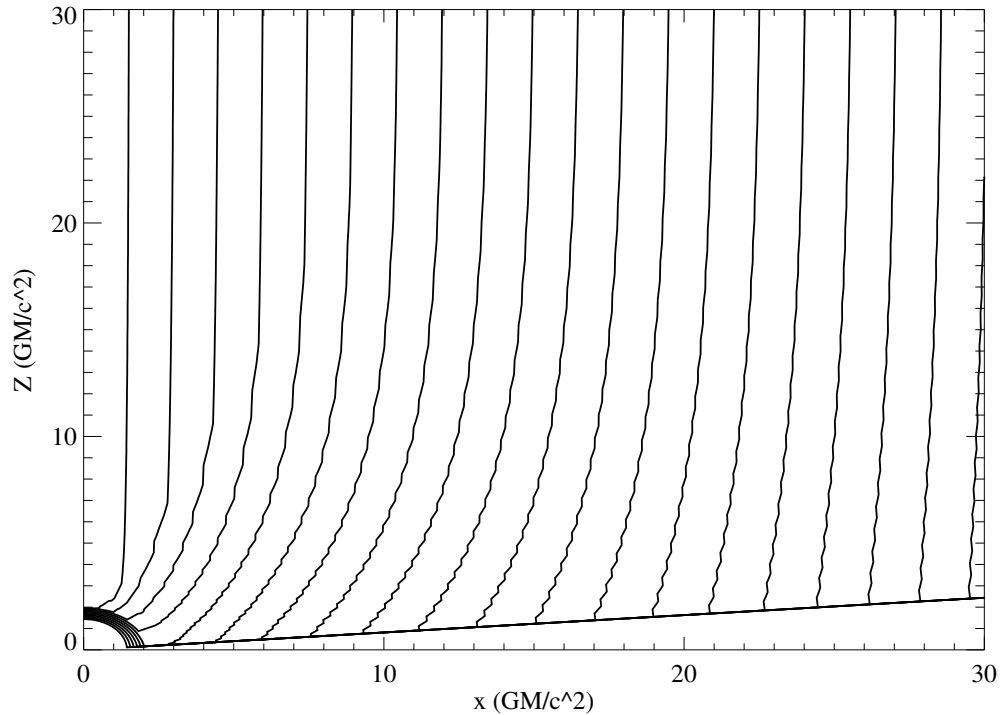
with

$$B^r = *F^{rb} u_b, \tag{4.20}$$

91

Figure 4.5: Lines of constant magnetic flux for a=0.85 Kerr black hole. Each side is 30 BL radii across. The marginally stable circular orbit is located at $r = 2.6$. Note how field lines are allowed to thread the equatorial plane for radial coordinate values that are smaller than for a spin zero disk (Fig. 3.6).

where $*F^{ab}$ is the dual Faraday tensor and u^b is the four-velocity of the ZAMO observers evaluated in the equatorial plane on the horizon membrane (in the sense of Thorne et al, 1986). The dual tensor components involve terms with derivatives of A_ϕ with respect to θ and therefore require the use of the boundary condition on the horizon membrane (eq. 4.1). The results depend on the value of B_0, the initial uniform field strength threading the horizon. The results are displayed in Figure 4.6. With these values of the horizon-threading magnetic fields, we can determine the BZ luminosity. This is shown in Figure 4.7. Despite possessing the largest hole-threading magnetic field, the Schwarzschild case, of course, produces no BZ power. Because of the low flux threading the horizon in the high spin case, the luminosity in this case is also low. The maximum BZ power is generated for $a \approx 0.8$. We note that the accumulated flux on the black hole depends
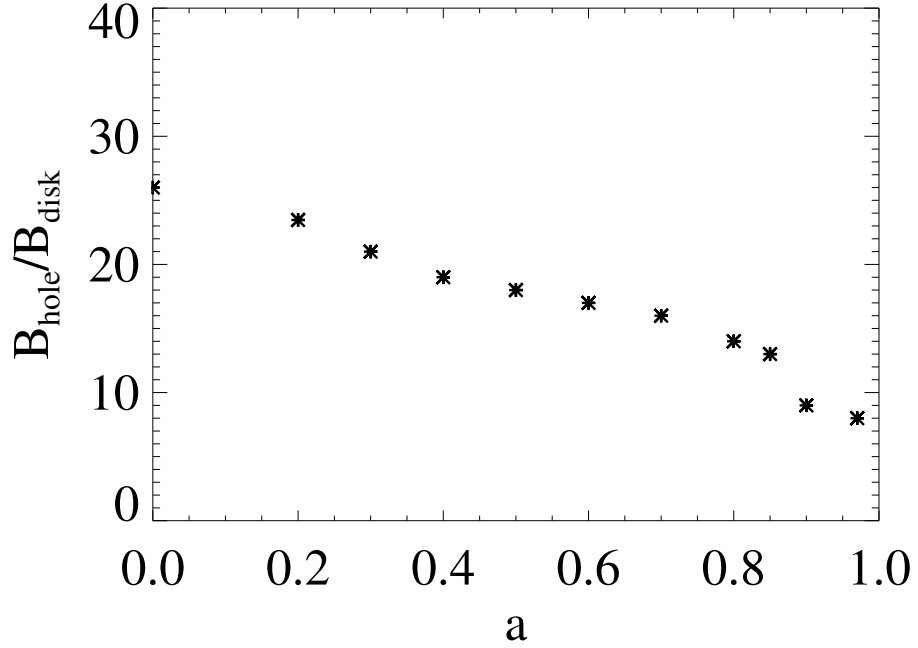
Figure 4.6: Ratio of the horizon-threading magnetic fields in the flux-trapping model and uniform field case.

linearly or almost so, on the radial coordinate value of the outer region of the active accretion disk. We have truncated the active region of our disk at $r_{dead} = 40$ outwards of which the disk fluid is characterized by zero radial velocity so the dragging of flux occurs only inwards of r_{dead}. As pointed out in Chapter 3, r_{dead} is one of the most artificial aspects of our model, but could be identified with the outer edge of the MHD-turbulence dominated accretion disk, or as the transition radius between an outer thin disk and an inner ADAF disk. We see, thus, that by increasing our active region of the disk and/or increasing the disk thickness, we could increase the generated luminosity. However, we remind the reader that our analysis is performed with large magnetic Prandtl number (i.e. 20) and thus with low diffusion. Chapter 3 shows that lower values of Pr_m will generate considerably lower black hole threading flux. One final point is in order. The outer boundary condition at $r = 54$ is fixed which means that field dragging by the
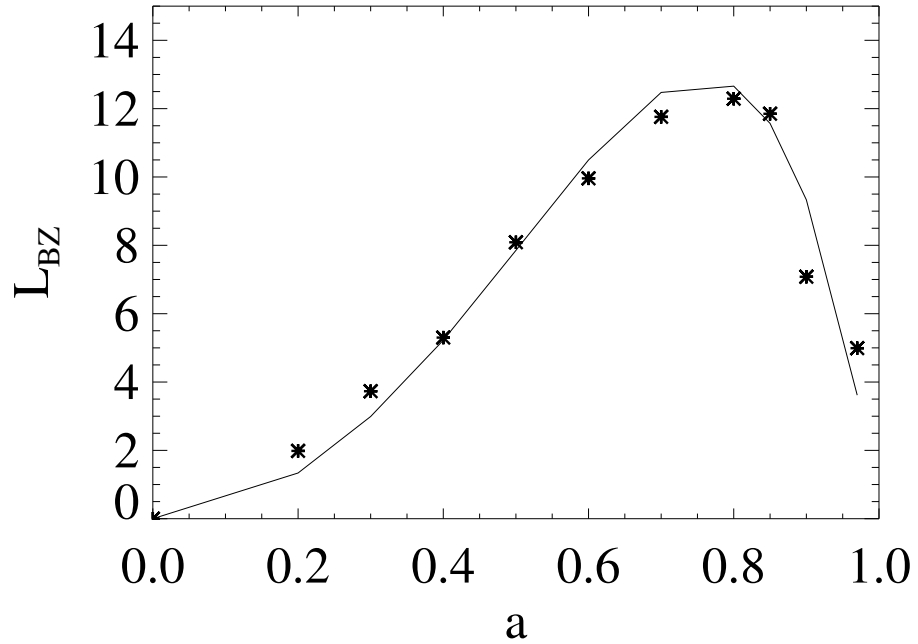
Figure 4.7: The individual points label the relative Blandford-Znajek luminosity as a function of spin. The solid line is the parametrization we adopt in the Nemmen et al. idl code.

disk towards the black hole will generate bending of field lines that is greater than an analogous simulation in which the outer boundary is at a larger radial coordinate. Since the bending of field lines increases the diffusion term in equation 4.15, the choice of fixed outer boundary not only decreases the overall flux accumulation on the hole, it does so more for smaller choice of outer radial coordinate value. Like r_{dead}, r_{out} is an artificial aspect of our model whose physical value might be interpretable as some kind of load region where flux-freezing forbids flux lines from being dragged along with the field threading the accretion disk. In Chapter 3, on the other hand, we did not fix the field at r_{out}, thereby allowing the field to be dragged unrestricted by the outer boundary value. Nevertheless, these caveats do not affect our basic qualitative result that the BZ luminosity is maximized for intermediate values of the black hole spin parameter. We consider this

an important and novel result.

4.3 Discussion - an application of the flux-trapping model to the $\dot{M}$-jet power correlation

In the previous section we showed that the magnetic field threading the black hole decreases as the spin increases. This produced a BZ power that is maximized for intermediate values of spin, with a peak at $a \approx 0.8$. We can accurately parameterize the behavior of L_{BZ} vs. a with the following overall empirically determined spin dependence

$$L_{BZ} \propto (1 - a^4)a^2. \tag{4.21}$$

This expression does a good job at reproducing the numerically determined points in Figure 4.7. Using this parametrization, we will now show that our model has immediate application to the curious properties of jetted AGN in nearby elliptical galaxies.

Allen et al. (2006) used the *Chandra* X-ray observatory to study nine nearby X-ray luminous elliptical galaxies. Assuming central black hole masses given by the M-σ relation, *Chandra* measurements of the ISM temperature and density on scales $\approx 10pc$ from the cores of these galaxies could be used to deduce the rate at which ISM accretes into the gravitational potential of the black hole. These estimates are based on the simple spherical accretion picture of Bondi (1952). In addition, *Chandra* reveals ISM cavities that have been blown by jet activity from the central AGN. Using "PdV" arguments (and assuming that the cavities have an age given by their sound crossing time), the jet powers could be deduced. It was found that

$$P_{jet} \approx \eta \dot{M} c^2 \tag{4.22}$$

where the average efficiency is $\eta \approx 3\%$ (See Fig. 4.8 which reproduces Fig. 4 from Allen et al. 2006). The object-to-object scatter about the correlation (eqn. 4.22) is small, with
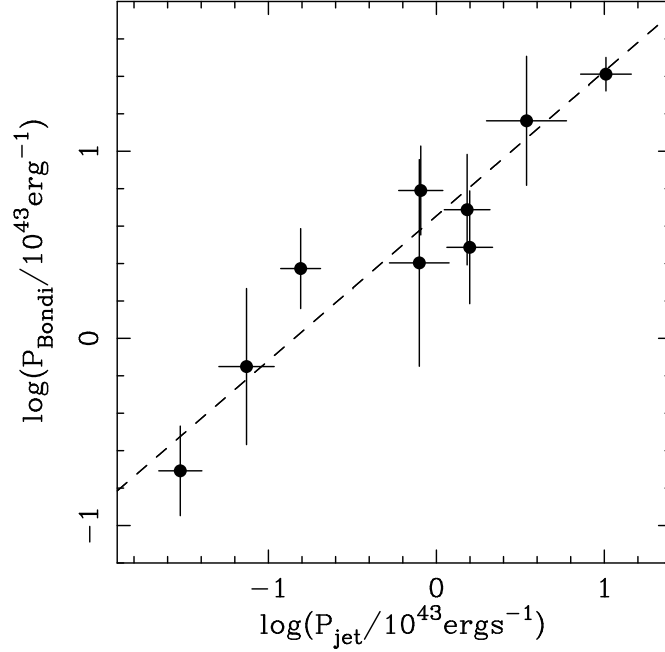
Figure 4.8: The logarithm of the Bondi accretion power (in units of $10^{43}\,\mathrm{erg\,s^{-1}}$) from Chandra X-ray data assuming an efficiency of 0.1 for conversion of rest mass into energy, versus the logarithm of the jet power (courtesy of Allen et al).

deviations in efficiency of only a factor of ≈ 2.

Nemmen et al. (2006) have explored whether the Allen et al. correlation is a natural result of the BZ mechanism. Employing the Narayan & Yi (1995) advection dominated accretion flow (ADAF) model, which is likely appropriate for the low accretion rates found in these elliptical galaxies, Nemmen et al. estimated the strength of the magnetic field in the central disk as a function of accretion rate and then estimated the BZ efficiency, η_{BZ}, as a function of black hole spin, where

$$\eta_{BZ} \equiv \frac{L_{BZ}}{\dot{M}c^2}. \tag{4.23}$$

They follow Meier (2001) to connect the jet power to the ADAF flow by enhancing the magnetic field in the inner accretion disk via frame-dragging. They showed that the Allen et al. results could only be reproduced if the elliptical galaxy black holes were all rapidly

spinning and there was rather little mass loss in the accretion disk between the Bondi radius and the black hole. Most disturbing, however, was that η_{BZ} was found to be a very sensitive function of spin a, especially for $a \approx 1$. See dashed line in Figure 4.9. Hence, all of the black holes in the Allen et al. sample would need to possess almost the same, high spin values. They found that η_{BZ} changed by almost a factor of 20 as one considers black holes with spin in the range $a = 0.8 - 1$ (see dashed line in Figure 4.9). Hence, to reproduce the tight correlation of the Allen et al. sample, all of the black holes in these nine galaxies would need to possess almost the same high spin value. In other words, the Nemmen et al. model suffers a fine tuning problem.
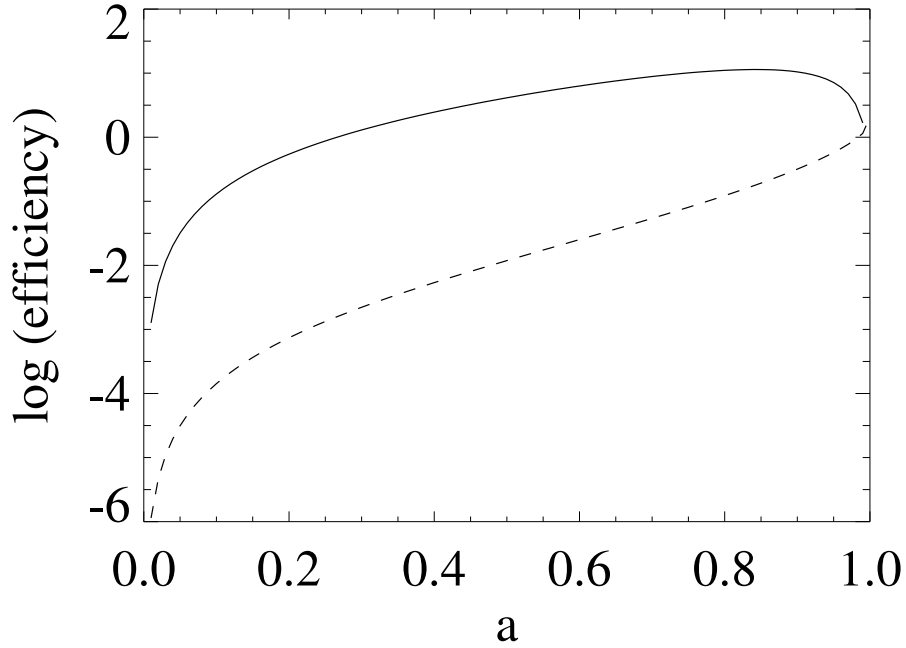
Figure 4.9: The efficiency η_{BZ} vs. spin for the BZ model for a standard horizon-threading magnetic field (dashed line) vs. that in the flux-trapping model (solid line).

We have taken the ADAF model of Nemmen and included the effects of flux trapping via our approximate parametrization. The resulting η_{BZ} as a function of a is shown in Fig.4.9 and compared with that of Nemmen et al. (2006). The fact that the BZ power in the flux trapping model is a maximum for intermediate values of spin results in η_{BZ} that is

a very flat function of spin for high spin. Furthermore, the efficiency that can be produced by the BZ mechanism in the flux trapping model is substantially higher reaching almost $\eta_{BZ} \approx 1000\%$. Of course, since the actual source of the energy is the black hole spin, the BZ efficiency as defined above (i.e., the BZ luminosity ratioed against the rest-mass energy of the accretion flow) can exceed unity without violating energy conservation. Thus we can tolerate a much larger mass loss between the Bondi radius and the black hole. Numerical investigation of rotating Bondi flows (e.g. Proga & Begelman 2003) suggests that only $\alpha\dot{M}$ reaches the black hole where $\alpha \approx 0.01 - 0.1$ is the effective viscosity parameter. Such a mass loss can be tolerated by these BZ models only if one includes the effects of flux trapping. We suggest that this provides a much more compelling framework for the exploration of the Allen et al. correlation than the more standard BZ model of Nemmen et al.

4.4   Conclusions

We postulated that given the dynamics of the plunge region of a thin black hole accretion disk, flux trapping can enhance the strength of the magnetic field threading the horizon by a significant factor. Our results indicate that a diffusive accretion disk will generate progressively weaker horizon-threading magnetic fields as the spin of the hole increases. Because the power generated via the BZ mechanism depends on the strength of the magnetic field threading the black hole horizon, our results indicate that high spinning black holes will not generate the maximum BZ luminosity. Therefore, if the trapping behavior of the plunge region operates in accretion systems around black holes, and if the energy emitted is BZ luminosity, the most powerful AGN jets occur for intermediate spin black holes. We then followed the program of Nemmen et al. to show that the enhancement due to the flux-trapping model on the BZ power is sufficient to explain the energies of the

nine jets in the Allen et al sample including an attractive indeterminacy in the black hole spin. In other words, we have shown that within the context of the flux-trapping model, we are not forced to assume a narrow range of spins for the central supermassive black holes of the nine elliptical galaxies. In addition, the jet efficiency in the flux-trapping model allows for greater mass loss in the accretion flow via BP winds.

This work has focused on the flux-trapping that results for the more stable co-rotating accretion disks. However, counter-rotating accretion disks where the black hole spin axis is oriented at 180 degrees to that of the accretion flow, may exist for relatively short time periods. The question arises as to what kind of BZ power would we obtain for such configurations. Because of the dependence of the strength of the hole-threading magnetic field on the locations of the marginally stable orbit and of the horizon, we expect that flux-trapping would be much greater for retrograde spins. This is because the marginally stable orbit moves further away from the horizon as the spin increases. In fact, as the black hole spin approaches $a \approx 1$, the marginally stable circular orbit of a counter-rotating accretion disk moves out to $r \approx 9r_g$. We see, therefore, that if counter-rotating accretion disks surround highly spinning supermassive black holes, the BZ power is not only much greater than we have determined for co-rotating accretion disks, it would also be greater for larger spin. The largest BZ power would occur for a maximally counter-rotating black hole accretion disk around a maximally spinning black hole. Such arguments could form the basis for understanding the enormous powers (up to $\approx 10^{48} \mathrm{ergs}^{-1}$) of the giant radio galaxies.

Chapter 5

Conclusions and Future Work

The emerging paradigm for the workings of AGN jets involves the interaction between supermassive black holes and large scale magnetic fields. But the presence of magnetic fields around black holes does not limit itself to the production of jets. Less collimated outflows may also have a magnetic origin and particular time-dependent phenomena in the inner disk region may also originate as a result of the presence of magnetic fields. In this dissertation we have investigated two types of interaction between the magnetic field and the surrounding black hole-accretion disk system that tend to appear in GRMHD simulations regardless of the initial seed magnetic field.

In Chapter 2 we studied the possible consequences of magnetic torques connecting the horizon or near black hole region with the inner accretion disk. We showed that this type of scenario produces a dissipation profile that is unlike that of the standard Shakura & Sunyaev or Novikov & Thorne models, with energy being deposited in the inner accretion disk. We then showed that this increased dissipation in the inner disk region can lead to a quenching of the X-ray flux further out in the disk corona and can serve as an explanation to the observed "Deep Minimum" State of the Seyfert galaxy MCG-6-30-15.

In Chapter 3 we studied the non-relativistic flux-trapping model to show that strong large scale magnetic field can thread the black hole horizon even though weak field may

thread the inner edge of the accretion disk. We found that the strength of the hole-threading magnetic field increases with disk thickness, the effective magnetic Prandtl number, and the location of the dead zone. We also discussed the relation of this to the behavior of jets during GBHB state transitions.

In Chapter 4 we extended the study of Chapter 3 to the relativistic regime in Kerr metric. We confirmed the appropriateness of the results of Chapter 3 for slowly spinning black holes and then studied the strength of the horizon-threading magnetic field as a function of spin. The crucial result from this study is that given the validity of the plunge region boundary condition, the largest Blandford-Znajek luminosity is produced for intermediate spins of $a \approx 0.8$. We then showed that our model provides the most natural explanation to the observed correlation between jet power and accretion rate for a sample of AGN in nearby elliptical galaxies. We show that the remarkable constancy in jet production efficiency can be explained without having to fine tune the spins of the black holes to their maximum values.

5.0.1 Future work

We have pointed out the fact that of the two main mechanisms for producing relativistic outflows, the Blandford & Payne mechanism may fail to produce the highly relativistic outflows observed. On the other hand, the Blandford & Znajek mechanism is a Poynting flux based process. Although a number of possible scenarios have been envisioned, it is not clear how a Poynting flux dominated jet in origin can convert this energy into kinetic form as the observations require. Perhaps this intermediate step is unneccessary. In other words, could magnetic fields in the central region of black hole accretion systems be the agent responsible for taking the azimuthal flows characteristic of accretion and directly generating axial flow of plasma?

The exploration of this idea depends, roughly speaking, on the details of the gravito-

magnetic interaction near the black hole. In order to produce the strong magnetic stresses that are required to produce the energy in the jet, the plasma and field must be brought in close to the horizon so that spacetime can twist magnetic field in tightly. There is a direct relationship between the twisting of field and the outflow energy. On the other hand, the closer plasma gets to the horizon of the black hole, the stronger gravity becomes. The horizon wants the plasma so there is an essential tension between gravity and Lorentz forces, both vying for the plasma. The details concerning the ultimate fate of plasma and of the nature of Poynting flux generated during this intense interaction between magnetic and gravitational forces is basically unclear. What is clear is that such issues arise specifically in the context of magnetic field brought to the black hole via a relatively thin accretion disk as a result of the fact that plasma and field approach the black hole in the plane of the disk. When dealing with accretion around black holes, is equatorial field dragging a ubiquitous phenomenon? In other words, is it possible to bring plasma and field close to the black hole, but say, near the pole of the hole as opposed to the equatorial plane? What kind of accretion system would produce magnetic field configurations that involve plasma near the pole of the black hole?

The azimuthal stretching of poloidal magnetic field that approaches the pole of the black hole leads to an acceleration of plasma along the axis of the hole as a result of magnetic field reconnection. For this to happen, though, we must first determine if poloidal fields can reach the polar axis above and below the black hole horizon. We have studied large scale magnetic configurations threading thin accretion disks, that under the dragging in the turbulent accretion flow, reach the black hole in the equatorial plane. We could imagine accretion tori of the kind expected to occur for advection dominated accretion flows, in which the large scale magnetic field structure approaches the black hole above and below the equatorial plane as well. Because the plunge region area is effectively smaller as the black hole spin increases, we propose the idea that as the spin of

the black hole increases, it becomes energetically more feasible for the poloidal magnetic field to survive being stretched to the polar axis, where it can be azimuthally twisted, leading to the reconnection described above. The other interesting thing to note is that the large geometrical thickness of the magnetic fields required for this process to occur, can only be brought to the near horizon region if the disk is geometrically large. Therefore, we find that energy in kinetic form can be transferred from the accretion disk to the jet only for thickest disks and for largest black hole spin. The large thickness of the disk suggests that what we should be modeling may be closer to a spherically accreting system. A quasi-spherical accretion system may also solve the issue of how fields are dragged to the polar axis above the hole, thereby overcoming the centrifugal barriers that arise in thinner accretion systems. In addition to the simplicity of the process compared to other magnetic models of jets, the gravitational redshift suffered by the plasma at the pole is less than that suffered in the plane of the disk for a given value of the radial coordinate. The issue that needs to be studied for this scenario to work is the extent to which the energy put into the magnetic field tracks the total conserved energy of the system, the killing energy. To the extent that it does or might, the idea is worth pursuing. This model is, therefore, appealing from various viewpoints and the idea behind this work would be to motivate full GRMHD simulations for very thick disks to test the idea in detail.

Appendix A

Acronyms

ADAF - Advection Dominated Accretion Flow

AGN - Active Galactic Nuclei

BZ - Blandford & Znajek

BP - Blandford & Payne

GR - General relativity

MHD - Magnetohydrodyamics

GRMHD - General relativistic magnetohydrodynamics

MRI - Magnetorotational instability

ZTBC - Zero torque boundary condition

HPB - Heyvaerts, Priest & Bardou

RPD - Radiation pressure dominated

GPD - Gas pressure dominated

GA 97 - Ghosh & Abrahmowicz

GBHB - Galactic black hole binary

LH - Low/Hard state

HS - High/soft state

Bibliography

Agol, E., Krolik, J.H., 2000, ApJ, 528, 161.

Allen et al., 2006, MNRAS, 372, 21.

Armitage P.J., Livio M., Pringle J.E., 1996, ApJ, 457, 332.

Balbus S.A., & Hawley, J.F., 1991, ApJ, 376, 214.

Balbus S.A., Hawley J.F., 1998, Rev. Mod. Phys., 70,1.

Bondi, H., 1952, MNRAS, 112, 195.

Blandford, R.D., & Payne, D.G., 1982, MNRAS, 199, 883.

Blandford, R.D., Znajek, R.L., 1977, MNRAS, 179, 433.

Brennemen, L.W., Reynolds, C.S.,2006, ApJ, 652, 1028.

Cunningham, C.T., 1973, PhD Thesis, Univ. of Washington.

Cunningham, C.T., 1975, ApJ, 202, 788.

Dabrowski, Y., Fabian, A.C., Iwasawa, K., Lasenby, A.N., Reynolds, C.S., 1997, MN-RAS, 288, 11.

De Villiers, J.P., Hawley, J.F., Krolik, J.H., 2003, ApJ, 599, 1238.

De Villiers, J.P., Hawley J.F., Krolik J.H., Hirose S., 2005, ApJ, 620, 878.

Di Matteo, T., Springel, V., Hernquist, L., 2005, Nature, 433, 604.

Eardley D., Lightman A., 1975, ApJ, 200, 187.

Fabian A.C., et al., 1989, MNRAS, 238, 729.

Fabian A.C., et al., 1995, MNRAS, 277, L11.

Fabian, A.C., Iwasawa, K., Reynolds, C.S., Young, A.J., 2000, PASP, 112, 1145.

Fabian A.C., Vaughan, S., 2003, MNRAS, 340, L28.

Fender, R., & Belloni, T., 2004, ARA&A, 42, 317.

Fender, R., Belloni, T.M., Gallo, E., 2004, MNRAS, 355, 1105.

Ferrarese, L., Merritt, D., 2000, ApJ, 539, L9.

Ford R.J., et al., 1994, ApJ, 435, L27.

Frank, J., King, A., Raine, D., 2002, in Accretion Power in Astrophysics, Cambridge Univ. Press, Cambridge.

Gammie, C.F., 1999, ApJ, 522, 57.

Gammie, C.F., Shapiro, S.L., McKinney, J.C., 2004, ApJ, 602, 312.

Gebhardt et al., 2000, ApJ, 539, L13.

Ghosh, P., & Abramowicz, M.A., 1997, MNRAS, 292, 887.

Greenhill, L.J., 1995, ApJ, 440, 619.

Haardt, F., Maraschi, L., 1991, ApJ, 380, 51.

Haardt, F., Maraschi, L., 1993, ApJ, 413, 507.

Harms, H.C., et al., 1994, ApJ, 435, L35.

Hawley, J.F., Krolik, J.H., 2000.

Hawley, J.F., Krolik, J.H., 2001, ApJ, 548, 348.

Hawley, J.F., Krolik, J.H., 2002, ApJ, 566, 164.

Heyvaerts J., Priest E.R., Bardou A., 1996, ApJ, 473, 403 (HPB).

Hirose, S., Krolik, J.H., De Villiers, J.P. & Hawley, J.F., 2004, ApJ, 606, 1083.

Iwasawa, K., et al., 1996, MNRAS, 282, 1038.

Kerr, R.P., 1963, PhRvL, 11, 237.

Koide S, Meier D.L., Shibata K., Kudoh T., 2000, ApJ, 536, 668.

Komissarov S.S., 2001, MNRAS, 326, 41.

Komissarov S.S., 2004, MNRAS, 350, 1431.

Komissarov S.S., 2005, MNRAS, 359, 801.

Krolik J.H., 1999, ApJ, 515, L73.

Krolik J.H., 1999, in Active Galactic Nuclei, Princeton University Press, Princeton, 139.

Li, Li-Xin, 2002, ApJ, 567, 463.

Lightman A., 1974, ApJ, 194, 419.

Livio M., Ogilvie G.I., Pringle J.E., 1999, 512, 100.

Lubow S.H., Papaloizou J.C.B., Pringle J.E., 1994, MNRAS, 267, 235.

MacDonald D.A., 1984, MNRAS, 211, 313.

MacDonald D.A., Thorne K.S., 198, 354.

McClintock J.E., Remillard R.A., 2006, ARAA, 44, 49.

McKinney J.C., 2005, ApJL, 630, L5.

McKinney J.C., Gammie C.F., 2004, ApJ, 611, 977.

McKinney, J.C., 2006, MNRAS, 368, 1561.

Meier, D.L., 2001, ApJ, 548, 9.

Meier D., 2005, in 'X-ray Binaries to Quasars: Black Hole Accretion on All Mass Scales',
eds., T.J.Maccarone, R.P.Fender, L.C.Ho (Dordrecht: Kluwer).

Miller, J.M., et al., 2002, AAS, 34, 1206.

Miniutti, G., Fabian, A.C., 2004, MNRAS, 349, 1435.

Miyoshi et al., 1995, Nature, 373,127.

Mizuno Y., Yamada S., Koide S., Shibata K., 2004, ApJ, 615, 389.

Moderski R., Sikora M., 1996, MNRAS, 283, 854.

Moderski R., Sikora M., Lasota J.-P., 1998, MNRAS, 301, 142.

Narayan, R., & Yi, I., 1995, ApJ, 452, 710.

Nemmen, R.S. et al., 2006, astro.ph., 12392N.

Nishikawa K.I. et al., astroph, December, 2006.

Novikov, I., & Thorne, K.S., 1973, in Black Holes, ed. C. DeWitt & B. DeWitt (New
York: Gordon & Breach), 345.

Page, D.N., Thorne, K.S., 1974, ApJ, 191, 499.

Phinney, E.S., 1983, Ph.D. thesis, Univ. Cambridge.

Proga, D., & Begelman, M.C., 2003, ApJ, 592, 767.

Punsly B., Coroniti F.V., 1990, ApJ, 354, 583.

Press, W.H., et al., 1992, Numerical Recipes in C. The Art of Scientific Computing (Cambridge Univ. Press).

Pringle J.E., 1981, ARAA, 19, 137.

Rees, M.J., 1966, Nature, 211, 468.

Reynolds C. S., Nowak M.A., 2003, Physics Reports, 377,389.

Reynolds C.S., Wilms J., Begelman M.C., Staubert R., Kendziorra E., 2004, MNRAS, 349, 1153.

Reynolds, C.S. & Fabian, A.C., astro-ph:0711.4158v1, ApJ accepted.

Reynolds, C.S. & Armitage, P.J., 2001, ApJ, 561, 81.

Reynolds, C.S., Brenneman, L.W., Garofalo, D., 2005, Ap&SS, 300, 71.

Riffert H., Herold H., 1995, ApJ, 450, 508.

Shakura, N.I., Sunyaev, R.A., 1973, A&A, 24, 337.

Speith, R., Riffert, H., Ruder, H., 1995, Computer Physics Communications, 88, 109.

Spruit H., Uzdensky D., 2005, ApJ, 629, 960.

Stirling A.M., Spencer R.E., de la Force C.J., Garret M.A., Fender R.P., Ogley R.N., 2001, MNRAS, 327, 1273

Tanaka Y., et al., 1995, Nature, 375.

Thorne K.S., Price R.H., Macdonald D.A., 1986, Black Holes: The Membrane Paradigm, Yale Univ. Press, New Haven CT.

Uzdensky D., 2004, ApJ, 603, 652.

Uzdensky D., 2005, ApJ, 620, 889.

van Ballegooijen, A.A., 1989, in Belvedere G., ed., Accretion Disks and Magnetic Fields in Astrophysics, Kluwer, Dordrecht, p.99.

Vaughan, S., Fabian, A.C., Nandra, K., 2003, MNRAS, 339, 1237.

Wilms J., et al., 2001, MNRAS, 328, L27.

Znajek, R.L., 1978, MNRAS, 185, 833.